



저작자표시-비영리-변경금지 2.0 대한민국

이용자는 아래의 조건을 따르는 경우에 한하여 자유롭게

- 이 저작물을 복제, 배포, 전송, 전시, 공연 및 방송할 수 있습니다.

다음과 같은 조건을 따라야 합니다:



저작자표시. 귀하는 원저작자를 표시하여야 합니다.



비영리. 귀하는 이 저작물을 영리 목적으로 이용할 수 없습니다.



변경금지. 귀하는 이 저작물을 개작, 변형 또는 가공할 수 없습니다.

- 귀하는, 이 저작물의 재이용이나 배포의 경우, 이 저작물에 적용된 이용허락조건을 명확하게 나타내어야 합니다.
- 저작권자로부터 별도의 허가를 받으면 이러한 조건들은 적용되지 않습니다.

저작권법에 따른 이용자의 권리는 위의 내용에 의하여 영향을 받지 않습니다.

이것은 [이용허락규약\(Legal Code\)](#)을 이해하기 쉽게 요약한 것입니다.

[Disclaimer](#)

공학박사 학위논문

Enhancement of Dispersion Stability on
the Polymer Nanocomposites with Clay
Nanoparticles through Analysis of
Moisture Absorption Behavior

흡습 거동 분석을 통한 점토 나노입자 강화 고분자
나노복합재료의 분산 안정성 향상에 관한 연구

지도교수 김윤해

2019년 8월

한국해양대학교 대학원

조선기자재공학과
박 수 정

본 논문을 박수정의 공학박사 학위논문으로 인준함

위원장	문 경 만
위 원	김 윤 해
위 원	김 국 진
위 원	신 도 훈
위 원	배 창 원



2019년 6월 28일

한국해양대학교 대학원

Contents

List of Tables	iii
List of Figures	v
Abstract	xi

1. Introduction

1.1 Trends of nanomaterial technology in advanced composites	1
1.2 Objectives of study	8

2. Literature review

2.1 Polymer matrix nanocomposites	11
2.1.1 Thermoset polymer composites	11
2.1.2 Nano-modification	15
2.2 Halloysite nanotubes based polymer nanocomposites	18
2.2.1 Halloysite nanotubes and crystallinity	18
2.2.2 Dispersion uniformity of halloysite nanotubes as fillers	21
2.3 Environment degradation of nano-structural materials	28
2.3.1 Hygrothermal behavior of polymer composites	28
2.3.2 Nanomaterials and environmental effect	30

3. Experimental works	
3.1 Halloysite nanotubes-FRP composites	33
3.2 Experimental procedure	38
3.2.1 Surface modification by thermal treatment	38
3.2.2 Nano-FRP manufacturing process	39
3.3 Evaluation and analysis	41
3.3.1 Structural property	41
3.3.2 Thermal property	42
3.3.3 Environmental degradation property	44
3.3.4 Mechanical property	45
3.3.5 Microscopic observation	46
4. Results and discussion	
4.1 Morphology effect	48
4.2 Thermal analysis	53
4.3 Moisture absorption behavior	63
4.4 Mechanical property	96
4.4.1 Tensile strength	96
4.4.2 Fracture behavior analysis	112
4.5 Dispersibility	124
5. Proposal for various applications	
5.1 High functional structural materials	137
6. Conclusions	141
Acknowledgement	144
References	145

List of Tables

Table 1 Composition and main specification of nanocomposites	34
Table 2 Sample' s code and their specifications	37
Table 3 Semi-autoclave process for HNT/EP nanocomposites	40
Table 4 Curing characteristics for HNT/EP nanocomposites system	54
Table 5 Open-hole tensile failure shape of HNT/FRP nanocomposites with immersion time in hygroscopic environment at 70°C; Neat GFRP and Neat BFRP	113
Table 6 Open-hole tensile failure shape of HNT/FRP nanocomposites with immersion time in hygroscopic environment at 70°C; C-0.5HNT/GFRP and C-0.5HNT/BFRP	114
Table 7 Open-hole tensile failure shape of HNT/FRP nanocomposites with immersion time in hygroscopic environment at 70°C; C-1HNT/GFRP and C-1HNT/BFRP	116
Table 8 Open-hole tensile failure shape of HNT/FRP nanocomposites with immersion time in hygroscopic environment at 70°C; C-3HNT/GFRP and C-3HNT/BFRP	117
Table 9 Open-hole tensile failure shape of HNT/FRP nanocomposites with immersion time in hygroscopic environment at 70°C; C-5HNT/GFRP and C-5HNT/BFRP	118
Table 10 Open-hole tensile failure shape of HNT/FRP nanocomposites with immersion time in hygroscopic environment at 70°C; A-0.5HNT/GFRP and A-0.5HNT/BFRP	119
Table 11 Open-hole tensile failure shape of HNT/FRP nanocomposites with	

immersion time in hygroscopic environment at 70°C; A-1HNT/GFRP and A-1HNT/BFRP	120
Table 12 Open-hole tensile failure shape of HNT/FRP nanocomposites with immersion time in hygroscopic environment at 70°C; A-3HNT/GFRP and A-3HNT/BFRP	122
Table 13 Open-hole tensile failure shape of HNT/FRP nanocomposites with immersion time in hygroscopic environment at 70°C; A-5HNT/GFRP and A-5HNT/BFRP	123

List of Figures

Fig. 1 Line representation between two points	1
Fig. 2 Industry trends of polymer nanocomposites market	3
Fig. 3 Effect of polymer viscosity on the state of dispersion of nanoparticles (nanotubes)	9
Fig. 4 Schematic diagram of curing reaction of thermosetting polymer; A-stage initial state, B-sate intermediate curing state, and C-state fully cured state	11
Fig. 5 Three district regions of resin change behavior on thermosetting resin cure system. V_i and V_f are the specific volume of the system at gelation and 100% cure, respectively	14
Fig. 6 Formation of cluster and surface bonding structure by adsorption of moisture on nanoparticle surface	16
Fig. 7 Chemical structure and composition of HNT	19
Fig. 8 Damage mechanism of polymer matrix FRP composites by moisture penetration	30
Fig. 9 Structure of thermosetting epoxy molecule	33
Fig. 10 Preparation of nanoparticle heat treatment	38
Fig. 11 FTIR analysis equipments	41
Fig. 12 DSC analysis equipments	43
Fig. 13 Equipments for moisture absorption tests	45
Fig. 14 Preparation for mechanical properties test	46
Fig. 15 Microscopic observation equipments; (a) Scanning electron microscopy and (b) Sputter coater	47

Fig. 16 Observation of crystallinity of HNT by Transmission Electron Microscopy (TEM)	49
Fig. 17 FTIR spectra of (a) HNT structures according to heat treatment and (b) HNT/EP colloidal solution structure	50
Fig. 18 Dynamic DSC analysis of Neat EP; (a) degree of cure and (b) rate of cure	56
Fig. 19 Dynamic DSC analysis of 0.5HNT/EP according to crystallinity of HNT; (a) degree of cure and (b) rate of cure	57
Fig. 20 Dynamic DSC analysis of 1HNT/EP according to crystallinity of HNT; (a) degree of cure and (b) rate of cure	58
Fig. 21 Dynamic DSC analysis of 3HNT/EP according to crystallinity of HNT; (a) degree of cure and (b) rate of cure	60
Fig. 22 Dynamic DSC analysis of 5HNT/EP according to crystallinity of HNT; (a) degree of cure and (b) rate of cure	61
Fig. 23 Absorption rate of Neat GFRP immersed in distilled water at 70 °C up to 336 h (14 days) according to laminated fiber plies	64
Fig. 24 Absorption rate of Neat BFRP immersed in distilled water at 70 °C up to 336 h (14 days) according to laminated fiber plies	65
Fig. 25 Absorption rate of C-0.5HNT/GFRP immersed in distilled water at 70 °C up to 336 h (14 days) according to laminated fiber plies	66
Fig. 26 Absorption rate of C-0.5HNT/BFRP immersed in distilled water at 70 °C up to 336 h (14 days) according to laminated fiber plies	67
Fig. 27 Absorption rate of C-1HNT/GFRP immersed in distilled water at 70 °C up to 336 h (14 days) according to laminated fiber plies	68
Fig. 28 Absorption rate of C-1HNT/BFRP immersed in distilled water at 70 °C up to 336 h (14 days) according to laminated fiber plies	69
Fig. 29 Absorption rate of C-3HNT/GFRP immersed in distilled water at 70 °C up to 336 h (14 days) according to laminated fiber plies	70

Fig. 30 Absorption rate of C-3HNT/BFRP immersed in distilled water at 70 °C up to 336 h (14 days) according to laminated fiber plies	71
Fig. 31 Absorption rate of C-5HNT/GFRP immersed in distilled water at 70 °C up to 336 h (14 days) according to laminated fiber plies	72
Fig. 32 Absorption rate of C-5HNT/BFRP immersed in distilled water at 70 °C up to 336 h (14 days) according to laminated fiber plies	73
Fig. 33 Absorption rate of A-0.5HNT/GFRP immersed in distilled water at 70 °C up to 336 h (14 days) according to laminated fiber plies	75
Fig. 34 Absorption rate of A-0.5HNT/BFRP immersed in distilled water at 70 °C up to 336 h (14 days) according to laminated fiber plies	76
Fig. 35 Absorption rate of A-1HNT/GFRP immersed in distilled water at 70 °C up to 336 h (14 days) according to laminated fiber plies	78
Fig. 36 Absorption rate of A-1HNT/BFRP immersed in distilled water at 70 °C up to 336 h (14 days) according to laminated fiber plies	79
Fig. 37 Absorption rate of A-3HNT/GFRP immersed in distilled water at 70 °C up to 336 h (14 days) according to laminated fiber plies	80
Fig. 38 Absorption rate of A-3HNT/BFRP immersed in distilled water at 70 °C up to 336 h (14 days) according to laminated fiber plies	81
Fig. 39 Absorption rate of A-5HNT/GFRP immersed in distilled water at 70 °C up to 336 h (14 days) according to laminated fiber plies	83
Fig. 40 Absorption rate of A-5HNT/BFRP immersed in distilled water at 70 °C up to 336 h (14 days) according to laminated fiber plies	84
Fig. 41 Moisture degradation of Neat GFRP by SEM; (a) before and (b) after distilled water immersion	86
Fig. 42 Moisture degradation of Neat BFRP by SEM; (a) before and (b) after distilled water immersion	87
Fig. 43 Effect of HNT on the moisture degradation of C-HNT/GFRP by SEM; (a) before and (b) after distilled water immersion	89

Fig. 44 Effect of HNT on the moisture degradation of C-HNT/BFRP by SEM; (a) before and (b) after distilled water immersion	90
Fig. 45 Effect of HNT on the moisture degradation of A-HNT/GFRP by SEM; (a) before and (b) after distilled water immersion	91
Fig. 46 Effect of HNT on the moisture degradation of A-HNT/BFRP by SEM; (a) before and (b) after distilled water immersion	93
Fig. 47 Effect of HNT on the moisture degradation by SEM; (a) C-HNT/GFRP and (b) C-HNT/BFRP after distilled water immersion over 700 h	94
Fig. 48 Effect of HNT on the moisture degradation by SEM; (a) A-HNT/GFRP and (b) A-HNT/BFRP after distilled water immersion over 700 h	95
Fig. 49 Effect of water absorption rate on tensile strength in (a) Neat GFRP and (b) Neat BFRP	97
Fig. 50 Tensile stress-tensile strain curves with water immersion time in (a) Neat GFRP and (b) Neat BFRP	98
Fig. 51 Effect of water absorption rate on tensile strength in (a) 0.5HNT/GFRP and (b) 0.5HNT/BFRP according to crystallinity of HNT ·	100
Fig. 52 Tensile stress-tensile strain curves with immersion time in (a) 0.5HNT/GFRP and (b) 0.5HNT/BFRP according to crystallinity of HNT ·	101
Fig. 53 Effect of water absorption rate on tensile strength in (a) 1HNT/GFRP and (b) 1HNT/BFRP according to crystallinity of HNT	103
Fig. 54 Tensile stress-tensile strain curves with water immersion time in (a) 1HNT/GFRP and (b) 1HNT/BFRP according to crystallinity of HNT	104
Fig. 55 Effect of water absorption rate on tensile strength in (a) 3HNT/GFRP and (b) 3HNT/BFRP according to crystallinity of HNT	106
Fig. 56 Tensile stress-tensile strain curves with water immersion time in (a) 3HNT/GFRP and (b) 3HNT/BFRP according to crystallinity of HNT	107

Fig. 57 Effect of water absorption rate on tensile strength in (a) 5HNT/GFRP and (b) 5HNT/BFRP according to crystallinity of HNT	109
Fig. 58 Tensile stress-tensile strain curves with water immersion time in (a) 5HNT/GFRP and (b) 5HNT/BFRP according to crystallinity of HNT	110
Fig. 59 Analysis of the state of HNT dispersion in composite laminates through moisture rate and variation with laminated fiber plies; (a) Neat GFRP and (b) Neat BFRP	126
Fig. 60 Analysis of the state of HNT dispersion in composite laminates through moisture rate and variation with laminated fiber plies; (a) C-0.5HNT/GFRP and (b) C-0.5HNT/BFRP	127
Fig. 61 Analysis of the state of HNT dispersion in composite laminates through moisture rate and variation with laminated fiber plies; (a) A-0.5HNT/GFRP and (b) A-0.5HNT/BFRP	128
Fig. 62 Analysis of the state of HNT dispersion in composite laminates through moisture rate and variation with laminated fiber plies; (a) C-1HNT/GFRP and (b) C-1HNT/BFRP	130
Fig. 63 Analysis of the state of HNT dispersion in composite laminates through moisture rate and variation with laminated fiber plies; (a) A-1HNT/GFRP and (b) A-1HNT/BFRP	131
Fig. 64 Analysis of the state of HNT dispersion in composite laminates through moisture rate and variation with laminated fiber plies; (a) C-3HNT/GFRP and (b) C-3HNT/BFRP	132
Fig. 65 Analysis of the state of HNT dispersion in composite laminates through moisture rate and variation with laminated fiber plies; (a) A-3HNT/GFRP and (b) A-3HNT/BFRP	134
Fig. 66 Analysis of the state of HNT dispersion in composite laminates through moisture rate and variation with laminated fiber plies; (a) C-5HNT/GFRP and (b) C-5HNT/BFRP	135

Fig. 67 Analysis of the state of HNT dispersion in composite laminates through moisture rate and variation with laminated fiber plies; (a) A-5HNT/GFRP and (b) A-5HNT/BFRP	136
Fig. 68 SEM observation of carbonized surface by flame; (a) A-HNT/GFRP and (b) A-HNT/GFRP (after UL 94 5V test)	138
Fig. 68 SEM observation of carbonized surface by flame; (a) A-HNT/BFRP and (b) A-HNT/BFRP (after UL 94 5V test)	139

Enhancement of Dispersion Stability on the Polymer Nanocomposites with Clay Nanoparticles through Analysis of Moisture Absorption Behavior

Park, Soo Jeong

Division of Materials Engineering
Department of Marine Equipment Engineering
Graduate School of Korea Maritime and Ocean University

Abstract

To begin with, nanomaterials are widely used as reinforcing materials with specific functionalities, because they have a characteristic broad particle surface area and excellent properties in small amounts. However, the use of nanomaterial fabrication technology has many limitations, such as the arrangement and dispersion of nanomaterials for use in composite materials and for the use of general structural materials. In order to overcome these limitations, researches on the physical and chemical surface treatment of nanomaterial based reinforcing materials and the development of mechanical techniques have been actively carried out. However, from the macro perspective, fiber reinforced plastics (FRP) composites such as shipbuilding, aerospace, automobiles, still have many technical limitations to their use for commercial purposes. In addition, since the conventional nanotechnology has a high price and a complicated

molding process, it has a disadvantage in that the production efficiency is inferior to the use of other materials and methods. Particularly, mass production of nanomaterials is difficult to control the structure such as particular particle size and length, and it is not easy to ensure uniformity of physical and chemical properties when working with these materials in a commercial environment.

Therefore, it is necessary to study the nanomaterial pretreatment method and the process of stabilization through a uniform dispersion with the polymer matrix, and it is required to develop nanomaterials for medium and large parts structural materials that exhibit uniform characteristics which can be used for a variety of other applications in other industries.

In this context, this study aims to establish the basis of a suitable manufacturing process of nanocomposite materials for general structure by applying FRP composites to applicable top-down processes, that will serve to control the grain and porosity of existing nanomaterials to below a few hundreds of nanometers, and therefore to significantly improve their properties.

In this study, halloysite nanotube/epoxy (HNT/EP) matrix glass fiber reinforced plastic (GFRP) and basalt fiber reinforced plastic (BFRP) nanocomposites were prepared by separating crystalloid-HNT (C-HNT) and amorphous-HNT (A-HNT) according to the crystallinity of HNT and the state of dispersion of HNT, which was evaluated at the interface of laminates. The state of dispersion of the laminate nanocomposites fabricated in a flat plate shape was analyzed by dividing a total of eight (A–H) columns in the direction of the air outlet in the vacuum molding.

The evaluation of the uniform dispersion was performed at 70 °C, and the tendency and the deviation of the moisture absorption rate when immersed in distilled water for 336 h. Based on these studies, the reliability of the state of dispersion criterion of nanomaterials was

suitably evaluated. As a result, the material design criteria for uniform dispersibility were obtained through a review of the identified moisture absorption characteristics. The effect of HNT on the interfacial bonding strength between EP and fiber reinforcements (GF, BF) was different depending on the notation of crystallinity that was found. In this regard, it is shown that moisture was important for controlling cohesion between HNTs. In the curing system, HNT was shown to have promoted the curing reaction, and the curing reaction caused the resin to develop properties related to shrinkage. The resin shrinkage affected the mobility of HNT and was a major factor involved in the re-aggregation. In addition, A-HNT has a strong bonding force with EP, which is relatively uniformly dispersed in EP compared with C-HNT, but also has a strong influence on the bonding strength of the interlaminar interface of laminates or weak bonds with the resulting fiber reinforcements. In other words, the crystallinity of HNT is closely related to the dispersibility of this material. In this study, the effect of HNT content and structure on the dispersion stability in GFRP and BFRP was investigated using the structural water characteristics of HNT.

KEY WORDS: Clay-polymer nanocomposites 점토-고분자 나노복합재료; Halloysite nanotube 할로이사이트 나노튜브; Particle aggregation 입자응집; Crystallinity 결정성; The state of dispersion 분산도.

1. Introduction

1.1 Trends of nanomaterial technology in advanced composites

Advanced nanocomposite materials are a core technology field of high-functionality new material and that is attracting attention in various higher value-added industries (see Fig. 1). Nanotechnology manipulates and analyzes material in the nanometer size category to create new material or systems. A new material is fabricated by changing the composition of the constituent components, or by changing the structure of the material, such as the crystal structure, or the size of the material (유선희, 2016). Nanotechnology can dramatically improve the performance of existing composite materials, and contribute to the development of multifunctional, high-performance new material by incorporating and hybridizing heterogeneous material at the nano level by physical or chemical methods.

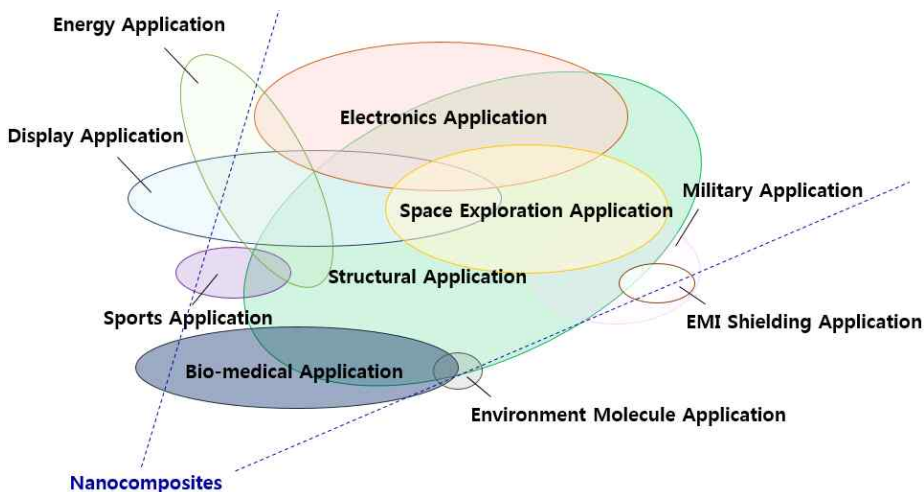


Fig. 1 Applications of nanocomposites

According to the technology trend report of the Korea Institute of Science and Technology (KISTI) (2002), nanomaterial is applied to functional materials used in molecular devices and various advanced electronic products, as well as the structural material of mechanical parts, through bonding with polymers. For this reason, the trend is toward nanotechnology in various fields, such as medical, environment, and energy.

The nanocomposites industry is located between the raw material industry and the applied product industry (see Fig. 2). It is composed of a rear industry that supplies raw materials for nanomaterial and base material, a nanocomposite materials industry part, and a front part manufacturing nanocomposite materials for the industry sector (INNOPOLIS Foundation, 2017). Among them, nanocomposite materials are being developed as promising material in fields related to transportation, such as automobiles, airplanes, and ships. These are business fields that focus on the development of lightweight material that is commonly used to improve fuel efficiency. Because nanocomposite materials can achieve high strength without changing specific gravity, impact resistance, etc., it is being studied as a major material in the development of products such as automobile engine room parts and door panels.

However, there are drawbacks, in that nanocomposite materials have high barriers to entry into the market due to low production, processing efficiency, ease of handling, and price competitiveness. Polymer nanocomposite materials technology is dominated by products that are classified as membrane (film) and coating. In addition, nanocomposite materials form a major product in industries related to real life, such as energy, construction, and the food packaging industry.

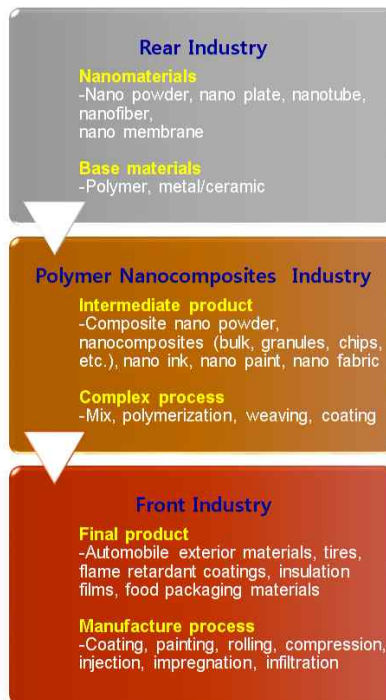


Fig. 2 Industry trends of polymer nanocomposites market
(INNOPOLIS Foundation, 2017)

A nanomaterial is a nanoscale material that has submicron size, and usually has a unit structure size of less than 100 nm. Nanomaterial, such as inorganic or metal particles, is separated and dispersed in a polymer material, such as a thermoplastic resin or a thermosetting resin, on a nano scale, to improve the mechanical properties of the material, or to impart specific functionality. Nanomaterial has a large surface area, so that it can obtain excellent physical properties with a small amount of addition, and it is mainly used for manufacturing various types of reinforcing material that are light and have high strength. In particular, it is possible to improve strength and stiffness, barrier properties against gas or liquid, abrasion resistance, heat resistance without deteriorating impact resistance, tensile strength, and transparency of the material by separating and dispersing the nano material in the polymer

material (Cho et al., 2006). In addition, nanocomposite materials have the advantages of lightweight and physical design, strong resistance to corrosion, the potential to provide electrical and thermal properties to material, and ease of manufacture of complex shapes. In order to expand the application range of nanomaterial in the industry, studies have been conducted on improving the affinity of nanomaterial by not only the protonation of polymeric material but also the mineralization of inorganic fillers. Research on the derivation of optimization parameters for the remediation process is required (KISTI, 2002).

As with the composites, nanocomposite materials also focus on creating synergies by macroscopically mixing heterogeneous materials, and expressing their useful properties. That is, two or more kinds of existing material are relatively homogeneously mixed with each other in a preserved state, which is opposite to alloy material. In order to minimize the deformation of the constituent materials and to project them onto the composite materials as much as possible, the state of dispersion, orientation, and interface of the nanomaterial as reinforcement are very important. In addition, it is possible to mix various material properties according to the manufacturing technology, and the material design can be made flexible, lightweight, and advanced. Therefore, in order to maximize the uniform dispersion of the reinforcement material, orientation method, and stress transmission efficiency, optimization of the interface design is a critical factor to be controlled for nanocomposite materials manufacturing. Among the various techniques, physical or chemical surface treatment of reinforcement, introduction of surfactants, and orientation by electrical or mechanical techniques are used as means for establishing such optimized process parameters (Choe, 2013).

Nanomaterial as advanced composites focuses on functionality. In the case of functional nanomaterial, there is a great demand for the fields of electronic material, lightweight high-strength material for automobiles, and

environment-friendly material. Functional nanomaterial is divided into carbon nanomaterial, metal nanomaterial, oxide nanomaterial, porous nanomaterial, and other nanomaterial, depending on chemical composition and structure of the raw material. These various structural differences and applications of physical, chemical, and biological properties have formed a broad spectrum.

One of the greatest advantages of such advanced nanocomposite materials is that the surface area of nanoparticle is relatively large, while the distance between particles is extremely short despite the low dispersion content, due to the finely dispersed particles. The increase in the surface area of the nanocomposite materials and the decrease in the intergranular distance form a continuous phase, that is, the interaction between the matrix and the particles, or the interaction between particles and particles, remarkably increases. As a result, the surface energy is greatly increased. This increase in interfacial energy makes it difficult to obtain a stable micro dispersion system. Therefore, the quality and competitiveness of the product depend on understanding the nanotechnology and nanomaterial fabrication techniques that are within 100 nm, so research on manufacturing technology has been carried out in various ways in order to utilize it properly.

Recently, studies on clay minerals and layered compounds as nanomaterial have been actively carried out. These inorganic nanoparticle layered compounds are highly diverse in their kind and characteristics, and have a very unusual property, compared to general inorganic or inorganic compound crystals. In particular, they have the properties of an organic polymer that are hardly possessed as an inorganic compound, such as swelling property, thixotropy, various reactivities with organic compounds, and ion exchange ability.

Nanocomposites using such layered silicates can be divided into exfoliated nanocomposites that completely disperse the silicate layer, and intercalated

nanocomposites that insert the polymer between the silicate layers. Methods for producing polymer composite materials using inorganic nanoparticles having a layered structure include melt intercalation, solvent intercalation, in situ polymerization, and compounding. Among them, compounding is a method of forming inorganic nanoparticles based on the original cluster in the matrix by a mixing technique used in conventional nanocomposite materials. In this method, a polymer chain is interposed between inorganic nanoparticles and various approaches have been attempted. Unlike solution and polymerization, the compounding method has the merit of the production efficiency being high, due to the relatively simple manufacturing process from a commercial aspect. However, since the final product quality is difficult to maintain at a certain level, and the risk of property deterioration is very high, there are many technical limitations in application and commercialization as material for medium- and large-sized machines, parts, and structural material. Also, the high price and complex molding process are disadvantageous to mass production. Therefore, in order to apply nanomaterial as an advanced composite material to industry, stabilization of the properties of nanomaterial should be prioritized. In particular, it is difficult to control the structure of mass-produced nanomaterial, such as particle size and length, and it is not easy to achieve uniformity of physical and chemical properties. Therefore, it is necessary to develop materials that exhibit uniform properties by stabilizing composite manufacturing techniques such as pretreatment methods of nanomaterial, and ensuring dispersion with matrix material.

In summary, nanotechnology is required to have a high degree of intensive technology to control the whole processes, such as analysis, control, and synthesis of nanostructure at the nanoscale level (유선희, 2016). In other words, the nanomaterial field for utilizing nanomaterial as advanced composites is a core technology that can dramatically change the direction of

technological progress in all fields of science, such as physics, chemistry, engineering, and medicine, and all fields of information electronics, materials, medicine, environment, and energy. In addition, technological change through nano-fusion materials is expected to have a great influence in the future in terms of industrial economics. Also, it is anticipated that new application products using innovative properties of nano-fusion material will form a large-scale market, and contribute to marketability. However, since the manufacturing technology of nanomaterial and nanocomposites is directly related to the quality of the structural material, it is necessary to secure a technology base from a macroscopic point of view, in order to improve the efficiency of the technology. This can be applied through advanced technology development study on nano-material surface modification and dispersion technology, nanotechnology to prevent recrystallization (agglomeration), and nanocomposite material process technology from a microscopic point of view.

1.2 Objectives of study

The goal of this research is to apply a top-down process that significantly improves physical properties by controlling and combining crystal grains and pores of existing material to a size of several hundreds of nanometers or less, to fiber-reinforced plastic (FRP) composites. Ultimately, it has the major purpose of opening up new horizons in the manufacturing process of new composite materials. The structural, physical, and chemical properties of nano-sized material highlight significant advantages in small quantities by creating new physical properties and functions in a variety of industries, while nanosize also limits the applications of nanomaterial. In particular, since the proper amounts of nanomaterial constituents are determined, they are relatively unaffected by the weight fraction between polymer and nanoparticles in mixing with a matrix, such as a polymer. In other words, in terms of excellent mechanical properties and light-weight, the efficiency of material property improvement is high, but the shape and size of the structure are restricted in manufacturing medium-and large-sized structures.

There are three approaches to apply nanoparticles to polymer-based FRP composites. The first is to impregnate the polymer matrix with nanoparticles, and mix them in the form of a uniform colloidal solution. The second is to uniformly bind the nanoparticles to the dry fabric (Yu, et al., 2019). The third is to uniformly disperse the nanoparticles on the surface of the prepreg formed by integrally molding the polymer matrix and the dry fabric. All of these have advantages and disadvantages in the molding process. A common factor among them is the change in state of the material due to resin curing, that is, the influence of resin fluidity on the nanoparticles. The combination of a polymer with viscosity and nanoparticles results in the generation of two or more molecular forces. Typically, the binding force between nanoparticles

and polymers is different, because the viscosity of the polymer limits the degree of freedom of nanoparticles. The binding force between nanoparticles affects the formation of clusters, by the binding force between nanoparticles according to the initial viscosity of the polymer. The attracting force between the nanoparticles is caused by the Van der Waals force, which is called agglomeration (aggregation). Since the aggregation phenomenon is strongly influenced by the viscosity of the polymer and the viscosity of the polymer varies with temperature, it is necessary to clarify the relationship between the temperature—viscosity and the viscosity—particle agglomeration (see Fig. 3). It is also observed in the form in which nanoparticles are incorporated into the polymer. In the case of the initial dry fabric and nanoparticles combined, the degree of freedom of the nanoparticles is limited, and the aggregation is relatively small. However, this is also not a negligible level, and an additional pretreatment step is required to increase the bonding strength between the dry fabric and the nanoparticles.

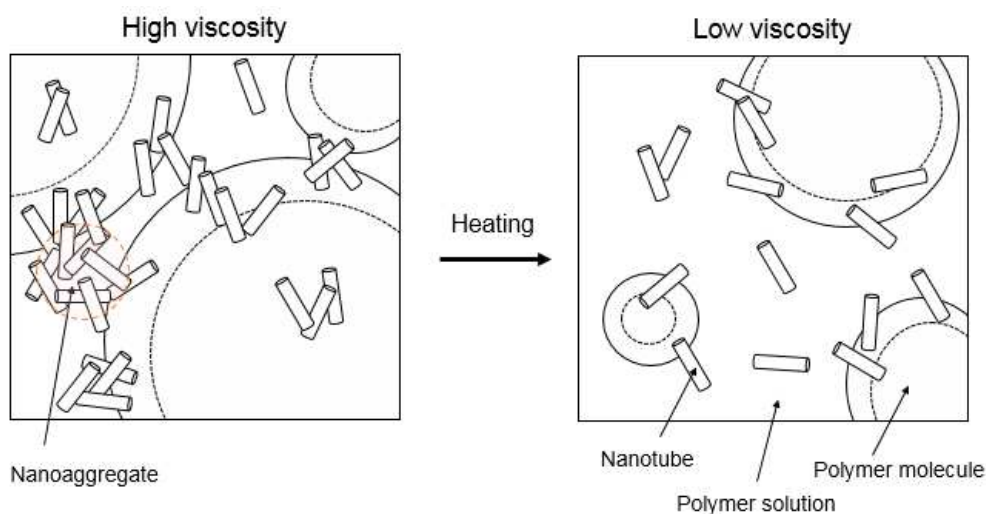


Fig. 3 Effect of polymer viscosity on the state of dispersion of nanoparticles (nanotubes)

It is necessary to study not only the initial uniform dispersion but also the approach, to prevent the re-coagulation phenomenon between the nanoparticles in the curing step, in the relation between the nanoparticles and the polymer. In particular, as the shape and size of structures are becoming more complex and larger, it is difficult to identify the state of dispersion from a microscopic point of view on a molecular scale. Therefore, an alternative process system is needed to simplify the manufacturing process, and improve the production efficiency. In addition, a practical research database from various perspectives must be accumulated, to ensure the process stability of nanoparticle-polymer matrix FRP composites.

Therefore, in this study, nanoparticle-polymer matrix FRP composites with excellent mechanical properties were fabricated, and the dispersibility between the polymer matrix and nanoparticles was observed using the inherent moisture absorption characteristics of the nanoparticles. In addition, the curing behavior and aggregation phenomenon of nanoparticles in the curing process of polymer were investigated. In order to investigate the mobility of nanoparticles according to the thickness of the laminate composite, the distribution of nanoparticles at the lamination interface and the bonding type with the constituent material was analyzed. Finally, the results of this study will contribute to establishing nanoparticle-reinforced laminate composite manufacturing process parameters. It is expected that this study will be used as important research material to accelerate the development of high-functionality nanocomposite materials by establishing a research base on curing behavior and dispersion of nanoparticles having similar components.

2. Literature review

2.1 Polymer matrix nanocomposites

2.1.1 Thermoset polymer composites

The polymers used in polymer matrix composites are classified into thermoplastic resins and thermosetting resins. A thermoplastic resin is a plastic that when heated, dissolves and becomes a liquid with high fluidity, and when cooled, becomes solid. It can be recycled with a reversible reaction. However, in the case of thermosetting resins, when heat and pressure are applied, they are melted, and become a fluid state. Once they are cured (solidified), they are not melted, even when heat is applied again. Thermoset polymer composites mainly consist of polymers such as epoxy and unsaturated polyester resin.

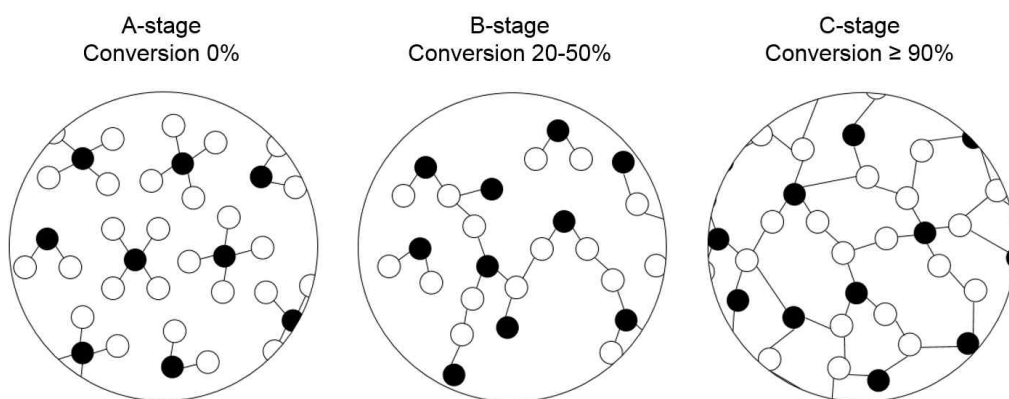


Fig. 4 Schematic diagram of curing reaction of thermosetting polymers; A-stage initial state, B-stage intermediate curing state, and C-stage fully cured state

The thermosetting resin is produced in the form of a final structure through a curing process. The curing of the thermosetting resin is caused by the crosslinking reaction between the base resin and the hardener to form a three-dimensional network structure (Shin, et al., 2015), which is classified into three stages, namely, A-stage, B-stage, and C-stage, including change of glassy and rubbery state (see Fig. 4). A-stage is the initial state of the thermosetting resin production reaction, and is a liquid state, and the conversion indicating the degree of reaction of the compound is 0 %. At this time, the thermosetting resin is dissolved by a specific solvent, and melted by heating. The B-stage means the intermediate curing state of the thermosetting resin, which is a partially cured solid state with (20—50) % conversion. It is softened by heating, and swells when contacted with a particular solvent, but is not completely melted or dissolved. Additionally, this state is referred to as gelation, which means that the liquid changes to a semi-solid state due to such chemical changes. The C-stage is the final state of the curing reaction, and has a conversion of more than 90 %, where the thermosetting resin is insoluble, and can be regarded as fully cured. Generally, the thermosetting resin maintains the B-stage state at room temperature (RT), and the viscosity gradually decreases as heat is applied, resulting in the A-stage state. When heat is applied and a specific temperature is reached, the reaction with the Hardener changes to B- or C-stage (Shin, et al., 2015).

The curing reaction is influenced by the pot life from the mixing of the resin and the curing agent to the progress of curing and gelation, and the curing time until solidification. The combination of specific time and temperature in the curing condition is called one cycle, and the degree of cure varies depending on the cycle of the step, which affects the characteristics of the resin and the durability of the material (Shin, et al., 2015). The degree of cure is used as an indicator of the chemical change of

the polymer resin, and the curing reaction is accompanied by a change in the physical and mechanical properties of the thermosetting resin, and is influenced by the curing temperature (Kwon, et al., 2014; Berglund & Kenny, 1991).

In addition, the most closely related factor to the curing process of thermosetting resins is viscosity. This is because the viscosity can induce diffusion control in the initial curing step. In the curing system of a thermosetting resin, the viscosity exhibits a complex temperature dependence, due to two phenomena. First, at constant molecular weight, the viscosity decreases with increasing temperature. Second, the increase in temperature promotes hardening, and as a result, increases the molecular weight and viscosity. Through this process, vitrification results are obtained in the post-curing stage (Vyazovkin & Sbirrazzuoli, 2000).

Shrinkage of thermosetting resin in composite structure design is one of the important factors to be considered (see Fig. 5). Shrinkage occurs during curing, which causes residual stress in composite structure, and causes thermal deformation, such as spring-in, spring-out, and warpage. Shrinkage difference occurs due to extreme temperature difference between the inside and outside of composite material. For this reason, it is necessary to analyze the cure shrinkage behavior of the resin, in order to minimize thermal deformation of the structure. In general, the initial curing reaction of the resin is dominated by chemical reactions, and after gelation, the diffusion reaction is more affected (Shin, et al., 2015).

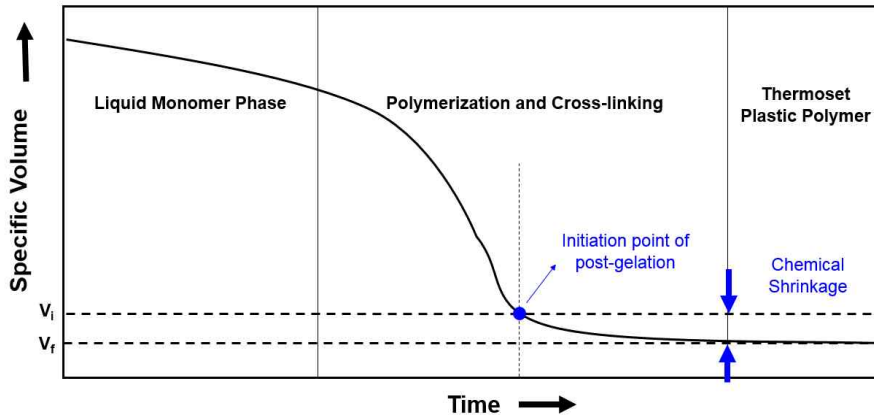


Fig. 5 Three distinct regions of resin change behavior on thermosetting resin cure system. V_i and V_f are the specific volume of the system at gelation and 100% cure, respectively (shah, & Schuble, 2010; Schubel, et al. 2013; Kwon, 2014)

Cure shrinkage occurs mainly in the B-stage, and begins with the formation of crosslinks, in which polymeric monomers in the resin have covalent bonds. The shrinkage of the resin does not occur at the initial stage of the curing reaction, but begins to increase sharply when the degree of cure reaches a certain level. However, when a certain level of hardening is reached, the shrinkage of the resin does not proceed any more. In addition, the higher the curing temperature of the thermosetting resin, the more shrinkage of the resin starts at a lower degree of cure; and since the shrinkage rate at the time of shrinking the resin is independent of the curing temperature, a precedent study on the relationship between degree of cure and volume shrinkage is necessary.

In particular, in order to use a reinforcing material, such as nanoparticles, in the production of a polymer matrix FRP, it is necessary to confirm the effect of the reinforcing material on the curing reaction of the polymer. In contrast, in order for the reinforcing material to perform its role, it is also

necessary to consider the risk of performance deterioration such as thermal deformation due to the curing reaction of the polymer.

2.1.2 Nano-modification

Nano-dispersion technology means that functional nanoparticles are stably dispersed in a matrix such as a polymer. Since nanoparticles can realize the originally intended characteristics and functions according to the uniformity and stability of dispersion, various dispersion techniques are being studied as a core element technology (Hwang, et al., 2016), to optimize dispersion technology and systems, and the development of techniques for dispersion stabilization is being actively carried out.

One of the greatest advantages of nanomaterials is that the dispersed particles are fine and the overall surface area of the nanoparticles is relatively large, while the distance between particles is very short, despite the low dispersant content. In the composite material using such a nanomaterial, the total surface area is remarkably increased while the inter-particle distance is reduced, so that interactions between the polymer matrix and nanoparticles, or between nanoparticles, and nanoparticles, are significantly increased. As a result, the surface energy is greatly increased. This increase in interfacial energy makes it difficult to obtain a stable micro dispersion system.

Nanoparticles such as nano-clay and nano-silica are used to improve the mechanical, thermal, and chemical properties of polymer matrix (Fatemeh, et al. 2013; Kibria, et al., 2015; Attia, et al., 2013). However, in nanocomposites, the surface area becomes exponentially larger as the particle reinforcement is reduced to nanoscale. As a result, if the addition amount is increased, the surface of the reinforcement becomes difficult to be wetted by the polymer matrix (Choe, 2013). In addition, nanoparticles aggregate to form a cluster (See Fig. 6). This is because the nanoparticle surface has an environment

where hydrogen bonding, moisture adsorption, and other chemical bonding actions are likely to cause aggregation phenomena between particles.

Therefore, the nanomaterial is chemically and structurally modified to overcome the limitations of the nano-dispersion technique. Proper surface modification can improve the dry state of nanomaterial and the dispersibility of polar and nonpolar solutions, polymeric compounds, and inorganic composite powders, and improve the effectiveness of nanomaterial. By modifying the nanoparticles, it is possible to improve the bonding and intercalation with the polymer material, and to lower the cohesion between the nanoparticles, thereby enabling uniform dispersion. At this time, the surface modification should be performed within a range that does not adversely affect the physical properties of the nanomaterial to be utilized.

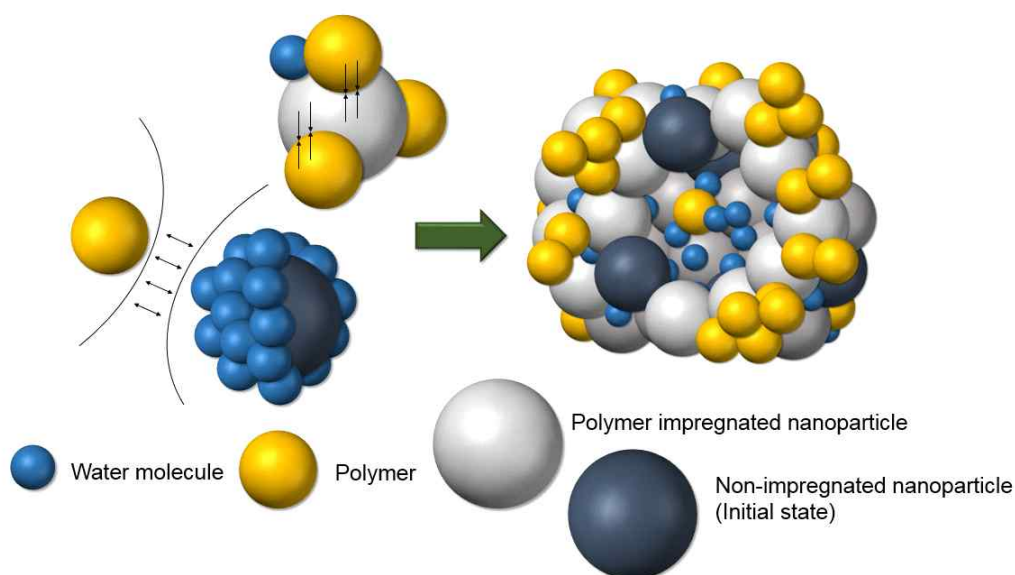


Fig. 6 Formation of cluster and surface bonding structure by adsorption of moisture on nanoparticle surface

For example, in the case of the surface modification method of silica nano powder, the surface property is modified by spray heating by a method in which the silica nano powder having mainly hydrophilic surface properties is modified to be hydrophobic. In addition, various surface modification methods have been reported for various inorganic-metal nanomaterial, depending on the characteristics of the nanomaterial, such as ultrasonic nano-surface modification, solid element plasma ion implantation, and surface treatment of functional nanoparticles, a surface-initiated atom transfer radical polymerization (ATRP) (Lee, et al., 2015; SunMoon University, 2012; 김용석, 2006; Li, et al., 2009).

For reference, the modified nanomaterial is strengthened to various matrix materials through various dispersion methods, such as medium dispersion, mechanical stirring dispersion, ultrasonic dispersion, electrostatic dispersion, dispersant dispersion and surface treatment. Typically, mechanical and ultrasonic dispersion are utilized as polymer-nanoparticle dispersion methods for structural materials of various sizes.

2.2 Halloysite nanotubes based polymer nanocomposites

2.2.1 Halloysite nanotubes and crystallinity

The minerals of the kaolin group include kaolinite, dickite, nacrite, phyllosilicate, feldspars, hematite, and halloysite, which are present in 1: 1 layers, but are stacked in different ways (Kadi, et al., 2012). Among them, halloysite nanotube (HNT) is an environmentally friendly nano material derived from geologically weathered or hydrothermally altered rocks, corrosion rocks, and soils, and has a relatively higher water content than the kaolin group minerals (Szczepanik, et al., 2015; Horvath, et al., 2003; Dong, et al., 2014). HNT has a hollow nanotube shape with an outer diameter of about (30 to 190) nm, a cylindrical pore (lumen) of about (10 to 15) nm, and an inner diameter of about (10 to 100) nm (Shu, et al., 2015; Cavallaro, et al., 2011). Chemically, HNT, which is similar to kaolinite and has the structural formula $\text{Al}_2(\text{OH})_4\text{Si}_2\text{O}_5 \cdot n\text{H}_2\text{O}$, is separated into a single layer of water molecules. HNT (n=2) refers to the hydrated form. At this time, the grain size is about 10Å, which means that there is one molecule of water between the multi-layers. HNT (n=0) is a dehydration structure, named 7Å, which is obtained by removing interlayer water molecules, whereas tubular morphology is maintained (Yuan, et al., 2009; Liu, et al., 2007; Dionisi, et al., 2016). HNT has a dominant form of tubular structure, with the 1: 1 type layer structure being divided into a silica tetrahedral sheet and an alumina octahedral sheet (see Fig. 7). HNTs have siloxane (Si-O-Si) groups, Silanol (Si-OH), and Aluminum Hydroxide (Al-OH) groups, and Thin layer of water between continuing layers (Yuan, et al., 2015; Szczepanik, et al., 2015; Duce, et al. 2015; Gasparini, et al. 2013). The zetapotential behavior of HNTs is almost negative at pH (6—7), due to the small surface potential of SiO_2 , and the positive cations on the Al_2O_3 inner surface. The chemistry of the outermost

surface of the HNT is similar to SiO_2 , and the properties of the inner cylinder core are related to the properties of Al_2O_3 (Liu, et al., 2007).

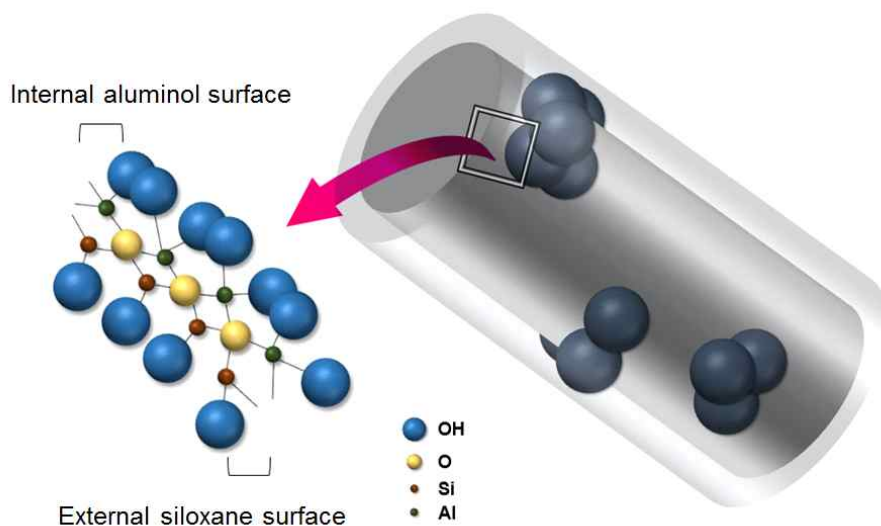


Fig. 7 Chemical structure and composition of HNT

HNT has a natural nanotube structure, high surface area, and unique surface properties, and is highly applicable as an additive filler of polymer plastics. The layered silicate structure of these HNTs forms a highly polar hydrophilic structure due to the OH group present at the end of the sheet, making it difficult to intercalate into a lipophilic material, such as a polymer. However, since naturally occurring HNTs have a unique crystalline structure, such as low hydroxyl density, as compared with other inorganic fillers of nano size, it is relatively easy to uniformly disperse the polymer in the polymer. In particular, this improves the mechanical properties, such as the Young's modulus and yield stress, by bonding with the polymer matrix (Nakamura, et al., 2013; Kaynak, et al., 2009; Lee, Park & Kim., 2017), and reduces the coefficient of thermal expansion, by forming a physical barrier during combustion, and delaying heat transfer. Also, as the particle size increases,

the fracture toughness increases. In other words, HNT is one of the nanofillers that is effective in improving mechanical properties, thermal stability, and flame retardancy. In addition, the intermediate water layer of HNT is a core structure for nano-modification, forming a structure that is capable of directly reacting with a solution such as an acid, and can be chemically and biologically loaded with various materials (Szczepanik, et al., 2015; Shchukin, et al., 2005). Therefore, HNT is widely used to synthesize complex structures. For example, template metal nanoparticle-HNT synthesis forms nanowires and porous carbon materials (Li, et al., 2009).

Generally, HNT is referred to as Hydro-HNT with 10Å and 7Å layers intermixed. Hydro-HNT is transformed into metakaolin by dehydroxylation reaction at (450 to 700) °C, which removes 10Å grain in Hydro-HNT, and leaves only 7Å grain (Gasparini, et al. 2013). These Hydro-HNT (-10Å, -7Å) and HNT (-7Å) are collectively called endelite, and are transformed into amorphous structures at temperatures above 700 °C. This is because the amorphous structure is clearly observed when the endelite is heated above 1,000 °C, and is called Meta-HNT (Park, 2016a, b, Kim, 2017; Hiller, et al., 2016). These changes are due to dehydroxylation, which removes water from the hydroxyl group, which is an important thermal dissociation reaction that occurs in the minerals, and natural and synthetic silicate materials of the kaoline group. The loss of the receiver caused by this process causes local buckling and deformation in the crystalline layer structure of the HNT. In addition, thermal decomposition reactions of some homogeneous clay minerals occur mainly in the temperature range of (30 to 1,000) °C, where the reaction rate of isothermal dehydration and dehydroxylation is the same as that of the first reaction (Duce, et al., 2015; Kiptsov, et al., 1988; Adhikari, et al., 1983; Liu, et al., 2012). However, this dehydroxylation reaction is controversial, because it depends on many factors of HNT structure, such as

particle size, shape, and defect density, and many factors, such as heating rate, sample treatment, temperature, and humidity. (Gasparini, et al., 2013). Therefore, it is necessary to set the process parameters suitable for the crystal structure of the HNT and the characteristics of the polymer matrix, and to optimize the system through surface modification and polymerization.

In particular, clay minerals such as HNT are used to support enzyme immobilization to solubilize the enzyme, or increase the recovery rate of the enzyme. As a result, research on the surface chemical polymerization of HNT is underway. Since the behavior of materials in the bond between HNT and polymer matrix is mainly limited to the constituents of HNT and polymer matrix, the efficiency of heterogeneous catalyst use is required (Rawtani & Agrawal, 2012; Kojima, et al., 1993; Okamoto, 2003).

Therefore, chemical compatibility is required between the single components, and the interfacial interaction with the HNT filler, which acts as a part of the microstructure, directly affects the properties of the material. Therefore, when nanoparticles are used as reinforcing materials for polymers, it is necessary to achieve uniform dispersion and to reduce cohesive force, by applying various techniques, such as the sol-gel process and the ultrasonic vibration method (Rosso, et al., 2006 ; Xiao & Ye, 2006).

2.2.2 Dispersion uniformity of halloysite nanotubes as fillers

In polymer nanocomposites, nano clay has a form that is peeled or dispersed in a polymer material, such as a thermoplastic resin or a thermosetting resin. Polymer chains are mainly inserted between layers of nano-clay, contributing to improvement of the mechanical properties or functionality (Tang, et al., 2010). As a direct/indirect method of inserting the polymer into the interlayer structure of the HNT, there are solution, polymerization and compounding methods (Pavlidou & Papaspyrides, 2008;

Idumah, et al., 2015). These are mainly considered in terms of high functionality, productivity, and commerciality. In general, high technology development is being carried out in order to maximize the utilization of nanoparticles, while minimizing structural and physical damage to the nano clay.

In the solution method, a polymer is dissolved in a solvent to prepare a solution and then mixed with an organic layered material. It is difficult to separate the polymer from the solvent of the solid component, because a high molecular weight polymer is inserted between the layers, and is non-commercial. In the polymerization method, an organic layered silicate is mixed with a monomer as the raw material of a polymer, and a part of the monomer is penetrated between the layers, and polymerized to obtain a nano-polymer solution. Since a monomer having a low molecular weight is intercalated between the nanoparticle layers, peeling occurs relatively easily, so that it is possible to disperse the layered silicate at nanoscale. However, it is difficult to apply to a large amount of nanoparticles, because the available monomers are limited, and the manufacturing process is complicated. On the other hand, in the compounding method, the organic layered material is mixed with the polymer resin in a molten state. Therefore, since processing equipment, such as an extruder and a ball mill, can be used, it is most efficient from a commercial viewpoint. Unlike the solution and polymerization methods described above, the compounding method has the advantages of ease of raw material supply and simplification of the process, since a large amount of nanoparticles can be handled. However, it is necessary to develop advanced technology to remove the layered material at the nanoscale, such as the use of a compatibilizer that enhances the affinity between the polymer resin and the layered material, modification of the polymer resin, and establishment of mixing conditions.

In general, the chemical species that can form interlayer complexes are limited to monomers and small molecules, and the polymers are difficult to intercalate between layers due to their size, and they are compounded by interlayer polymerization (Ryu, et al., 1998; Barrientos-ramirez, et al., 2011; Gao, 2004). When a load is applied to nanocomposites fabricated through this process, microcracks are generated between the weakly bonded layers. The interlayer polymerized nano clay inhibits the growth of microcracks, resulting in high fracture energy. In this case, the impact strength of the composite with nano clay is increased more than two times, depending on the kind of nano clay (Tang, et al., 2010; Basara, et al., 2005; Deng, et al., 2007). Tang, et al. (2011) and Deng, et al. (2010) reported that when intercalated HNTs were used to produce uniformly dispersed HNT-Epoxy colloidal solutions, the fracture toughness was significantly improved, without sacrificing properties such as the strength, glass transition temperature, and thermal stability (Ye, et al., 2007, Ng, et al., 2010). This increase in fracture toughness is mainly due to mechanisms such as crack bridging, crack deflection, plastic deformation of matrix around HNT clusters, fiber breakage, fiber segregation, and pull-out of HNT. In other words, the increase of contact area with epoxy through HNT modification affects the improvement of fracture toughness.

Recently, the application of nano clay in industry has been rapidly increasing. Ultimately, uniform dispersion is emerging as a core technology of nano clay composite, and dispersion is closely related to intergranular aggregation. Agglomeration of nanoparticles has a direct effect on the physical properties of the material (Deng, et al., 2007). In particular, agglomeration between nanoparticles degrades the activity of nanoparticles, making it very difficult to produce nanoparticles, and to apply nanoparticles as fillers (Esbati, et al., 2018).

The major causes of nanoparticle aggregation phenomena can be classified

as follows. First, since conventional materials absorb a large amount of mechanical energy and thermal energy in the process of nanosynthesis, the new nanoparticles have high surface energy. These nanoparticles try to reach a stabilized state by lowering their high surface energy, which causes mutual aggregation of nanoparticles. Second, when the particles reach a specific particle size, the inter-particle distance becomes extremely short, and the Van der Waals force between particles becomes larger than the inherent gravity of the particles, resulting in mutual agglomeration between particles. Thirdly, the hydrogen bonding, moisture adsorption and other chemical bonding action on the surface of the nanoparticles cause agglomeration between the particles.

Therefore, these nanoparticle agglomerates form voids in the polymer or matrix, and act as stress concentrations, thereby lowering the strength. These nanoparticles are influenced by the interlayer distance (Brindley, 1979). In addition, studies have been carried out to improve the mechanical strength and high-temperature characteristics by increasing the inter-layer distance by inserting various organic molecular ions into swellable clay such as HNT, thereby ensuring dispersion stability (Ryu et al., 1998; Blumstein, 1965 ; Kanatzidis, et al., 1989, Deng, et al., 2008). HNT has a structurally wide surface area, high porosity, and adjustable surface chemistry, and imparts specific functionality by grafting HNT to substrates, such as thin film and polymers, through the deformation and surface modification of nanotubes. In addition, HNTs are easy to use as fillers for polymer composites, because of their individual nano-particles with small surface charge (Deng, et al., 2009). However, HNTs do not have uniformly dispersed nanotube structures, and tend to aggregate under the influence of Van der Waals forces, due to their relatively large surface energies. In other words, HNT can act as a potential defect (Deng, et al., 2009; Levis & Deasy, 2002). Therefore, the binding force

between the nanoparticles and the polymer must be further increased through the modification of the HNT and surface functionalization treatment. In addition, nanoparticle dispersion methods should be considered to minimize the problems that can arise from nanoparticles (Lun, et al., 2014; Hu & Yang, 2012).

Natural HNTs also exist as aggregates of various diameters and lengths in a natural state, similar to conventional inorganic nano-clay (Lun, et al., 2013). It is highly likely that the coagulation phenomenon occurs due to surface denaturation, such as moisture adsorption, during the process of storage or manipulation after the nano-forming process. However, HNT is widely used for nanocatalysis, because it can obtain higher specific surface area and larger void area due to its uniform dispersion, and is applied as an effective impact modifier in highly brittle polymers. (Liu & Zhao, 2008). In addition, there is a need for a new methodology to solve this problem.

However, in general, primary aggregation occurs in the process of bonding with the polymer. Secondary aggregation (re-aggregation) occurs in the curing stage of the polymer, depending on the change of the state of the polymer, and the degrees of freedom of nanoparticles, and a large cluster is formed. Therefore, in order to uniformly disperse the nanoparticles, it is important to combine the nanoparticles with the polymer in a 1:1 ratio to form a complete bond. The conventional dispersion method has been studied, in order to prevent agglomeration of the nanoparticles themselves by mechanical agitation, which breaks the particle agglomeration. In contrast, mechanical agitation has the disadvantage that the nanoparticle lumps float, due to the flow of liquid.

To overcome this, ultrasound dispersion was applied to force the nanoparticles to break the cohesive force into a larger energy. Ultrasonic dispersion is the most common method for peeling and inserting polymers into

nano clay. At this time, the ultrasonic strength is controlled, and the ultrasound exposure time for the nanoparticles is adjusted to uniformly disperse the coagulated nanoparticles temporarily. In addition, absorption of ultrasound energy by the polymer causes the temperature of the solution to rise and the viscosity to lower, thus allowing the uniform dispersion of nanoparticles. However, dispersion by mechanical blending methods, such as ultrasonic vibration and shear mixing, cannot completely prevent particle agglomeration. In recent years, various studies have been conducted to improve the dispersibility of nanoparticles by clay surface modifier through deformation, functionalization, and mixing techniques (Brantseva et al., 2018).

One of them is to modify the surface of nano-clay to improve the compatibility of nano-clay with polymer and to promote uniform dispersion (Liu, et al., 2003). Surface modification of HNT can extend the base spacing of HNTs by the intercalation of inorganic and organic compounds in the interlayer, which can form a strong bond between the HNT and the polymer through such surface modification (Rawtani & Agrawal, 2012; Levis & Deasy, 2002). In addition, surface modification and ball mill homogenization have improved the dispersion of particles, which is due to the improved mechanical properties (Deng, et al., 2009). Therefore, in order to select an appropriate nano clay modifier, the polymerization process with the polymer and the chemical structure of the crosslinking agent should be considered. It is also necessary to pay attention to the increase of shear and peel strength by nano-fillers (Brantseva, et al., 2018). In particular, since HNT has a hollow nanotube form, surface damage occurs when exposed directly to ultrasonic energy. It is difficult to optimize the dispersion parameters of HNTs with various grain sizes, such as HNT-7 Å and HNT-10 Å. Therefore, a dispersant is used as a method to uniformly disperse HNT in a polymer suspension (Zhang, & Choi, 2012). Dispersants include inorganic dispersants, polymeric

dispersants, and anionic and cationic dispersants, and are classified according to the nature of the nanoparticles. According to Lun, et al. (2013), sodium dodecyl sulfate (SDS) is adsorbed on HNT as a dispersant, and is mainly used in silica-based nanoparticles similar to natural nanotubes, thereby improving the stability and dispersibility of the polymer suspension. However, additional studies are needed to maintain consistency of the HNT concentration and HNT particle size for polymer suspension applications.

2.3 Environment degradation of nano-structural materials

2.3.1 Hygrothermal behavior of polymer composites

The aerospace, shipbuilding, marine, and automobile industries deal with typical composite materials. The light weight, specific strength, integral molding, and ease-of-design features that are possessed by composite materials are rapidly growing, not only in terms of mechanical properties, but also in terms of their structural, chemical, and physical properties, as well as their economic and industrial applications. Furthermore, the environmental resistance of composite materials, such as corrosion resistance, hygroscopicity, and fire resistance, prolongs material life, and secures structural stability under specific environmental conditions, as compared with conventional metals. While composite materials that are composed of two or more different materials are complementary to reinforcements and matrix materials, in extreme environments, the properties of a single material determine the properties of the composite material.

In particular, these characteristics are clearly observed in polymer composites. Polymers are highly vulnerable to environmental degradation by moisture, solvents, oil, temperature, mechanical load, and radiation (Akil, et al., 2014). When a polymer composite is exposed to high humidity or water environment for a long time, the polymer generally undergoes large influence from moisture. Generally, a polymer composite absorbs moisture, and this water molecule simultaneously affects the fibers, polymer matrix, and interface. In this case, the water molecule acts like a plasticizer in the polymer matrix, resulting in a deterioration of the mechanical properties (weakness of interfacial strength) finally (Akil, et al., 2014; Mazuki, et al., 2011; Lee, et al., 2010). The water-softened polymer is plasticized to increase

the fracture toughness of the nanocomposite, but the surface becomes rough, and becomes a potential cracked part (Saharudin, et al., 2017). This deterioration also causes micromechanical damage to the fiber reinforcement and polymer matrix interface. Therefore, in order to improve the durability of the material, it is necessary to understand the moisture diffusion mechanism of the nanocomposite.

In the polymer degradation mechanism, initial moisture penetrates the polymer matrix, and diffuses according to Fick's law (Picard, et al., 2008; Xu, et al., 2006). The diffusion of moisture penetrates into the nonuniform interface between the silane portion of the polymer composite laminate and the reinforcing fiber interface, causing swelling of the material, and deterioration of the physical properties (see Fig. 8). A large amount of water generates tensile stress on the fiber, causing swelling and peeling of the polymer resin to cause permanent damage, such as separation of the fiber and resin interface and fiber breakage. In the case of fiber-reinforced materials, relatively little water directly influences penetration into the fiber or surface damage. In other words, fatal damage to the fiber surface occurs from the polymer matrix being degraded by water rather than being directly affected by water. The moisture absorbed in the polymer matrix chemically bonds with the polymer. However, some water molecules are not chemically bonded, because they diffuse into the free volume, and are removed by drying, without affecting the mechanical properties of the polymer. As such, the swelling and drying of the polymer due to moisture causes shrinkage of the material, and weakens the interfacial bonding strength between the polymer and the reinforcing fiber. According to Kim, et al. (2008), when the specific non-conversion point is observed in terms of the amount of water in the material or the exposure period of water, the swelling phenomenon and the interfacial fracture due to moisture are generated within the material. At

this time, it is impossible to recover the physical properties of the material by drying. Therefore, it is necessary to alleviate the conditions for this non-conversion point in the polymer composite.

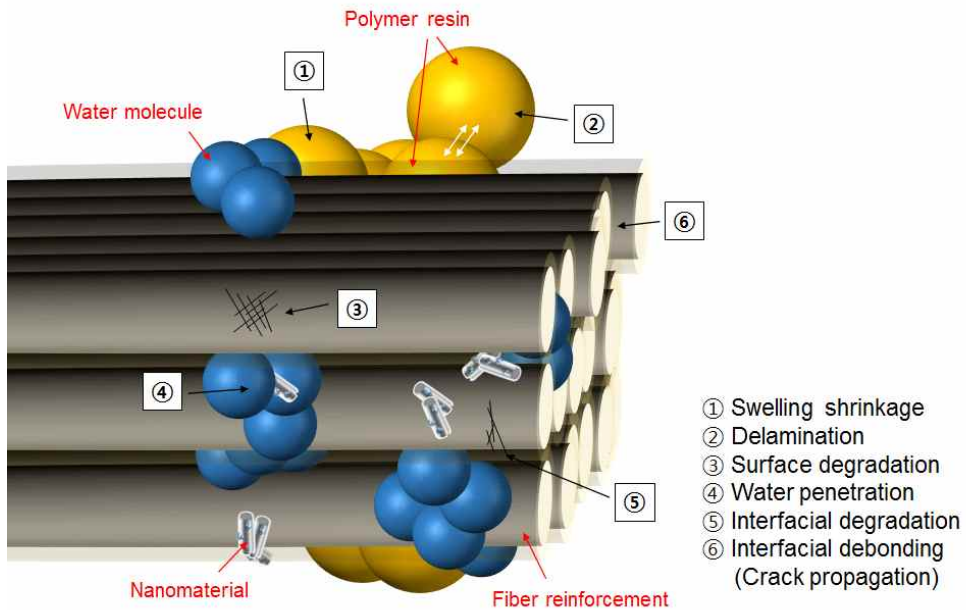


Fig. 8 Damage mechanism of polymer matrix FRP composites by moisture penetration

2.3.2 Nanomaterials and environmental effect

Although water acts as a factor to inhibit the polymerization and synthesis of polymers and nanoparticles (Kornmann, et al., 2001; Manfredi, et al., 2008; Saharudin, et al., 2015), a large amount of water diffuses into polymer matrix by clay nanofiller (Kim, et al., 2005). High aspect ratio nanofillers can create a skewed path, where water molecules diffuse into the complex. In addition,

nanoparticles can reduce the cross-linking density of polymers (Lan et al., 1996; Fellahi, et al., 2001; Manfredi, et al., 2008). At this time, the moisture absorption rate with respect to moisture tends to decrease gradually, as the content of the clay nanofiller increases. The clay nanopiller is added in an amount of about 1 wt.%, mainly because it exhibits high functionality, even in a small amount. Above 1 wt.%, the tendency of aggregation between nanoparticles increases the moisture absorption rate, resulting in a significant decrease in fracture strength and tensile stress, due to the physical damage of nanocomposites (Irshidat & Al-Saleh, 2018; Park & Kim, 2019; Park, et al., 2019). However, when the dispersion uniformity of the nanoparticles is achieved, the clay nanofiller can greatly reduce the equilibrium moisture content and diffusion coefficient of the composite material (Mohan & Kanny, 2011). In other words, the equilibrium moisture content and diffusion coefficient of the composite materials are greatly reduced by the clay nanofiller (Mohan & Kanny, 2011). This is because the tortuosity effect increases with increasing filler content. For example, in polymer epoxy-based nanocomposites, the maximum absorption rate has been observed through the addition of a layered silicate, Al_2O_3 nanoparticles (Alamri & Low, 2012; Zhao & Li, 2008; Liu, et al., 2014; Becker, et al., 2004). On the other hand, the fracture toughness and impact strength were increased, due to the plasticizing effect of moisture absorption. This is due to the fact that the penetration and diffusion of moisture into the polymer matrix increases the ductility of the polymer matrix, as well as the mobility of polymer chains, resulting in improved toughness of the nanocomposites (Alamri & Low, 2012; Zhao & Li, 2008). Therefore, in a polymer nanocomposite, a liquid medium caused by external environmental factors, such as water, diffuses through microcracks, and induces stress cracking. In order to improve the stress cracking resistance, a detailed study of nanoparticle-reinforced polymer polymers is needed. In particular, it is important to study the relationship between the

external liquid medium and stress cracks of composites, improvement of interfacial bonding strength in the nanocomposites, and micro crack prevention (Saharudin, et al., 2015).

In addition, the HNT used in this study has also been reported to be added to the polymer composite to reduce the water absorption rate, and to improve the mechanical properties of the nanocomposite after moisture absorption (Saharudin, et al., 2016; Georga, et al., 1998; Saharudin, et al., 2017). Since HNT is hydrophilic, the addition of HNT to the polymer increases the water resistance of the surface, due to the different wettability of the surface (Liu, et al., 2014; Kim, et al., 2018). However, as mentioned above, when HNT is dehydrated at high temperature, it forms a relatively stable structure compared with nanotubes; but since it is not effective in intercalating the polymer in the HNT, additional surface modification is required (Deng, et al., 2009).

3. Experimental works

3.1 Halloysite nanotubes-FRP composites

The main material used in this study is polymer matrix fiber reinforced plastic (FRP) composites with HNTs (see Table 1). In this case, glass fabric and basalt fabric were used as fiber reinforcements, and they have a unidirectional woven arrangement as an inorganic material. Glass fiber (GF) and basalt fiber (BF) form a similar chemical composition. GF and BF are relatively low in mechanical properties compared to CF, but GF in general use in industry as an economical fiber. BF is an environmental-friendly material made of basalt ores, has mechanical properties similar to GF, has excellent heat resistance properties, as well as mechanical and chemical properties, and is being studied and applied in various industries.

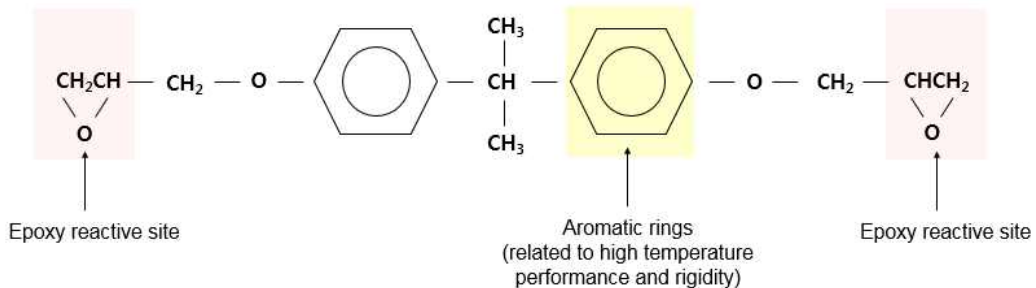
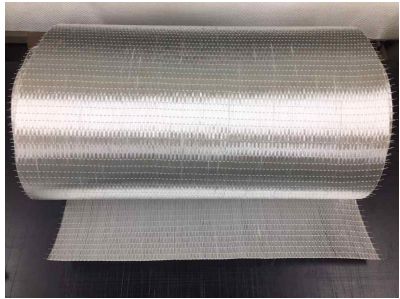





Fig. 9 Structure of thermosetting epoxy molecule

A bisphenol-A type epoxy resin (EP) was used as the matrix, and it was a low viscosity liquid type and had a post-curing condition at 80 °C for 4 h. Bisphenol-A (BPA)-type epoxy resin has mainly excellent chemical resistance, solvent resistance, high mechanical strength, and dimensional stability (see Fig. 9), and is used in various industrial fields such as adhesives, coatings, and matrix materials for composites (Kim, et al., 2015).

Table 1 Composition and main specification of nanocomposites

Materials			
Components	Model	Type	
Reinforcement	Glass fabric (EJ30)	Unidirectional fiber (UD)	
		Specification	
		<input checked="" type="checkbox"/> Supplier: Hankuk Carbon Co., LTD, South Korea <input checked="" type="checkbox"/> Areal weight: 450 g/m ² <input checked="" type="checkbox"/> Thickness: 0.177 mm <input checked="" type="checkbox"/> Chemical composition (E-glass): SiO ₂ , Al ₂ O ₃ , CaO, MgO, Na ₂ O, K ₂ O, B ₂ O ₃	
		Unidirectional fiber (UD)	
	Basalt fabric (HB-300)	Specification	
		<input checked="" type="checkbox"/> Supplier: GM Composite Co., South Korea <input checked="" type="checkbox"/> Areal weight: 300±24 g/m ² <input checked="" type="checkbox"/> Thickness: 0.115±0.013 mm <input checked="" type="checkbox"/> Chemical composition: SiO ₂ , TiO ₂ , Al ₂ O ₃ , Fe ₂ O ₃ +FeO, CaO, MgO, MnO, Na ₂ O+K ₂ O, SO ₃	

Components	Model	Type	
Matrix	Epoxy resin (KFR-120V)	Liquid	
		Specification	
		<ul style="list-style-type: none"> ☑ Supplier: Kukdo Chemical Co., Ltd, South Korea ☑ Hardener: KFH-141 (Mixing ratio of epoxy resin/ hardener=100:30±2 wt.%) ☑ Density of Mixture: 1.0~1.2 g/mL ☑ Viscosity of Mixture: 150~300 cps ☑ Glass transition temperature (T_g): (70—80) °C ☑ Post curing: 80 °C for 4 h 	

Components	Model	Type	
Nano-fillers	Halloysite nanoclay	Powder	
		Specification	
		<ul style="list-style-type: none"> ☑ Supplier: Sigma-Aldrich, South Korea ☑ Synonym: Kaolin clay ☑ Density: 2.53 g/cm³ ☑ Molecular weight: 294.19 g/mol ☑ CAS No. 1332-58-7 	

In particular, epoxy composite materials using bead, talc, CNT, silica, fiberglass, carbon fiber, and aramid fiber show excellent light weight, adhesion, mechanical properties, and durability, and are widely used in aerospace, automobile, civil engineering structural materials, shipbuilding, and marine industries. HNT was used as a nanofiller, and impregnated with GF and BF in EP mixed form. HNTs are classified into crystalline and amorphous types depending on the crystal structure.

In this study, hydro-HNT ($\text{Al}_2\text{Si}_2\text{O}_5(\text{OH})_4 \cdot 2\text{H}_2\text{O}$), crystalline HNT ($\text{Al}_2\text{SiO}_5(\text{OH})_4$), and amorphous Meta-HNT ($\text{Al}_2\text{SiO}_5(\text{OH})_4$) were used, and they were named Neat HNT, C-HNT, and A-HNT, respectively. They form a uniform crystal structure according to the heat treatment. In the case of C-HNT, when Neat HNT was annealed at 700 °C for 4 h, it had only the 7 Å crystal structure of the Neat HNT precursor, which is a mixture of (7 and 10) Å (quartz or silicon oxide). In addition, when exposed to temperatures above 1,000 °C for extended periods of time, C-HNT turns into an amorphous form, A-HNT (Kim, et al., 2008; Park, 2016a; Park, 2016b). These forms differ in crystallinity, depending on the presence or absence of the H_2O layer in the structure of the HNT; their inherent physical properties also differ. In other words, since HNT is affected by heat, it is necessary to study the crystal structure and properties according to the temperature range to understand the basic crystal structure, except that the crystal structure is manipulated artificially, such as chemical surface treatment. Therefore, the material properties and manufacturing process to improve the physical properties of polymer matrix FRP composites based on the basic structure of HNT were examined.

In particular, in the case of nanoparticles, the physical properties vary depending on the viscosity and molecular size of the polymer to be mixed, the addition amount of nanoparticles, and the dispersion technique. Therefore,

the addition amounts of HNT were classified into (0.5, 1, 3, and 5) wt.%, depending on the crystal structure of HNT. Table 2 shows the specifications of the samples used in this study. They are classified according to EP type, amount of HNT, and crystal structure of HNT.

Table 2 Sample' s code and their specifications

Code	Epoxy resin (g)	Resin type	Clay content (phr)	Clay type
Neat GFRP	100	Liquid	0	NA
Neat BFRP	100	Liquid	0	NA
C-0.5HNT/GFRP	100	Liquid	0.5	Crystalloid
C-0.5HNT/BFRP	100	Liquid	0.5	Crystalloid
C-1HNT/GFRP	100	Liquid	1	Crystalloid
C-1HNT/BFRP	100	Liquid	1	Crystalloid
C-3HNT/GFRP	100	Liquid	3	Crystalloid
C-3HNT/BFRP	100	Liquid	3	Crystalloid
C-5HNT/GFRP	100	Liquid	5	Crystalloid
C-5HNT/BFRP	100	Liquid	5	Crystalloid
A-0.5HNT/GFRP	100	Liquid	0.5	Amorphous
A-0.5HNT/BFRP	100	Liquid	0.5	Amorphous
A-1HNT/GFRP	100	Liquid	1	Amorphous
A-1HNT/BFRP	100	Liquid	1	Amorphous
A-3HNT/GFRP	100	Liquid	3	Amorphous
A-3HNT/BFRP	100	Liquid	3	Amorphous
A-5HNT/GFRP	100	Liquid	5	Amorphous
A-5HNT/BFRP	100	Liquid	5	Amorphous

3.2 Experimental procedure

3.2.1 Surface modification by thermal treatment

Heat treatment was performed for the surface modification of HNT. Through the heat treatment at high temperature, the water layer remaining inside the HNT structure according to the chemical composition was removed. The annealing process was carried out at (700 and 1,000) °C in the electric furnace, and maintained under the isothermal condition for 4 h. The electric furnace was PyroTech's PT-16EF030 instrument and has a maximum temperature range of 1,500 °C (see Fig. 10 (a)). Neat HNT was placed in an alumina crucible, and annealed in an electric furnace container (see Fig. 10 (b)). For uniform heat treatment, the temperature difference between the inside and the outside of the alumina crucible was checked in advance, and then the isothermal holding time and the amount of heat-treated sample were set.



(a) Electric furnace



(b) Heat treated HNTs

Fig. 10 Preparation of nanoparticle heat treatment

In particular, after the heat treatment, the HNT was sealed in a vacuum, in order to prevent prolonged exposure to moisture in the atmosphere. This was to prevent the hydrolyzed HNT from recombining with moisture. Since the processed HNT is mixed with the polymer, the effect of moisture should be minimized.


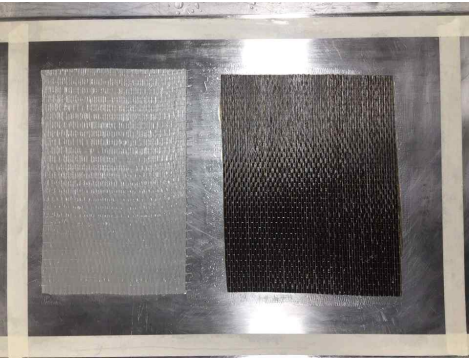

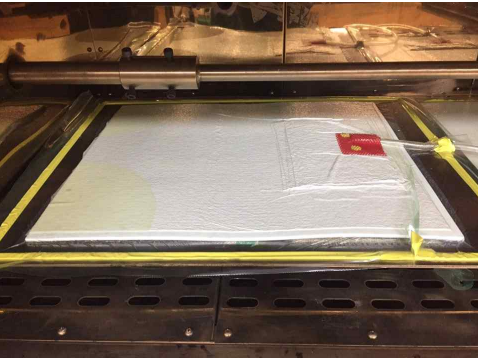
3.2.2 Nano-FRP manufacturing process

HNT-reinforced FRP nanocomposites were fabricated through a semi-autoclave process. The semi-autoclave is vacuum-bag molding after laminating wet prepreg made by a Hand lay-up method. FRP samples prepared by this method have many advantages, such as a high resin impregnation rate, uniform fiber-resin volume ratio, and uniform surface. Table 3 shows that the process is divided into 6 stages:

Step 1. Ultrasonication. HNT was uniformly dispersed in EP using an ultrasonic processor. The ultrasonic processor is a K-CORPORATION Sonicator with a capacity of 500 watt and 20 kHz. In the ultrasonic dispersion process, the operating time and the activation time of the ultrasonic wave are (1,680 and 1,200) s respectively, the amplitude is 50 % of the maximum input power, and the duration of one energy pulse is set to 5 s. Based on the above conditions, (0.5, 1, 3, and 5) wt.% of HNT were dispersed with EP.

Steps 2—6. Manufacture of HNT/GFRP and HNT/BFRP nanocomposites. Flat plate molds were prepared for HNT-reinforced GFRP and BFRP, and SAFELEASE #30 from AIRTECH was used for mold release. The wet-prepregs were laminated one-by-one, to form laminate composites. Then, the residual resin was removed by vacuum-bag molding, and the surface was flattened. After being fully vacuumed, high-temperature curing was carried out at 80 °C for 4 h.

Table 3 Semi-autoclave process for HNT/EP nanocomposites

	
<p>Step 1 Ultrasonication</p>	<p>Step 2 Mold release treatment</p>
	
<p>Step 3 Wet-prepreg production</p>	<p>Step 4 Vacuum-bag molding</p>
	
<p>Step 5 High temperature cure (at 80°C for 4 h)</p>	<p>Step 6 Vacuum-dry oven (temperature-time)</p>

3.3 Evaluation and analysis

3.3.1 Structural property

In this study, it was necessary to clarify the crystal structure of HNT in the analysis of interfacial bonding and dispersibility between EP and HNT. In order to establish the crystallinity of HNTs annealed at (700 and 1,000) °C, the structure of HNT was observed from a microscopic point of view using Transmission Electron Microscopy (TEM), and the relationship between the surface and coherency of HNT was investigated.

The effect of HNT on the molecular structure of EP was analyzed by Fourier-transform infrared spectroscopy (FTIR) test (see Fig. 11). The FTIR equipment was an iS50 FT-IR from Thermo Scientific Solutions LLC. The important physicochemical characteristics of EP were confirmed (Seo, et al., 2015).



Fig. 11 FTIR analysis equipments

FTIR is a method of quantitatively and qualitatively analyzing a substance by irradiating the molecule of the compound by Infrared. When a molecule is irradiated with infrared rays, it absorbs and emits a wavelength of (2.5–25) μm = (4,000–400) cm^{-1} of intrinsic vibration energy region depending on the

bonding structure between atoms in the molecule, and this change is measured. This is based on two theories, the first being that the molecules in the compound have a unique wavelength of the vibrational energy domain, depending on the type of functional group, such as —OH, C=O, COOH, N—H, C=C, which is directly involved in the reaction. The second is that the amount of absorbed wavelength is proportional to the concentration.

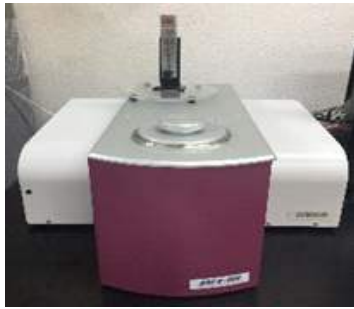
3.3.2 Thermal property

Differential Scanning Calorimetry (DSC) test was performed to analyze the thermal properties and structure of the EP/HNT colloidal solution. The DSC equipment was a DSC N-650 from SINCO Co., Ltd. (see Fig. 12).

The heating rate was divided into (10 and 20) °C/min, and the enthalpy change, and the maximum exotherm temperature according to the heating rate were observed. The degree of cure, rate of cure, and heat flow of HNT/EP colloidal solution according to crystallinity and addition amount of HNT were compared and analyzed. At this time, EP was mixed with a curing agent at 100:30 vol/vol, and it was possible to measure the curing temperature and the melting point. The samples used were HNT/EP colloidal solution, which was in a liquid state before curing. About (5–7) mg was added to the aluminum hermetic pan and sealed with aluminum lid. This is because the polymer is cured according to the temperature rise at the time of the DSC, and the proper amount of the sample is checked in advance, in order to prevent the polymer from overflowing out of the container, due to volume expansion.

The DSC device measures the heat flux (dQ/dt) as a function of the sample temperature, while heating the sample and reference materials according to the set temperature conditions (Chen, et al., 2018). A qualitative analysis of the sample is possible from the position, shape, and number of peaks in the

DSC curve. Since the width of the peak is related to the change of enthalpy when the sample is denatured, it enables quantitatively calculation of the parameters of the substance causing the reaction, or the heat of the sample in the sample.



(a) Differential scanning calorimetry (DSC) device



(b) Aluminum lid, hermetic pan, tools

Fig. 12 DSC analysis equipments

Equation (1) shows the basic theory of measuring the degree of cure, and the rate of cure is calculated by differentiating the degree of cure with respect to time.

$$\% \text{ cure} = \frac{dH(\text{uncure}) - dH(\text{cured})}{dH(\text{uncure})} \times 100 \quad (1)$$

In particular, the curing reaction of epoxy is an exothermic reaction, in which an epoxy end functional group reacts with a curing agent (hardener) to form a crosslinked structure to release energy. Therefore, assuming that the calorific value generated during the reaction is proportional to the consumption of the functional group, the conversion can be expressed as in Eq. (2), and the total calorific value measured at the temperature elevation condition is used (Kwon, et al., 2018).

$$\alpha = \frac{\Delta H_t}{\Delta H} \quad (2)$$

where, α is the conversion, ΔH_t is the cumulative calorific value from (0 to t), and ΔH is the total calorific value when the conversion is 1.

3.3.3 Environmental degradation property

In this study, the state of dispersion of HNT was predicted according to the number of fiber layers of laminate composites by using the excellent water resistance of HNT as a measure to determine the dispersibility of HNT. The absorption test equipment was a VB-55G from Lab. Companion (see Fig. 13 (a)). The experimental conditions of moisture absorption properties were determined by immersing HNT/GFRP and HNT/BFRP in 70 °C (=158 °F) distilled water for up to 336 h (14 days), according to the Standard Test Method for Moisture Absorption Properties and Equilibrium Conditioning of Polymer Matrix Composite materials (American Society for Testing and Materials, ASTM D5229). Fig. 13 (a) (right side) shows that the laminate composites were divided into (A–H) columns, the average value of the moisture absorption rate was calculated by processing four samples corresponding to each column, and the change of the moisture absorption rate was observed. The average moisture content was measured by Eq. (3):

$$M(\%) = \frac{W_i - W_o}{W_o} \times 100 \quad (3)$$

where M is the average moisture content, W_i is the current specimen mass (g), and W_o is the oven-dry specimen mass (g). The number of fiber layers was (1, 2, 4, 6, and 12) plies, respectively, and the effect of HNT on interfacial bonding with polymer and fiber was investigated.

Ultimately, this study was carried out in order to obtain the optimal dispersion process technology of HNT in laminate composites, by confirming the secondary aggregation phenomenon in the curing process due to the structural, physical and chemical characteristics of HNT. In addition, Fig. 13

(b) shows the distillation unit used to conduct long-term moisture absorption tests and to replenish water evaporated at high temperatures. Fig. 13 (c) shows the precision balance, which can be measured up to the third decimal place.



(a) Constant-temperature water bath and samples for water absorption test



(b) Distilled water output



(c) Precision balance

Fig. 13 Equipments for moisture absorption tests

3.3.4 Mechanical property

The evaluation was carried out according to the Standard Test Method for Open-Hole Tensile Strength of Polymer Matrix Composite Laminates (ASTM D5766) for mechanical properties test and analysis (see Fig. 14 (d)). The tensile strength of each of the C-HNT/GFRP, C-HNT/BFRP, A-HNT/GFRP, and A-HNT/BFRP specimens prepared by varying the amount of HNT was

measured by immersing them in water at (0 (dry sample), 60, 180, and 336) h. The effect of HNT crystallinity on the mechanical tensile strength of GFRP and BFRP nanocomposite laminates was investigated by measuring the change in moisture absorption rate. Fig. 13 shows the test equipment, which was a KDMT-136 UNIVERSAL TESTING MACHINE (see Fig. 14 (a)) and holes were machined into the flat typed nanocomposite laminates (see Fig. 14 (b), (c)).

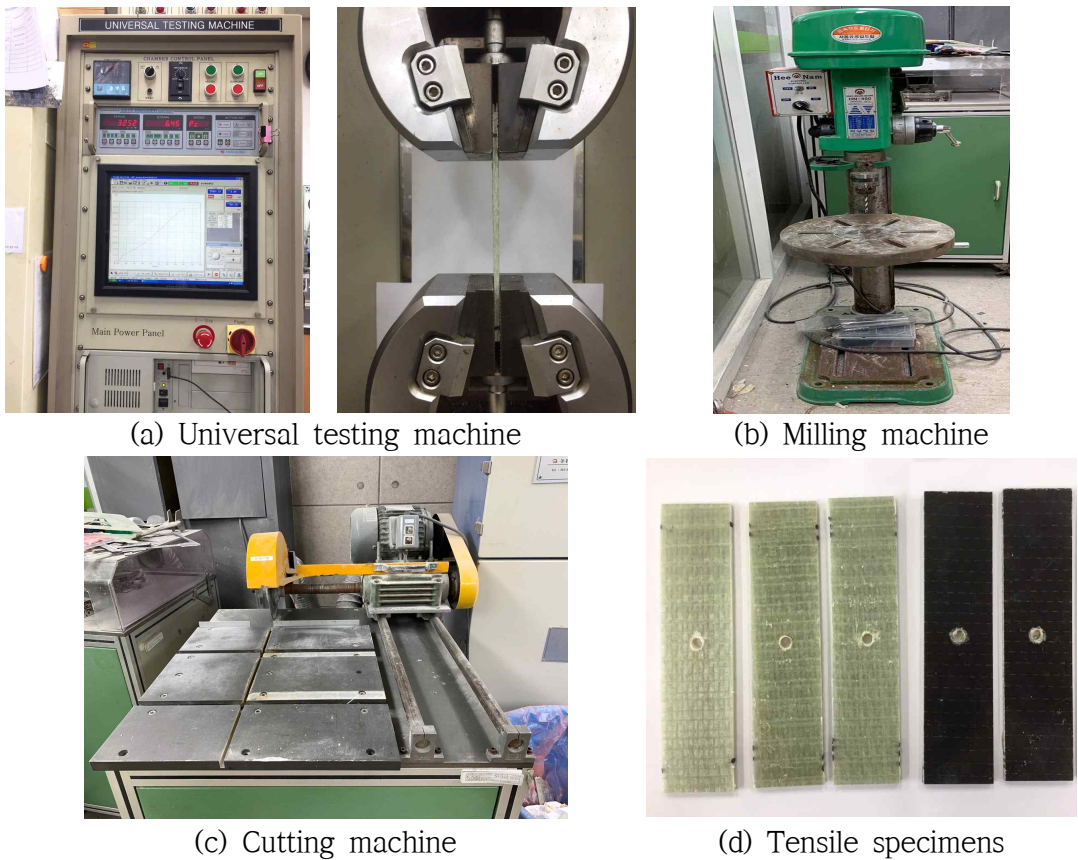
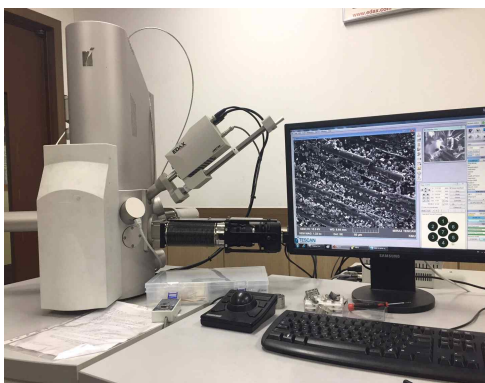


Fig. 14 Preparation for mechanical properties test

3.3.5 Microscopic observation

Scanning electron microscopy (SEM) analysis was performed to microscopically analyze the degradation phenomena through surface

observation of the HNT/EP nanocomposites exposed directly to moisture. The SEM used is a device of TESCAN Corporation (see Fig. 15 (a)). Composites are nonconductive samples. This causes a charge-up phenomenon, in which electrons accumulate in the sample, or on the surface of the sample. Therefore, to prevent this, Ion sputtering method was applied to provide a gold (Au) or platinum (Pt) coating at 15 mA for 120 s, and the surface was observed. The Scatter coater was a device of Quorum Technologies Ltd. (see Fig. 15 (b)). The prepared samples were analyzed for the moisture penetration mechanism of GF, BF, EP, and HNT in each case, by comparing the surface singularities with time, before and after water immersion.



(a)



(b)

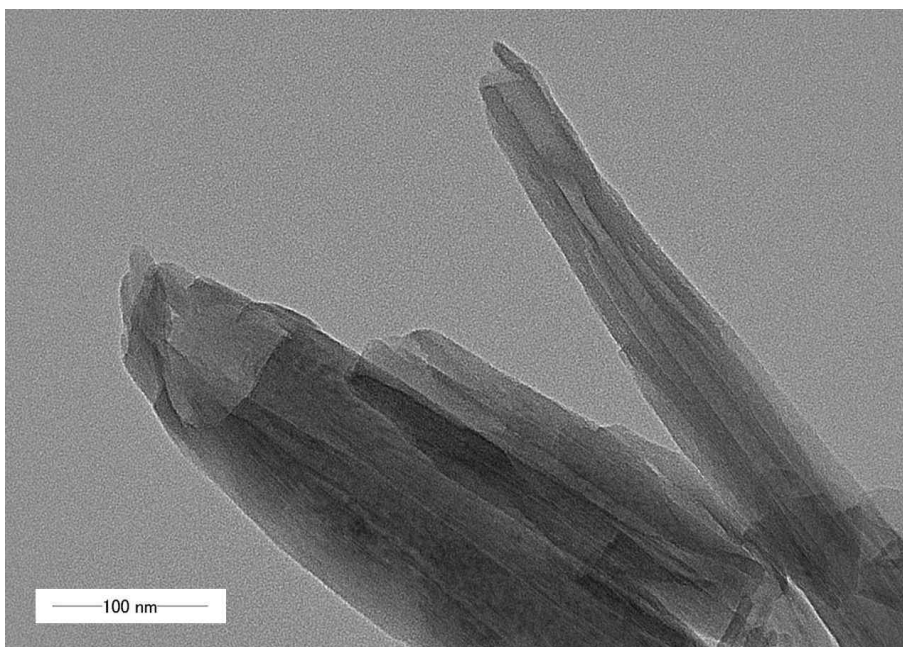
Fig. 15 Microscopic observation equipments; (a) Scanning electron microscopy and (b) Sputter coater

4. Results and discussion

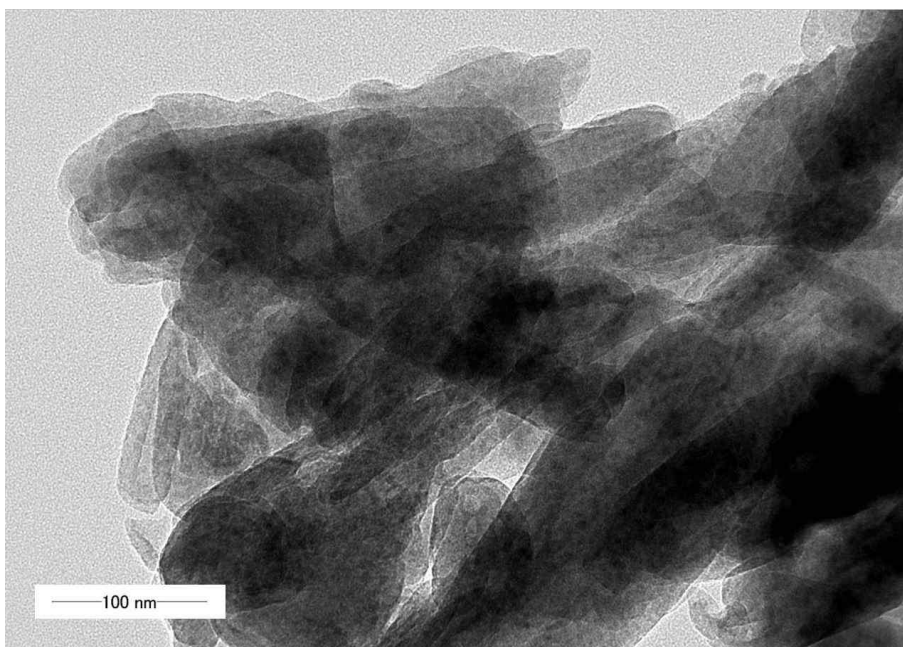
4.1 Morphology effect

In order to distinguish the crystallinity of HNT, C-HNT and A-HNT were prepared by heat treatment of existing Hydro-HNT at (700 and 1,000) °C, respectively. Generally, HNTs are classified into Hydro-HNT, Dehydrated HNT (Crystalline) and Meta-HNT (Amorphous). As mentioned in the introduction, Hydro-HNT does not have a constant structure at room temperature (RT), and is sensitive to relative humidity and temperature. Therefore, in this study, C-HNT and A-HNT were distinguished through the heat treatment process so that HNT had a uniform structure and constant physical property. The structural changes of the heat-treated HNT were analyzed through TEM and FTIR, to ensure the reliability of the heat treatment process.

First, Fig. 16 shows the results of the TEM observation of C-HNT and A-HNT. HNTs generally formed agglomerates in powder state, regardless of crystallinity (Kim, et al., 2017). In the case of A-HNT (see Fig. 16 (b)), there was almost no residual hollow tubular morphology. Also, the shape of the surface was uneven, and HNT shrinking was observed. In addition, the balance of HNT particle bonding force was broken, and the particles showed a tendency to clump together with each other. This is due to the oxidative dehydrogenation after the formation of amorphous SiO_2 and $\gamma\text{-Al}_2\text{O}_3$, which fundamentally changes the clay form of HNT (Samir, et al., 2012; Kim, Choi & Park, 2019). According to Park, (2016a, b), the dehydroxylation reaction occurs while the physically bound water layer is removed, and structural failure occurs in the inner part of the HNT. As a result, HNT suffers structural rearrangement. In other words, HNTs annealed at temperatures above 1,000 °C result in chemical changes, which are due to structural change.

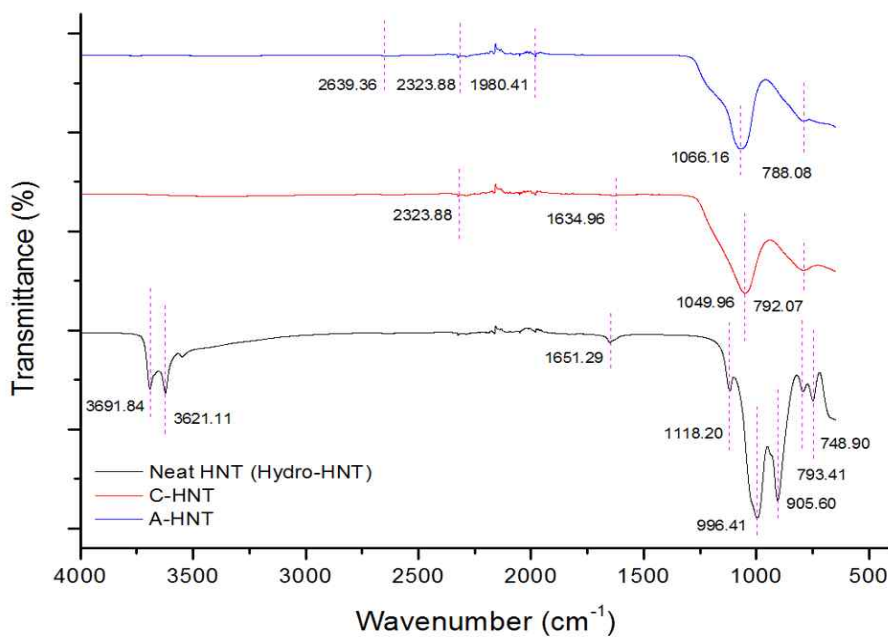


(a) C-HNT

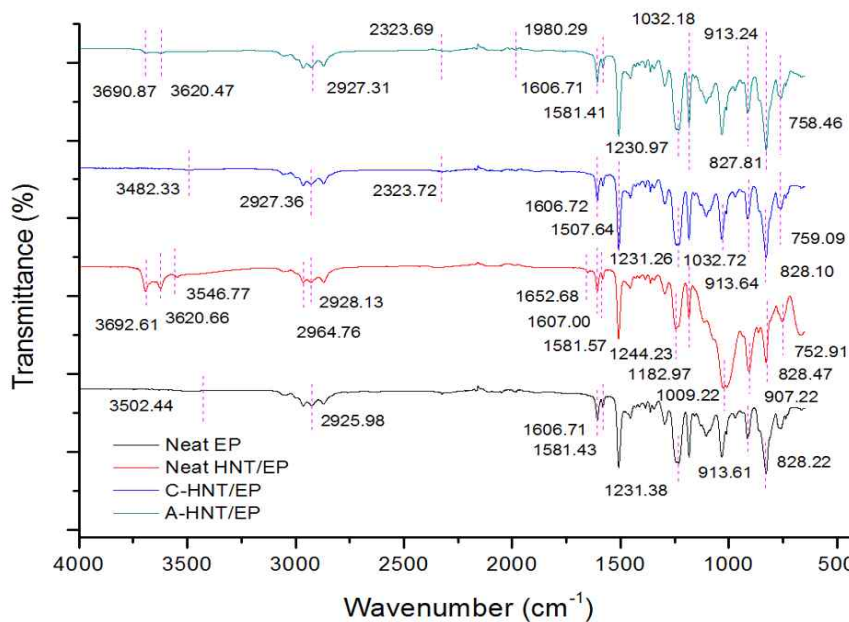


(b) A-HNT

Fig. 16 Observation of crystallinity of HNT by Transmission Electron Microscopy (TEM)



(a)



(b)

Fig. 17 FTIR spectra of (a) HNT structures according to heat treatment and (b) HNT/EP colloidal solution structure

FTIR analysis was carried out to investigate the effect of heat treatment on the structural bonding type of HNT. Fig. 17 shows the structural change of HNT by annealing and bonding type of EP and HNT colloidal solution that were observed. In Fig. 17 (a), (3,700–3,600) cm^{-1} peaks were disappeared in C-HNT and A-HNT based on the Neat HNT, and a new band at (2,600–2,300) cm^{-1} was generated. It was also found that the band was expanded at (1,100–1,000) cm^{-1} . In the Neat HNT, (3,691.84 and 3,621.11) cm^{-1} are stretching vibrations of the hydroxyl groups, which means that the HNT was dehydroxylated by heat treatment. In particular, 3,691.84 cm^{-1} is assigned to the inner hydroxyl stretching group, and 3,621.11 cm^{-1} represents the inner hydroxyl stretching vibration band (Samir, et al., 2012; Beata, et al., 2015). In other words, the initial Neat HNT before heat treatment forms two Al_2OH stretching bands, one in which two Al atoms are bonded to one OH. The peaks of 1,651.29 cm^{-1} in Neat HNT and 1,634.96 cm^{-1} in C-HNT mean that it is strongly bonded with the vibrations of adsorbed water, but the bonding strength of C-HNT becomes considerably weakened.

In general, it had a structure such as Si—O—Si, Al—OH, OH vibrations at (1,000–400) cm^{-1} , and OH translational vibration was generated in OH units of HNT near 793.41 cm^{-1} of the Neat HNT, and 792.07 cm^{-1} of C-HNT. The 2,323.88 cm^{-1} bands of C-HNT exhibit a quartz structure, while the A-HNTs exhibit a calcite structure of 2,639.36 cm^{-1} and a quartz structure of 2323.88 cm^{-1} , resulting in an amorphous structure. Also, 1,066.16 cm^{-1} extended from 1,049.96 cm^{-1} of C-HNT showed amorphization of the structure (Samir, et al., 2012; Beata, et al., 2015; Sohlberg, et al., 1999).

However, according to Sohlberg, et al. (1999) and Samir, et al. (2012), three or more bands should be observed in the (3,900–3,600) cm^{-1} region of A-HNT, which corresponds to a hydrogen bond between the hydroxyl groups used in γ -alumina; but this was not observed in the test analysis results. This

suggests that the heat treatment for a long time does not form an activating group of A-HNT in a specific region. As a result, it is believed that the crystallinity of C-HNT and A-HNT will contribute to the analysis of the effect of functional groups on the formation of functional groups such as EP.

Fig. 17 (b) shows the bonding type when various HNTs were added to the typical Bisphenol-A type Neat EP. First, the O—H peak was observed at $3,502.44\text{ cm}^{-1}$, which was weak, but was of broad area. C—H stretching structure was found at $2,925.98\text{ cm}^{-1}$ wavelength region, and C—C bond of benzene ring was confirmed at the $(1,606.71\text{ and }1581.43)\text{ cm}^{-1}$ regions. The C—H of the benzene ring observed at $(1,231.38, \text{ and } 913.61)\text{ cm}^{-1}$ means the oxirane ring at the epoxy resin end, and the 828.22 cm^{-1} peak showed the =C—H structure (Seo, et al. 2015). In other words, Neat EP showed the physical/chemical properties of a typical EP (Seo, et al., 2015). When Neat HNT was dispersed in EP, the bands of $(3,692.61\text{ and }3,620.66)\text{ cm}^{-1}$ indicated the stretching vibrations of the hydroxyl groups, and the peak of $3,546.77\text{ cm}^{-1}$ was interlayer water due to the stretching vibration band of HNT. In the case of C-HNT, the stretching vibrations of hydroxyle groups disappeared, and $(3,690.87\text{ and }3,620.47)\text{ cm}^{-1}$ peaks were found in A-HNT/EP, which seems to be the hydrogen bond observed by A-HNT. That is, it is considered that a weak hydroxyl group is activated by the O—H functional group of the Neat EP (Seo, et al., 2015; Beata, et al., 2015).

In summary, the results of the FTIR test showed that EP and HNT have chemically similar components and bonding forms, and thus they mainly affect the strength of bonding force, due to changes in bonding types, such as single bonds and double bonds between atoms. EP and HNT partially form chemical bonds, but EP and HNT can form bonds in independent form. In other words, the FTIR results suggest that HNT can be structurally modified for uniform dispersion in polymers such as EP to improve bonding strength.

4.2 Thermal analysis

Table 4 shows the curing characteristics of HNT/EP nanocomposites that were analyzed by DSC. Dynamic DSC analysis was performed to analyze the effect of crystallinity, and ultimately, the addition amount of HNT on the EP curing system. The correlation of heat flow-time with the change of heating rate for each sample type was compared based on Temperature- T_p . The faster the heating rate of Neat EP, the higher the peak temperature, which is common to all C-HNT and A-HNT fillers. However, no significant trends were observed other than these. Except for C-5HNT/EP, T_p of Neat EP was high when the heating rate was 10 °C/min, but T_p was high by C-HNT and A-HNT at heating rate of 20 °C/min.

Overall, the starting point of the endothermic/exothermic reaction was measured to be at least 38% higher than the heating rate 10 °C/min at a heating rate of 20 °C/min. As a result of analyzing the heat of reaction according to the heating rate, the heat of reaction was increased as the heating rate increased. However, A-1HNT/EP and A-3HNT/EP showed the opposite tendency, and the difference of heat of reaction between A-0.5HNT/EP and A-5HNT/EP was insignificant.

It is considered that this is influenced by the particle dispersity of HNT. If the HNT is not uniformly dispersed in EP, it will delay the curing reaction; and the longer the exposure time to the activation curing temperature, the greater the heat of reaction. Therefore, A-HNT has a higher Van der Waals force than C-HNT, which causes clustering in the EP, which slows the curing reaction.

Table 4 Curing characteristics for HNT/EP nanocomposites system

Types	Heating rate (°C/min)	$\Delta H_{\text{reaction}}$ (J/g)	T _{onset} (°C)	T _p (°C)	T _{endset} (°C)	Types	Heating rate (°C/min)	$\Delta H_{\text{reaction}}$ (J/g)	T _{onset} (°C)	T _p (°C)	T _{endset} (°C)
Neat EP (Liquid)	10	69.95	52.48	122.27	181.17						
	20	233.35	81.54	132.71	209.81						
C-0.5HNT/EP (Liquid)	10	69.85	39.38	121.68	195.98	A-0.5HNT/EP (Liquid)	10	121.98	36.94	115.92	188.82
	20	168.30	92.99	138.37	190.22		20	125.26	96.49	137.53	185.05
C-1HNT/EP (Liquid)	10	69.85	39.38	121.68	195.98	A-1HNT/EP (Liquid)	10	497.78	55.01	112.93	203.57
	20	142.03	92.90	136.85	192.77		20	122.15	95.80	139.24	186.45
C-3HNT/EP (Liquid)	10	510.56	37.62	118.71	205.46	A-3HNT/EP (Liquid)	10	249.84	79.99	114.55	162
	20	798.41	85.25	138.86	204.47		20	155.59	93.19	137.42	184.74
C-5HNT/EP (Liquid)	10	54.63	49.80	122.65	181.21	A-5HNT/EP (Liquid)	10	82.90	37.22	121.30	192.15
	20	162.06	86.60	138.07	198.5		20	84.29	82.38	134.20	178.83

Fig. 18 shows the results of Neat EP's degree of cure and rate of cure with heating rate. The degree of cure was calculated by integrating the calorific value over time. In the degree of cure and rate of cure, α and the rate of cure tended to increase with increasing temperature. In the degree of cure, the curing reaction was slowed again, after reaching the maximum rate of cure. It was confirmed that this is an autocatalytic reaction of a typical amine-based curing agent of S-shaped curve (jeong, et al. 2018). Also, as the heating rate increased to 20 °C/min, the degree of cure at the same time was lower, and the degree of cure was higher at a higher temperature than the heating rate of 10 °C/min. The higher the heating rate, the higher the rate of cure. That is, in the case of Neat EP, the higher the heating rate, the higher the degree of cure at a higher temperature, and the rate of cure is promoted.

Fig. 19 shows a comparison of the degree of cure and rate of cure between C-0.5HNT/EP and A-0.5HNT/EP. In general, the same S-curve shape as Neat EP was maintained, but the total curing reaction time was relatively short in C-0.5HNT/EP. In particular at the heating rate of 20 °C/min, the rate of cure was accelerated, regardless of the crystallinity of HNT. C-0.5HNT/EP and A-0.5HNT/EP have similar shapes, but as the heating rate decreases, the maximum temperature of the degree of cure increases, and the rate of cure is drastically reduced by half in a level similar to that of the Neat EP. This is considered to require a sufficient time for curing. In other words, C-0.5HNT was dispersed in the EP, lowering the relative curing temperature, and instantaneously accelerating the curing reaction. However, it was found that A-0.5HNT had little influence on the chemical bond in EP, so that it could participate in the curing reaction in only a small amount. This is because HNT is difficult to disperse uniformly, due to the unevenness and unstable state in EP.

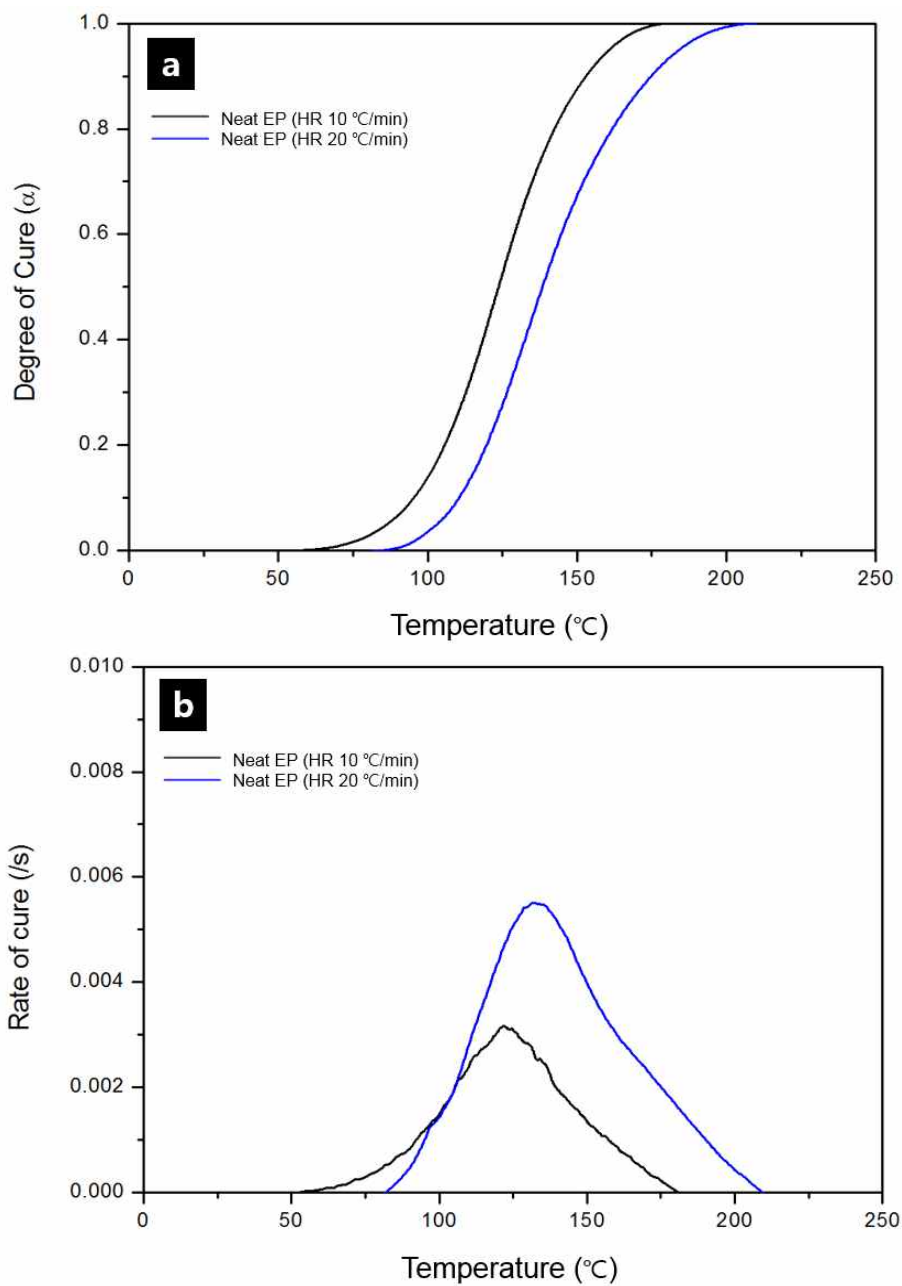


Fig. 18 Dynamic DSC analysis of Neat EP; (a) degree of cure and (b) rate of cure

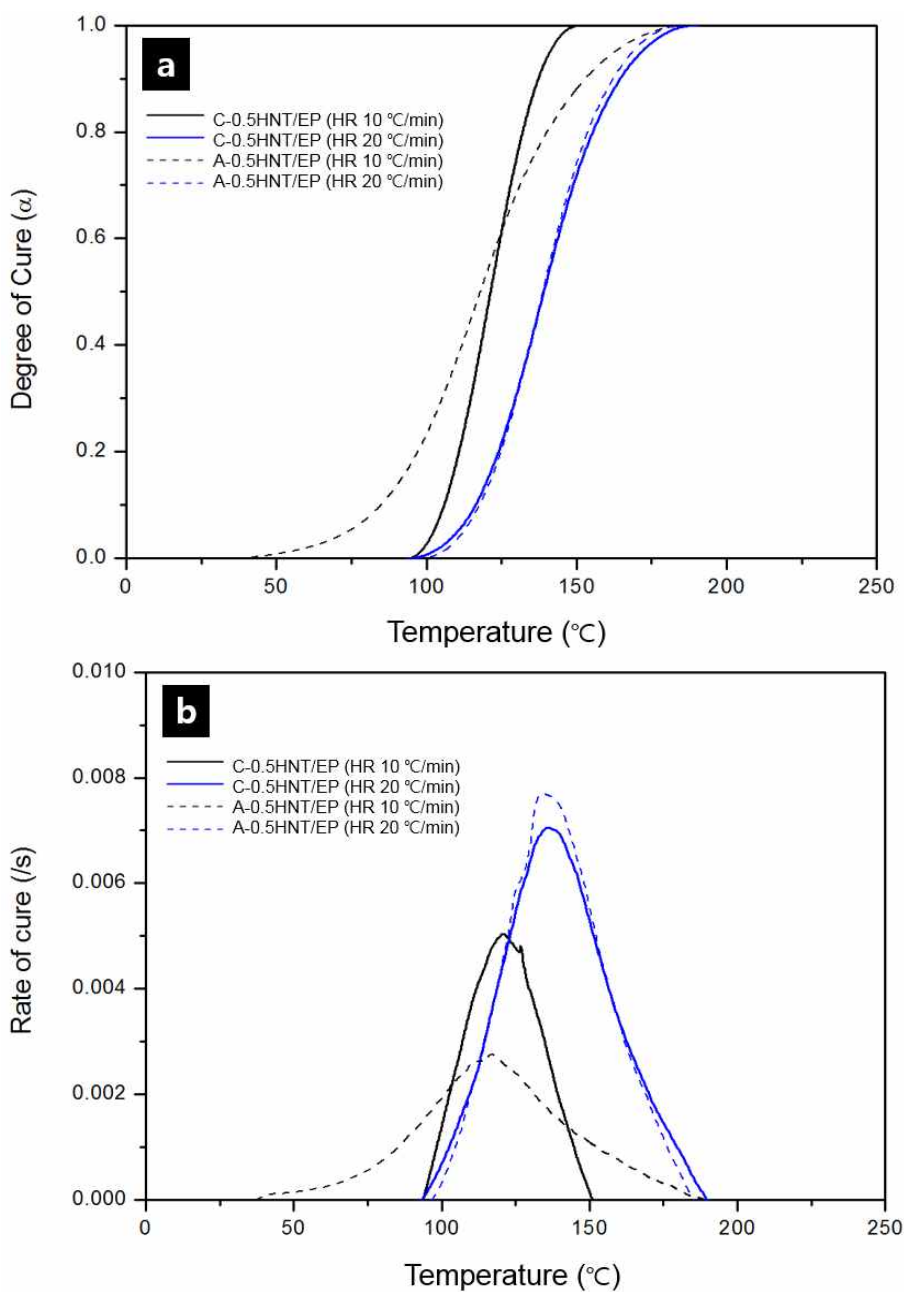


Fig. 19 Dynamic DSC analysis of 0.5HNT/EP according to crystallinity of HNT; (a) degree of cure and (b) rate of cure

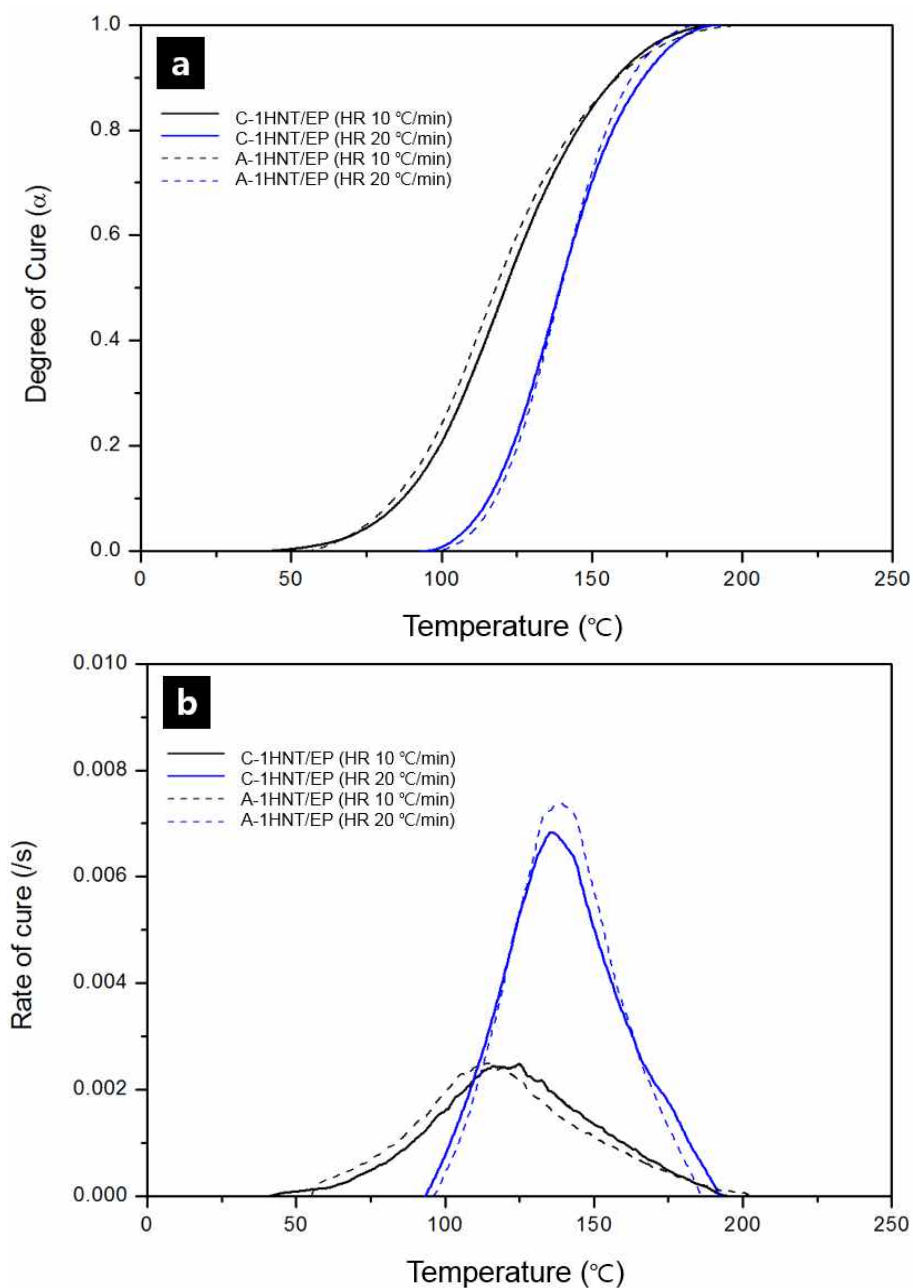


Fig. 20 Dynamic DSC analysis of 1HNT/EP according to crystallinity of HNT;
(a) degree of cure and (b) rate of cure

Fig. 20 shows the calculation of the degree of cure and rate of cure of C-1HNT/EP and A-1HNT/EP. The addition of 1 wt.% HNT showed a tendency to be independent of the crystallinity of HNT, and almost the same value was observed for the change of heating rate. In particular, the curing reaction was terminated at the same temperature regardless of the heating rate. At a heating rate of 20 °C/min, HNT lowered the maximum temperature of the degree of cure and promoted the rate of cure. However, at a heating rate of 10 °C/min, the fully cured temperature was higher than that of Neat EP, and the rate of cure decreased. Therefore based on the observed results, it is considered that sufficient time and temperature are required for curing.

Fig. 21 shows the degree of cure and rate of cure of C-3HNT/EP and A-3HNT/EP. Unlike the previous results, the A-3HNT had low fully cured temperature, shortened total curing reaction time, and accelerated rate of cure. However, the rate of cure was still lower than that of (0.5 and 1) wt.% of small HNTs. This suggests that HNT may partially contribute to accelerate curing, but it may also act as a factor to inhibit curing from a point where it exceeds a certain amount.

Fig. 22 shows the degree of cure and rate of cure between C-5HNT/EP and A-5HNT/EP. In 5 wt.% HNT, C-5HNT/EP showed the most similar tendency to Neat EP as the heating rate increased or decreased. At this time, the fully cured temperature was lowered. In the case of A-5HNT/EP, the fully cured temperature was relatively low at the heating rate of 20 °C/min, and the rate of cure was greatly accelerated, compared with C-5HNT/EP.

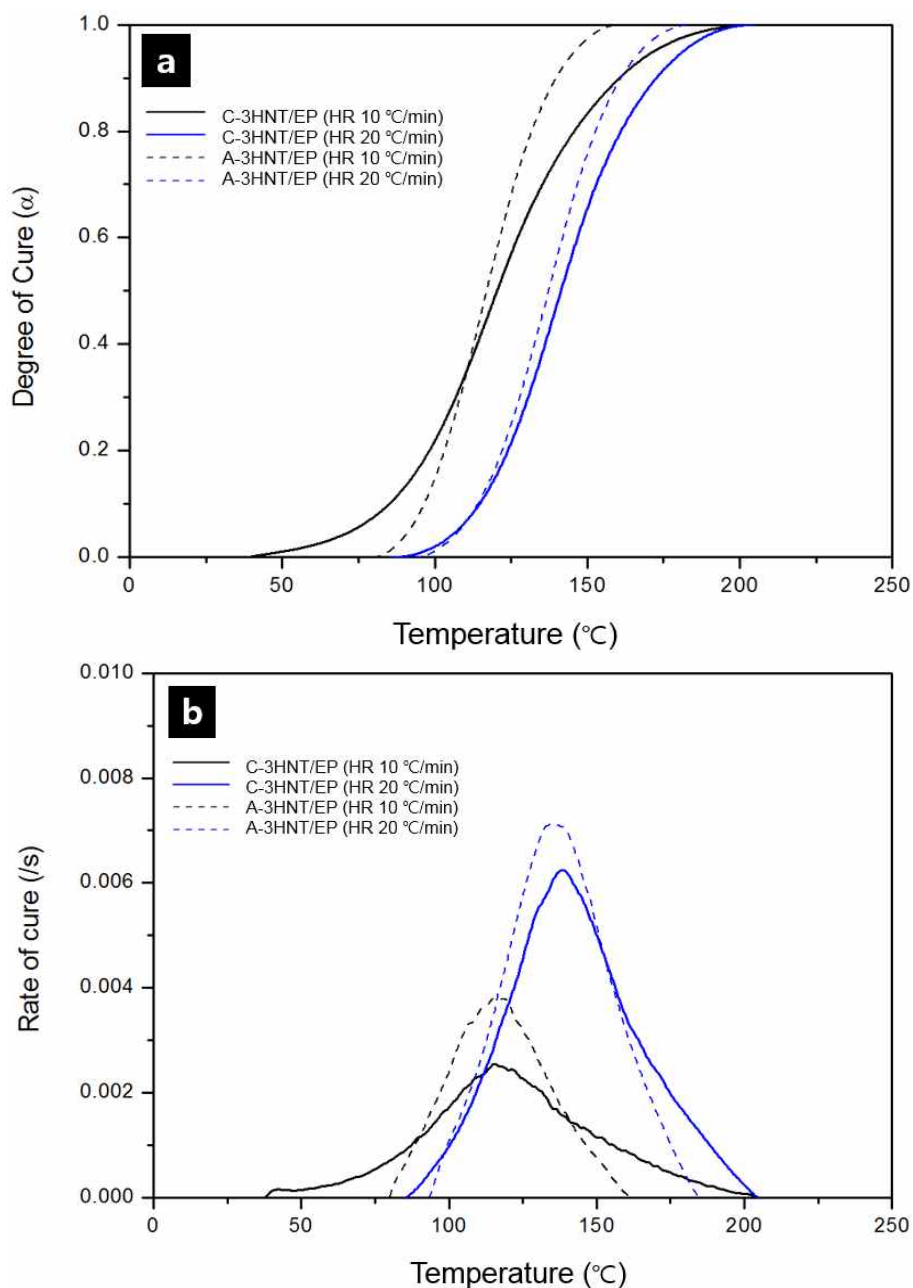


Fig. 21 Dynamic DSC analysis of 3HNT/EP according to crystallinity of HNT;
(a) degree of cure and (b) rate of cure

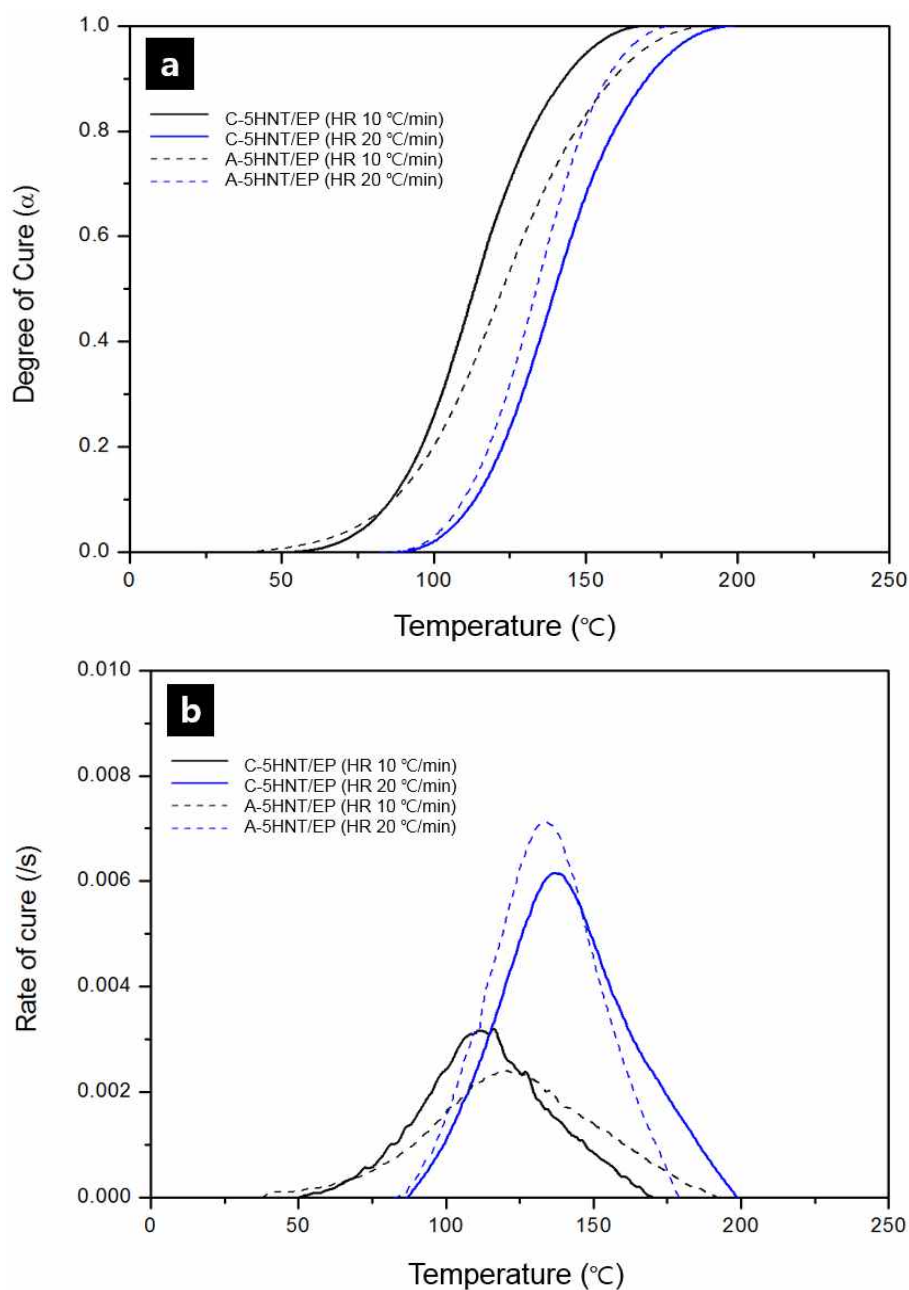


Fig. 22 Dynamic DSC analysis of 5HNT/EP according to crystallinity of HNT;
(a) degree of cure and (b) rate of cure

In summary, regardless of the crystallinity of the HNT structure, HNTs were involved in reducing the fully cured temperature or improving the rate of cure within a range similar to that of EP curing. Previous studies have reported that the incorporation of nanosilica-based particles into the EP has the effect of promoting the curing behavior, due to increased interfacial interaction between the nanoparticles and the matrix (Zhang, et al., 2002). In this context, a similar conclusion was drawn in the DSC analysis conducted in this study. In all cases, the rate of cure decreased rapidly, as the heating rate decreased. This is because sufficient time is required for curing. Also, the faster the heating rate, the higher the cure temperature and the fully cured temperature. In the case of 1 wt.% HNT, the degree of cure and rate of cure were almost similar, regardless of the heating rate. At the relative heating rate of 10 °C/min, the curing reaction time was long, and required high temperature. C-HNT maintained almost similar curing reaction conditions from more than 1 wt.%. A-HNT showed a stable curing reaction at a heating rate of 3 wt.%, and efficient curing conditions were obtained at the fully cured temperature, rate of cure, and total curing reaction time. However, it is considered that it is necessary to set finer dispersion conditions than C-HNT, because it is sensitive to dispersion with EP, depending on the amount of HNT added.

4.3 Moisture absorption behavior

In this study, moisture absorption tests were carried out to investigate the effect of the crystallinity of HNT on the state of dispersion of HNT/GFRP and HNT/BFRP. The composite laminates were divided into eight columns from (A—H) and their moisture absorption behaviors were analyzed (for each region) to evaluate the dispersion stability of HNT.

Fig. 23 shows the moisture absorption rate of each region exposed to distilled water at 70 °C for a maximum of 336 h and the number of fiber layers in them. Neat GFRP showed a rapid increase in the moisture uptake within 24 h and a gentle curve at around 48 h. At this time, the moisture absorption rate was about 1-2%. The edge A and H columns of neat GFRP-1 and neat GFRP-4 showed a large difference in hygroscopicity. Neat BFRP (Fig. 24) also showed similar tendency because of the edge loss of EP during vacuum forming.

Fig. 25 shows the moisture absorption rate of C-0.5HNT/GFRP as a function of the laminated fibers. Compared to neat GFRP, C-0.5HNT/GFRP showed a relatively low moisture absorption rate, suggesting that C-HNT prevented the degradation of EP. In the case of C-0.5HNT/GFRP-2 and C-0.5HNT/GFRP-4, the moisture absorption rate was relatively high in the C and D columns. The moisture absorption rate was high in the E, G, and H columns. We believe that HNT moved to the center part during the vacuum forming step in the direction of air discharge to form aggregated clusters, which contributed to the increase in the water absorption rate. These aggregated clusters also reduced the permeability of water into the fibers, resulting in the non-uniform dispersion of HNTs. Fig. 26 shows the hygroscopic results of C-0.5HNT/BFRP. It showed a trend similar to that shown by C-0.5HNT/GFRP. The moisture absorption rate was slightly higher but not significantly different.

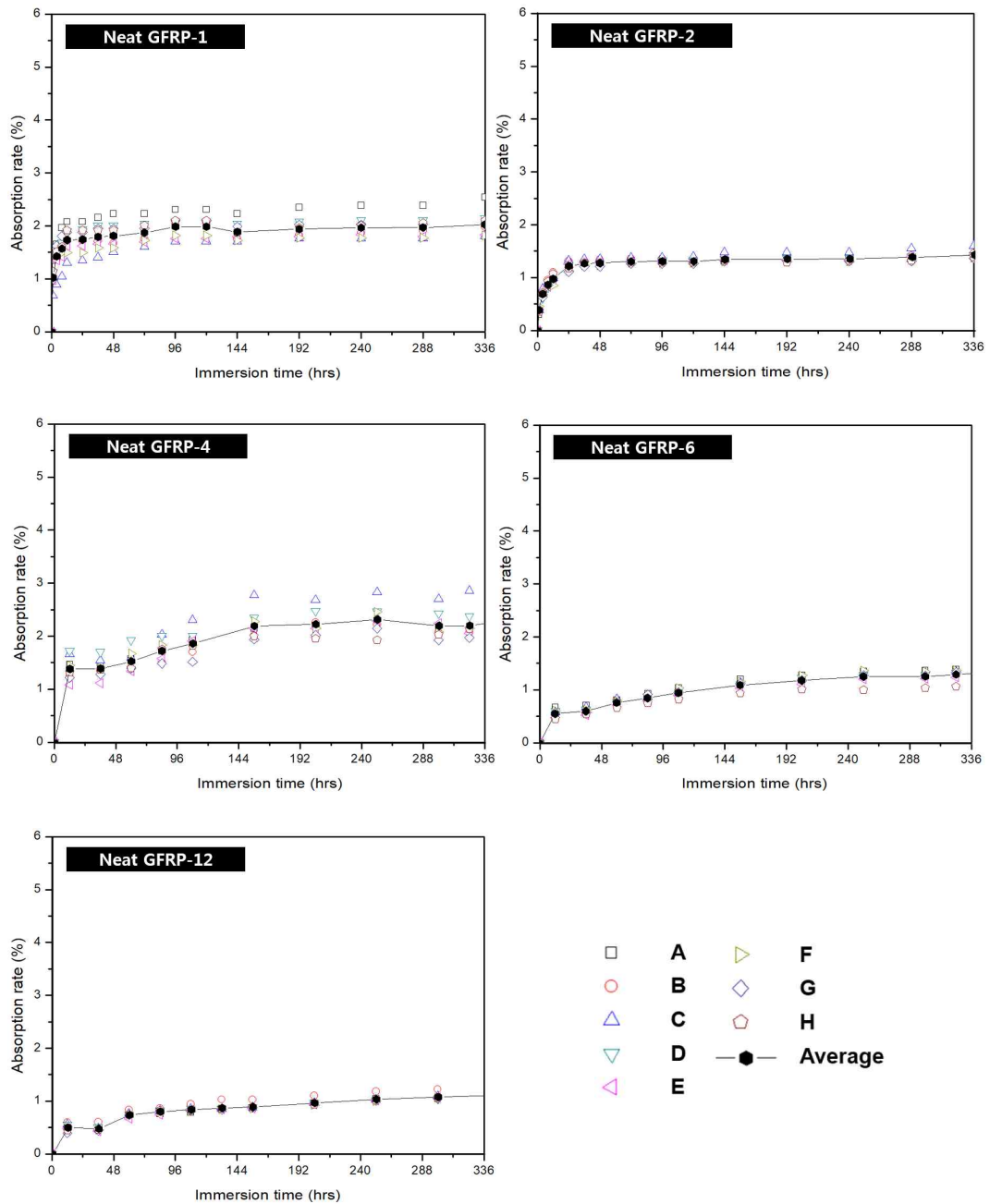


Fig. 23 Absorption rate of Neat GFRP immersed in distilled water at 70 °C up to 336 h (14 days) according to laminated fiber plies

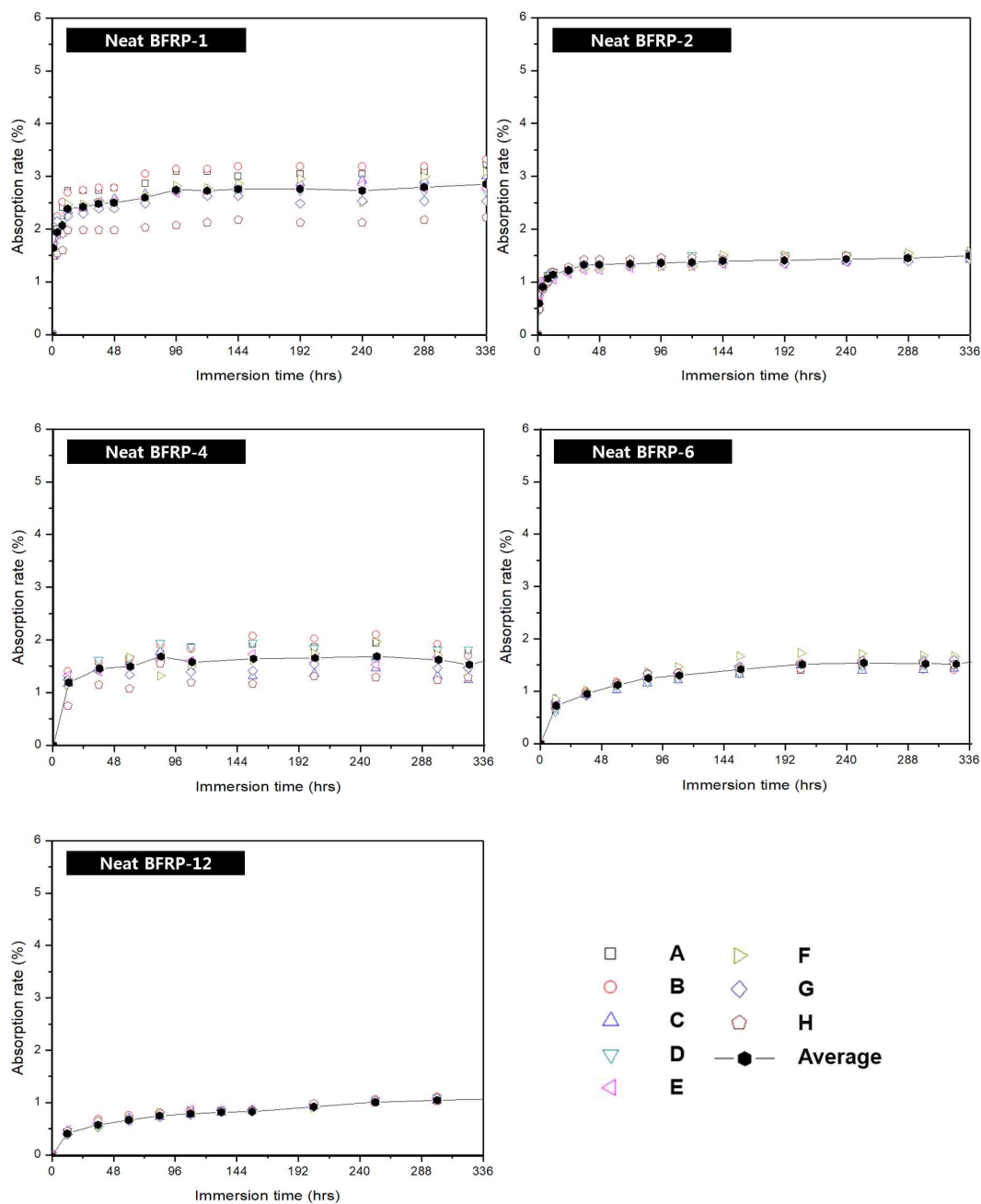


Fig. 24 Absorption rate of Neat BFRP immersed in distilled water at 70 °C up to 336 h (14 days) according to laminated fiber plies

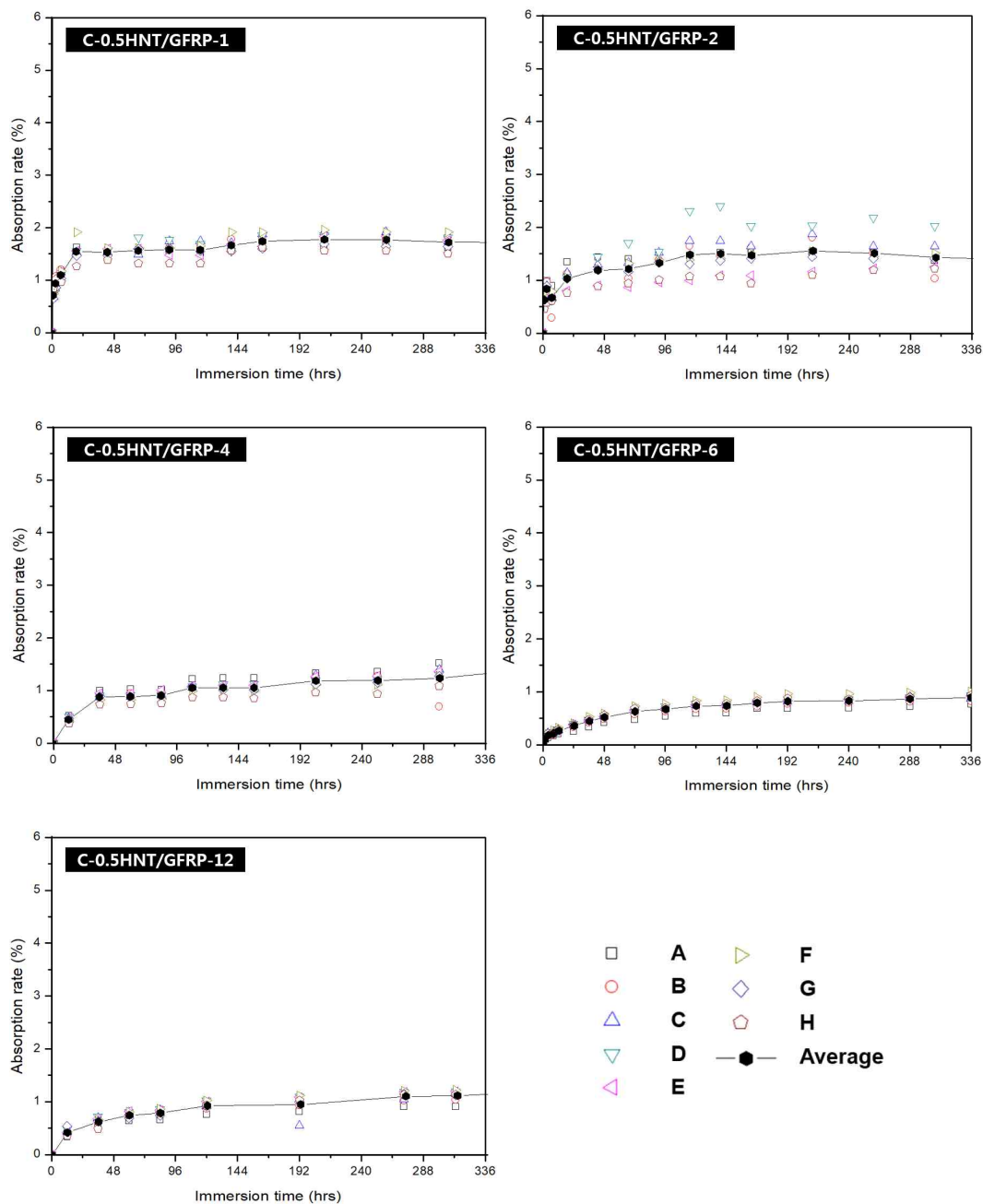


Fig. 25 Absorption rate of C-0.5HNT/GFRP immersed in distilled water at 70 °C up to 336 h (14 days) according to laminated fiber plies

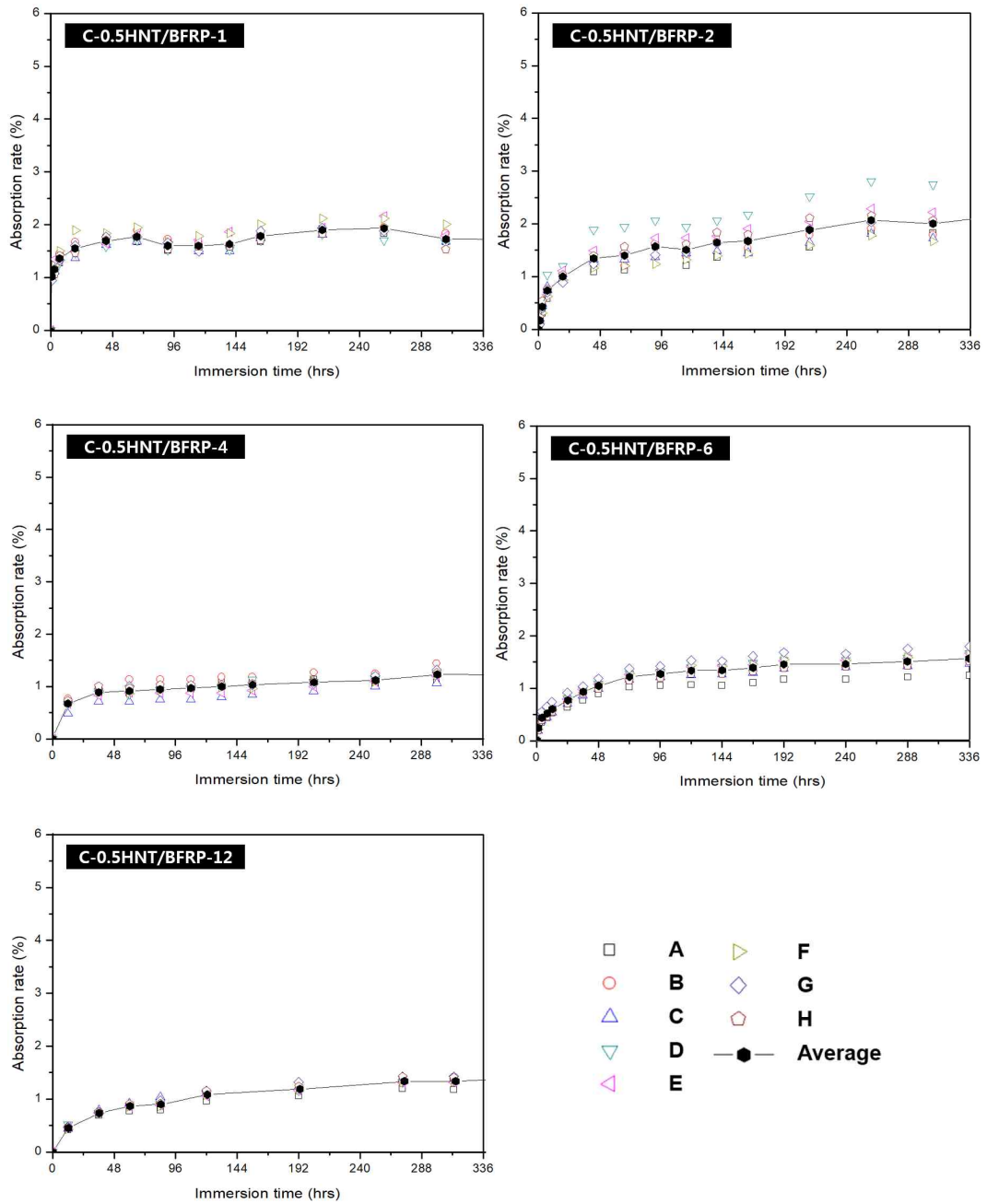


Fig. 26 Absorption rate of C-0.5HNT/BFRP immersed in distilled water at 70 °C up to 336 h (14 days) according to laminated fiber plies

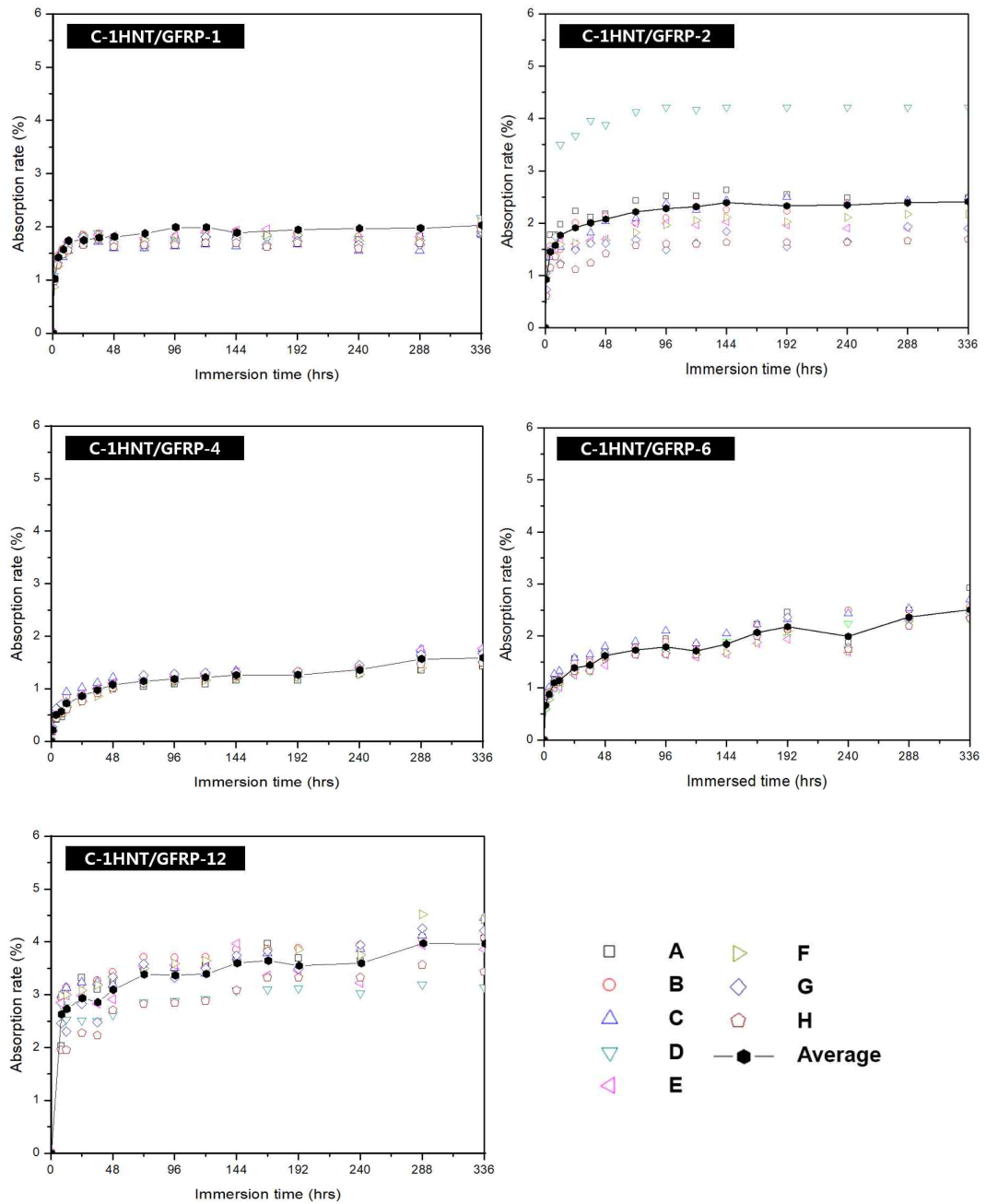


Fig. 27 Absorption rate of C-1HNT/GFRP immersed in distilled water at 70 °C up to 336 h (14 days) according to laminated fiber plies

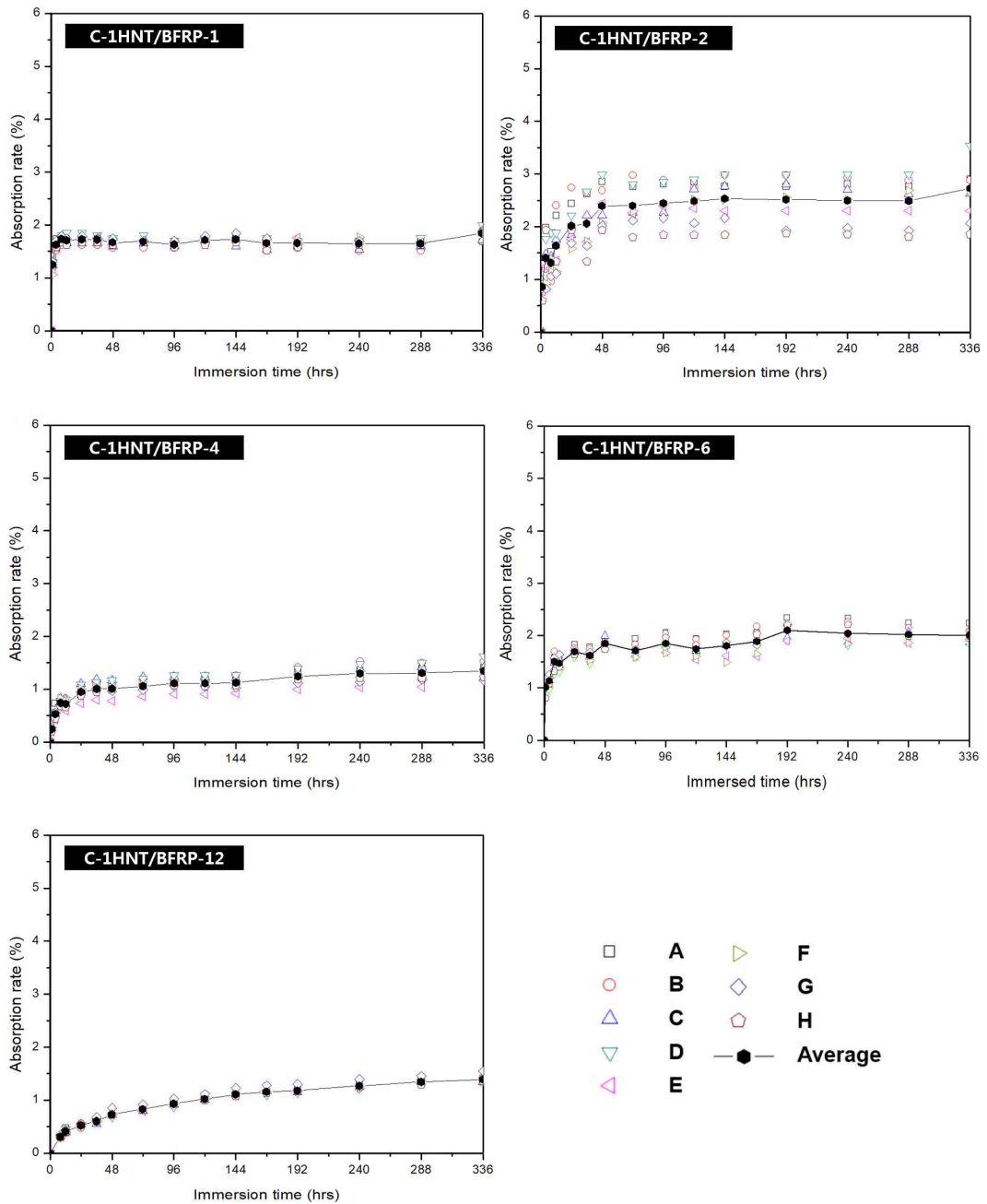


Fig. 28 Absorption rate of C-1HNT/BFRP immersed in distilled water at 70 °C up to 336 h (14 days) according to laminated fiber plies

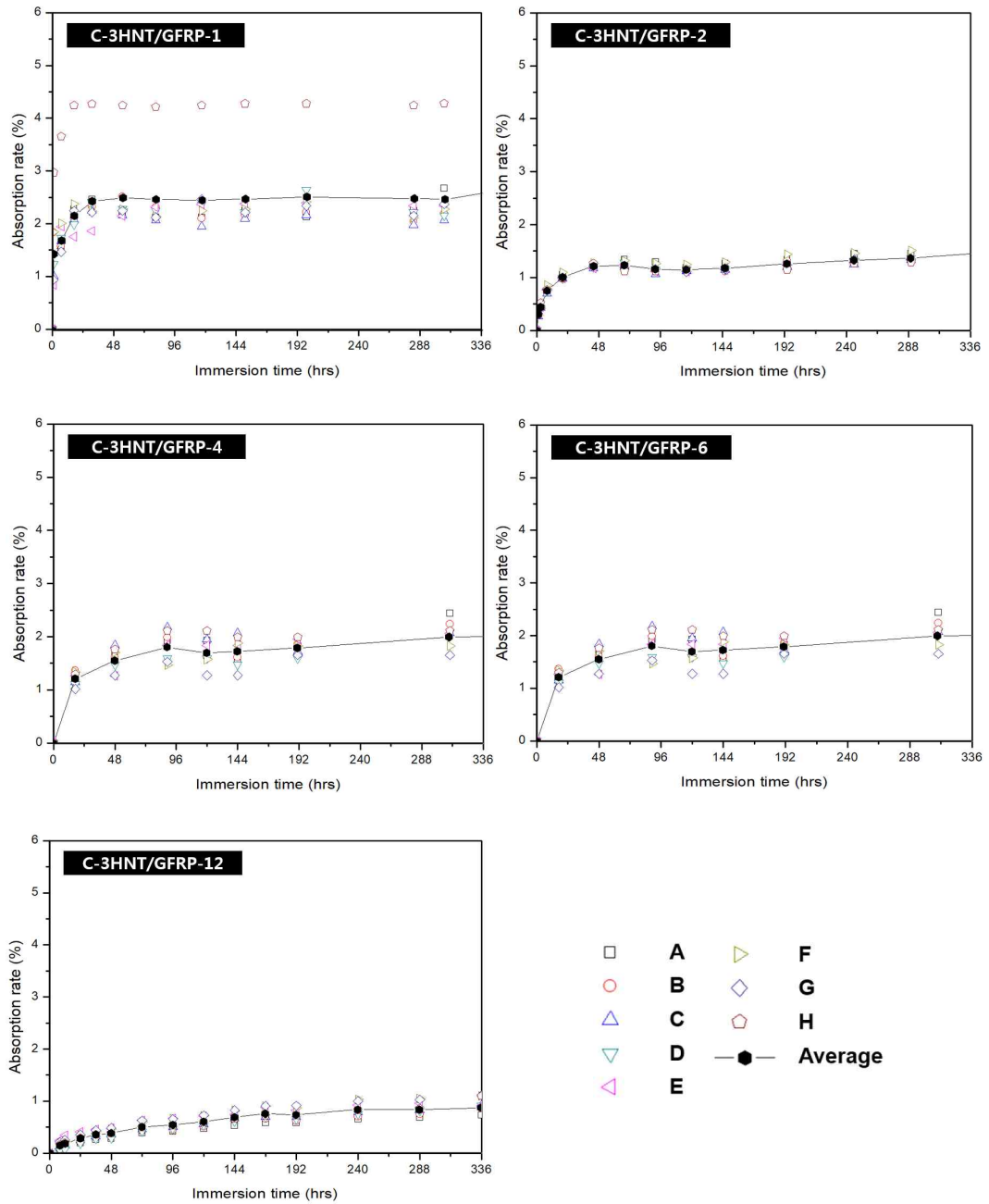


Fig. 29 Absorption rate of C-3HNT/GFRP immersed in distilled water at 70 °C up to 336 h (14 days) according to laminated fiber plies

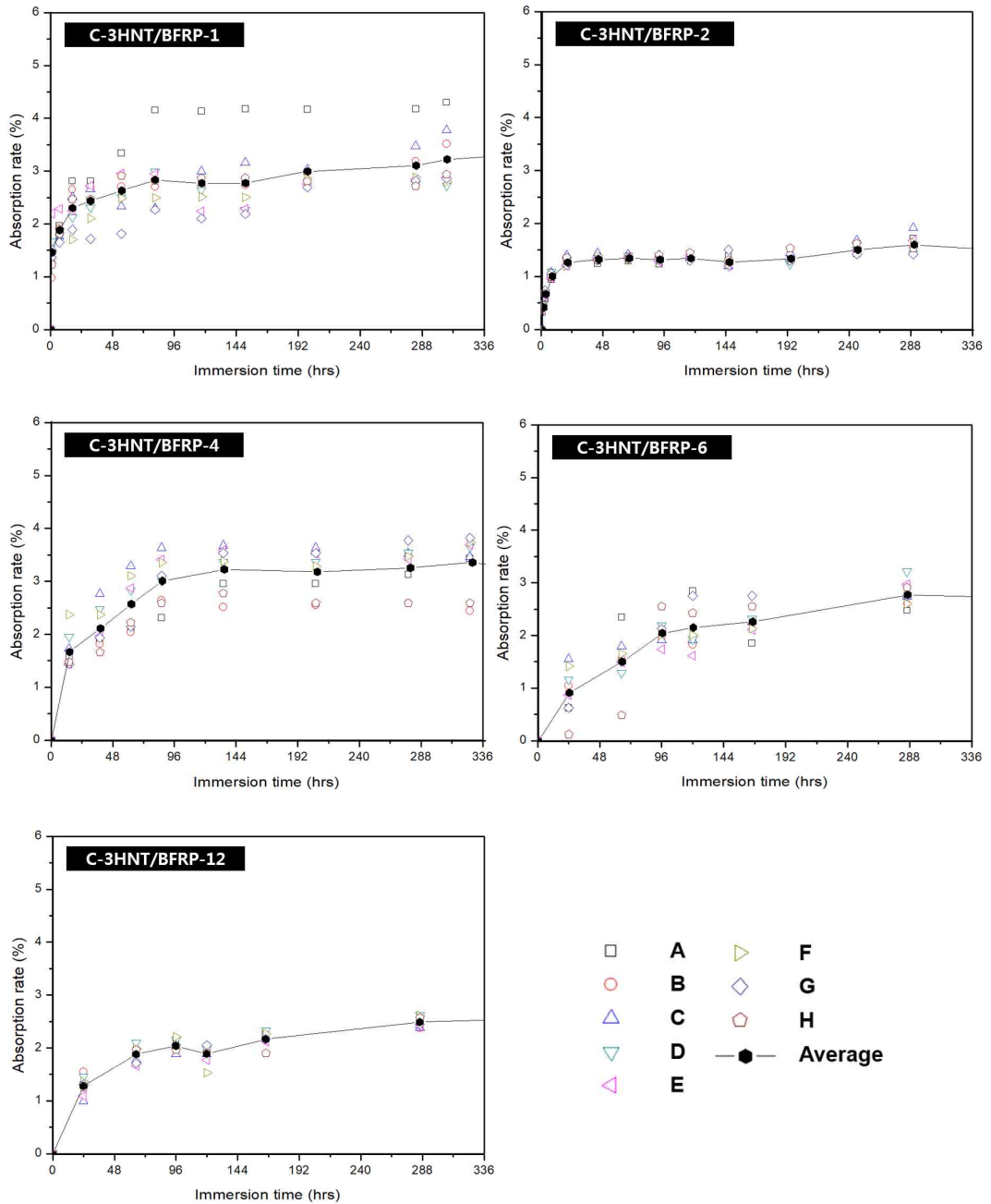


Fig. 30 Absorption rate of C-3HNT/BFRP immersed in distilled water at 70 °C up to 336 h (14 days) according to laminated fiber plies

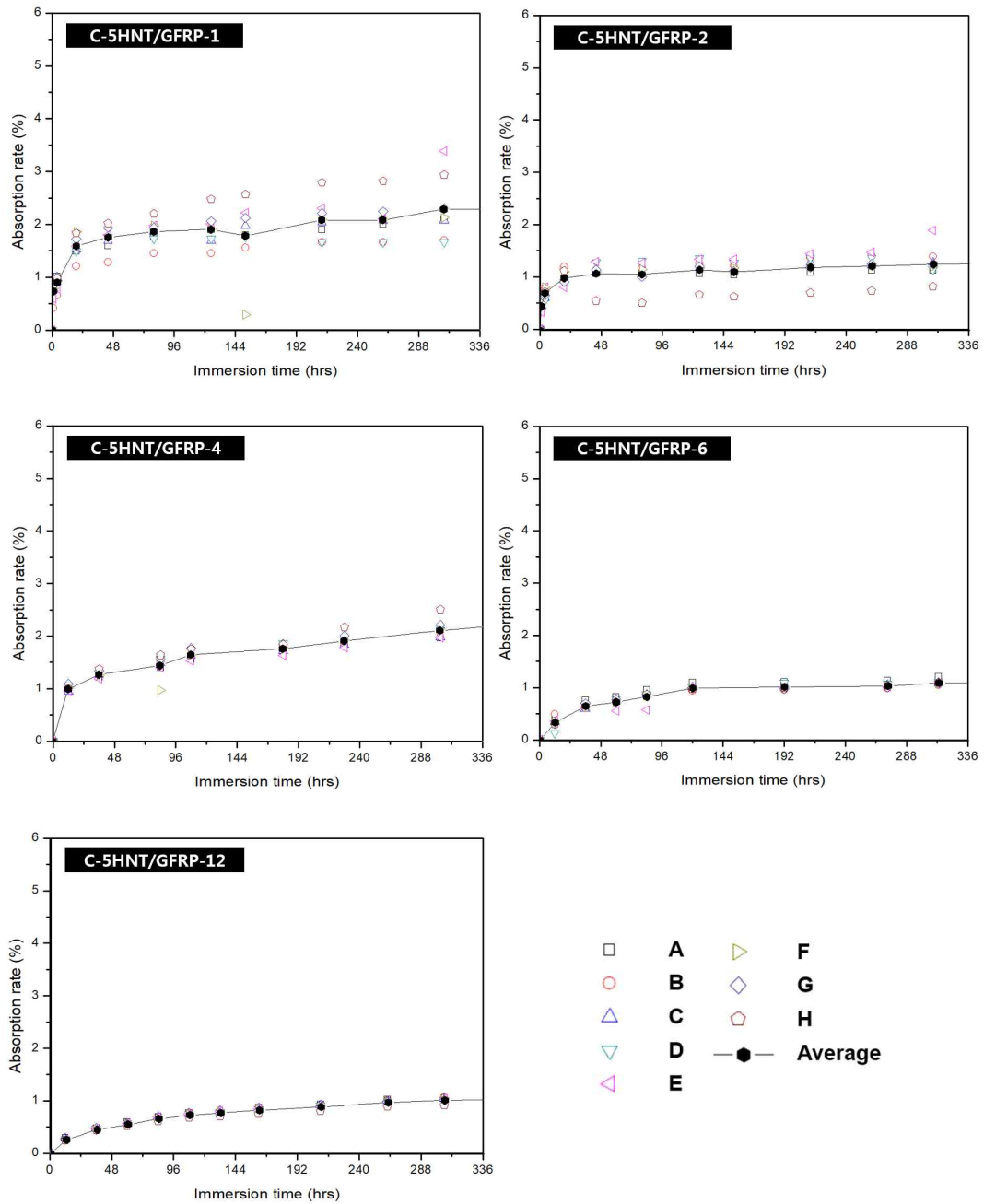


Fig. 31 Absorption rate of C-5HNT/GFRP immersed in distilled water at 70 °C up to 336 h (14 days) according to laminated fiber plies

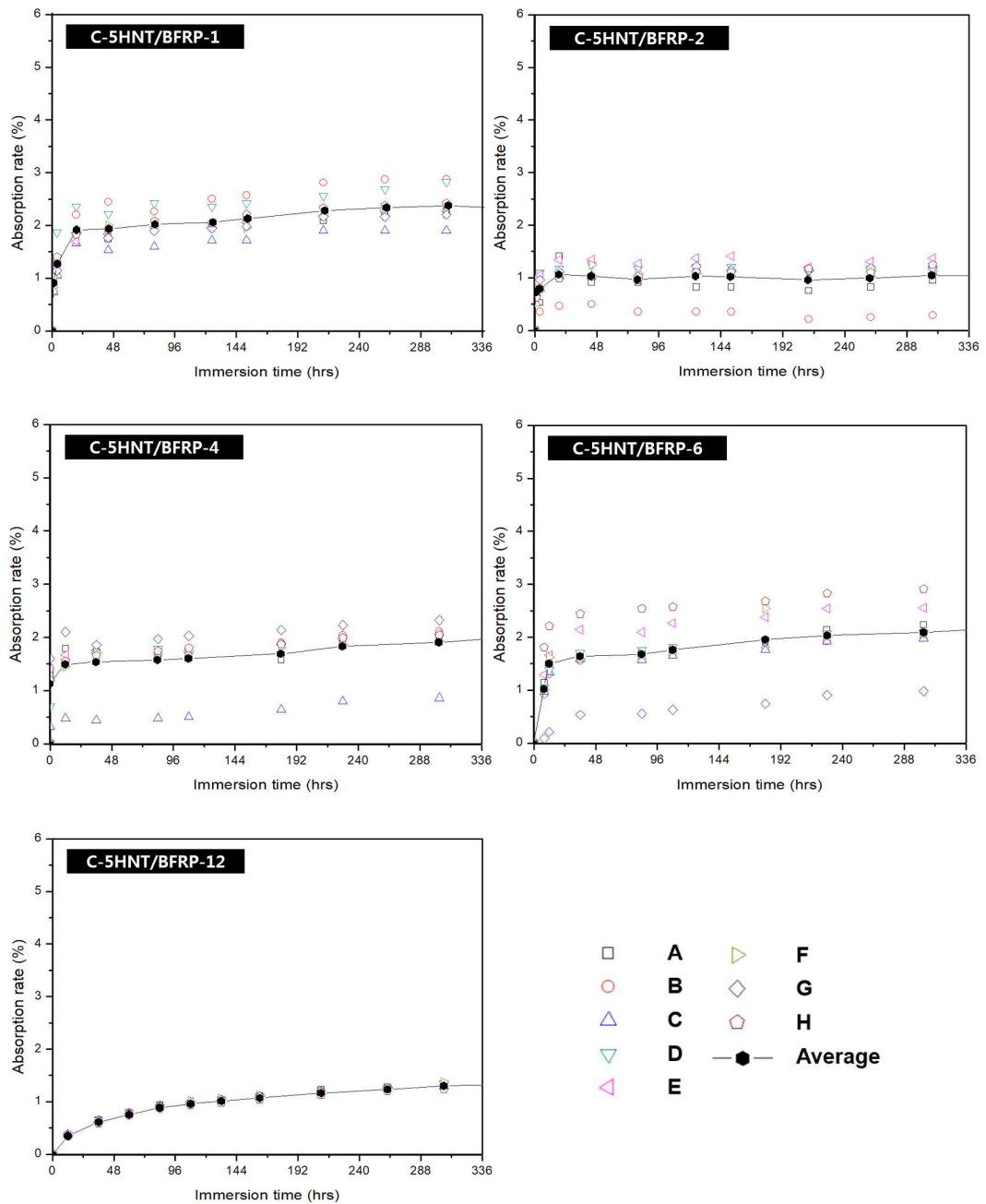


Fig. 32 Absorption rate of C-5HNT/BFRP immersed in distilled water at 70 °C up to 336 h (14 days) according to laminated fiber plies

As shown in Figs. 27 and 28, C-1HNT/GFRP and C-1HNT/BFRP showed similar tendency depending on the laminates layer. However, when 2 layers and 12 plies were used, the difference in the moisture absorption rate was large in each area. In addition, the moisture absorption rate changed rapidly from the D and E columns onwards. With an increase in the number of laminate layers, C-1HNT/BFRP retained its initial bond between HNT and EP and showed uniform dispersion and bonding behavior.

Figs. 29 and 30 show the changes in the moisture absorption rates of C-3HNT/GFRP and C-3HNT/BFRP, respectively. It can be observed from the figures that the number of laminate layers or regions did not affect the moisture absorption rates of C-3HNT/GFRP and C-3HNT/BFRP. However, with an increase in the amount of HNT up to 3 wt.%, these samples showed unstable moisture absorption over the entire area. In the case of C-3HNT/BFRP, the absorption rate increased rapidly within the initial 24 h and then, increased sharply up to 144 h. In addition, the combination of EP and HNT was incomplete and HNT was activated in the water environment. In addition, EP also showed degradation in water.

Figs. 31 and 32 show the moisture absorption rates of C-5HNT/GFRP and C-5HNT/BFRP, respectively. When the number of laminate layers was 12, C-5HNT/GFRP and C-5HNT/BFRP showed similar moisture absorption rates and behaviors. These moisture absorption rates and behaviors were similar to those of neat GFRP and neat BFRP. In addition, the state of dispersion was uniform over the entire region. Overall, intergranular aggregation due to de-bonding with EP was observed in C-5HNT/BFRP. This is because the moisture absorption rate was measured in the region corresponding to column H located opposite to the columns A, B, and C. This can partly be attributed to the deterioration of EP.

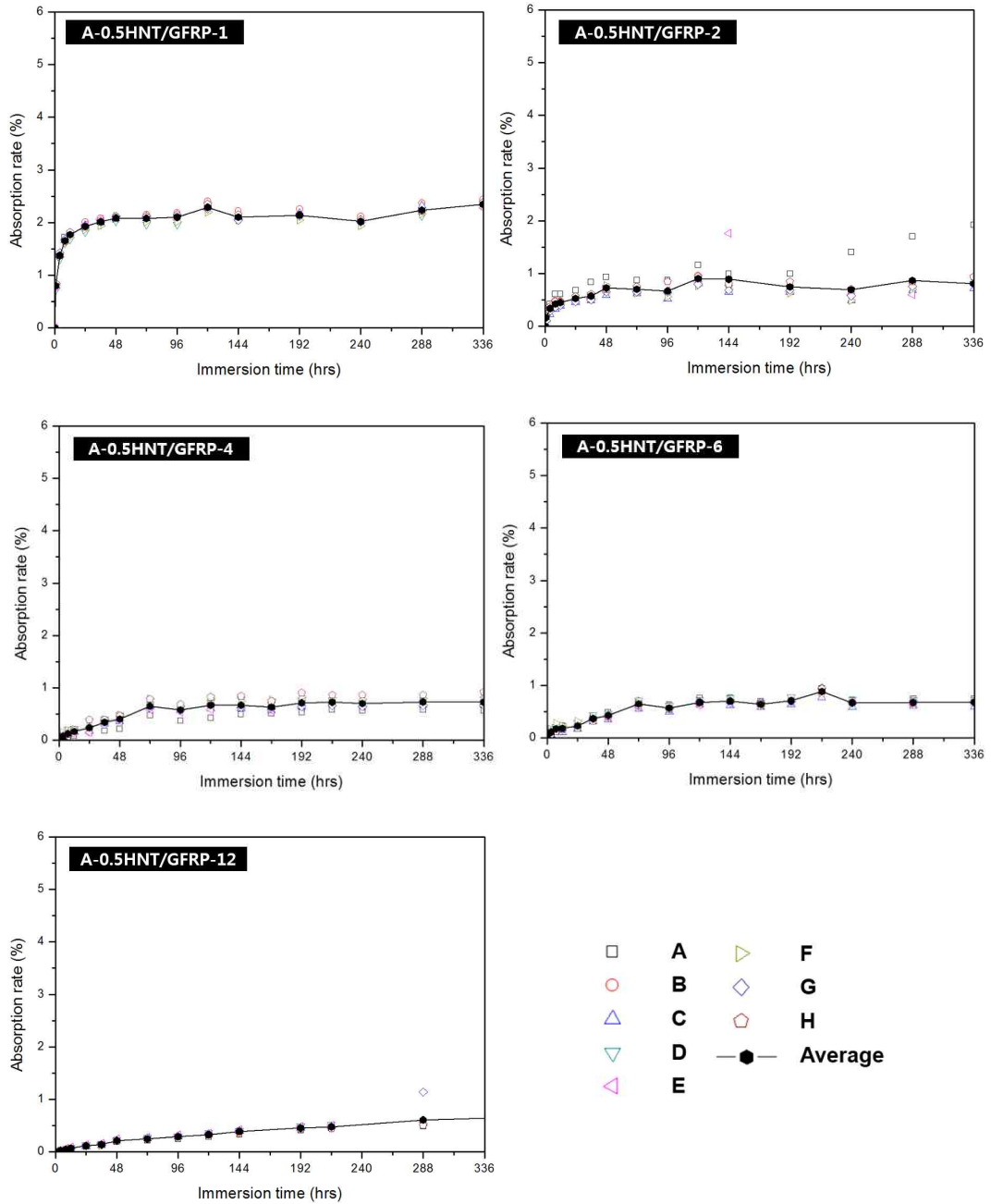


Fig. 33 Absorption rate of A-0.5HNT/GFRP immersed in distilled water at 70 °C up to 336 h (14 days) according to laminated fiber plies

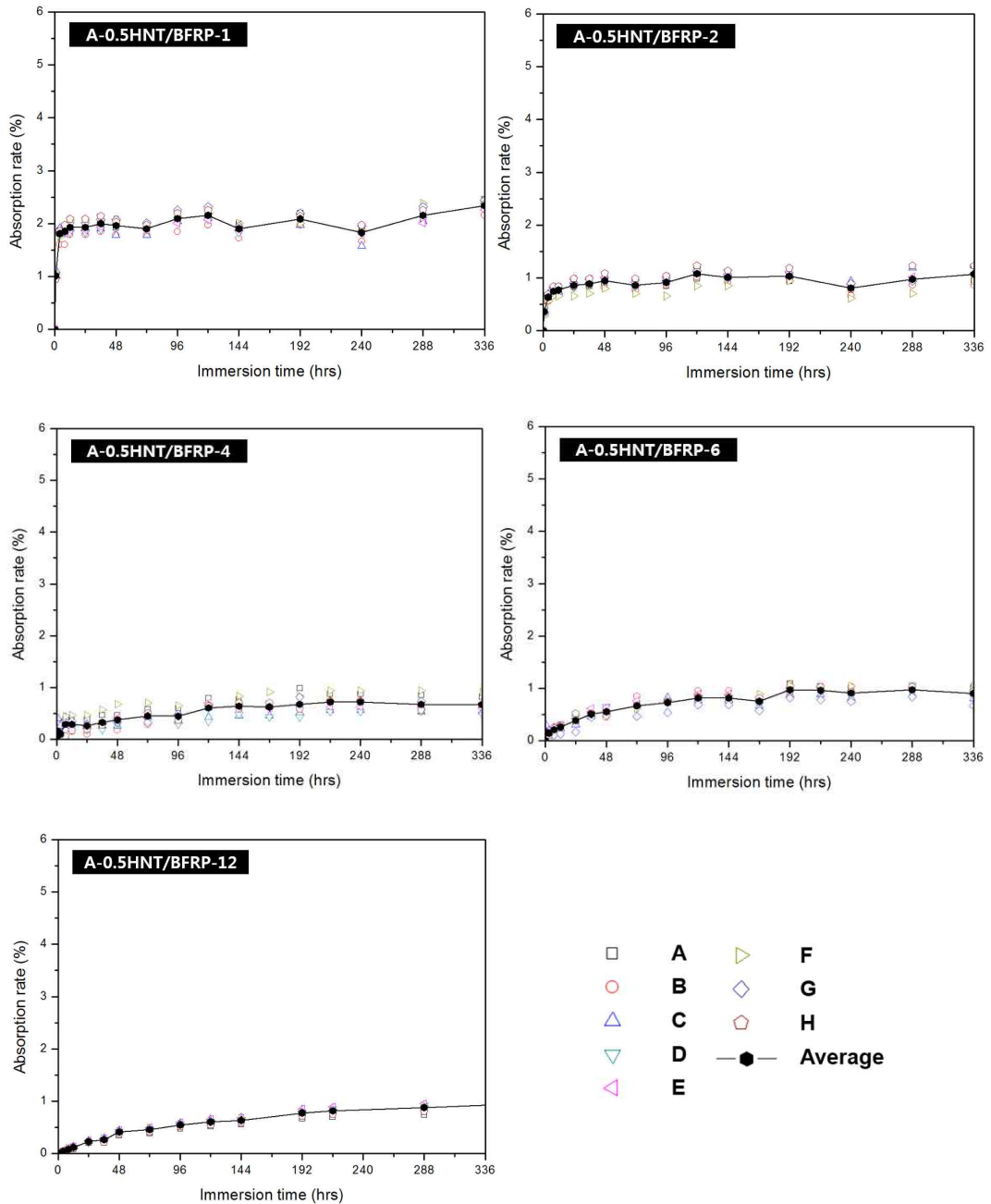


Fig. 34 Absorption rate of A-0.5HNT/BFRP immersed in distilled water at 70 °C up to 336 h (14 days) according to laminated fiber plies

As shown in Figs. 33 and 34, at higher laminate thicknesses, the hygroscopicity of both A-0.5HNT/GFRP and A-0.5HNT/BFRP was lower than that of neat GFRP and neat BFRP. This can be attributed to the high mobility of A-HNT on the binding surfaces of the fiber and EP in one ply laminate, which activated the re-aggregation process. In addition, the deterioration of EP was observed in the F, G, and H columns, and the A, B, and C columns showed different moisture absorption rates because of HNT. This confirmed the formation of a stable bond between A-HNT and EP/BFRP.

Figs. 35 and 36 show the hygroscopic graphs of A-1HNT/GFRP-1 and A-1HNT/BFRP-1, respectively. EP/HNT delamination occurred partially in the specimens exposed to high temperatures (70 °C). The moisture absorption rate decreased with an increase in the laminate layer thickness. In particular, the variations in the moisture absorption rates in the F, G, and H columns of A-1HNT/BFRP-1 were large. The moisture absorption rate of A-1HNT/BFRP was larger than that of A-1HNT/GFRP.

In Figs. 37 and 38 show that the moisture absorption rate of A-3HNT/GFRP showed little variation with the thickness of the laminates. However, the moisture absorption rate varied with time. The moisture absorption rates of the A and B columns in the case of A-3HNT/GFRP were higher than those in the case of A-3HNT/BFRP. This is because in BFRP, the binding force of A-HNT was stronger than that in GFRP and re-aggregation hardly occurred. The moisture absorption rates of A-3HNT/GFRP-12 and A-3HNT/BFRP-12 were similar.

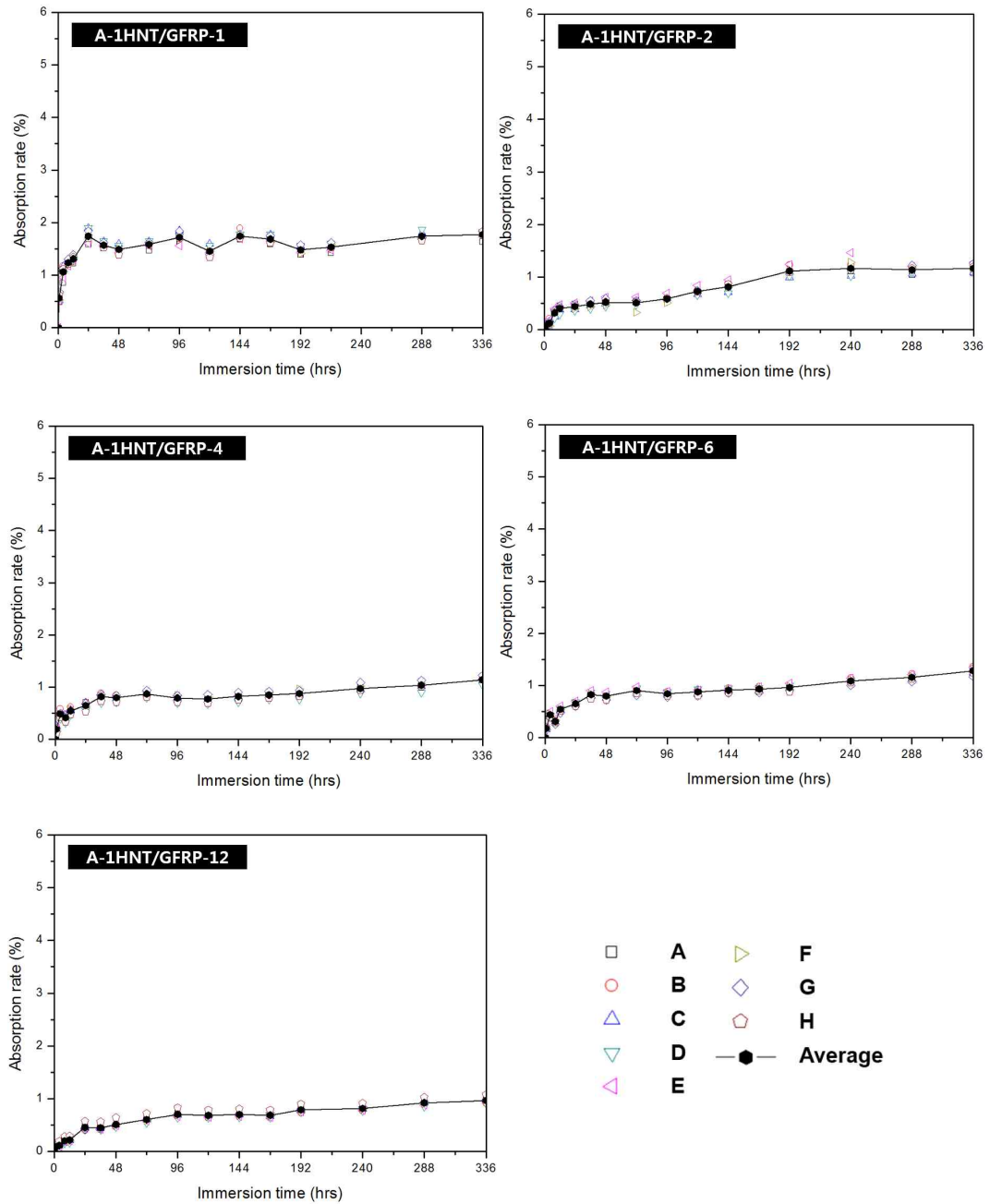


Fig. 35 Absorption rate of A-1HNT/GFRP immersed in distilled water at 70 °C up to 336 h (14 days) according to laminated fiber plies

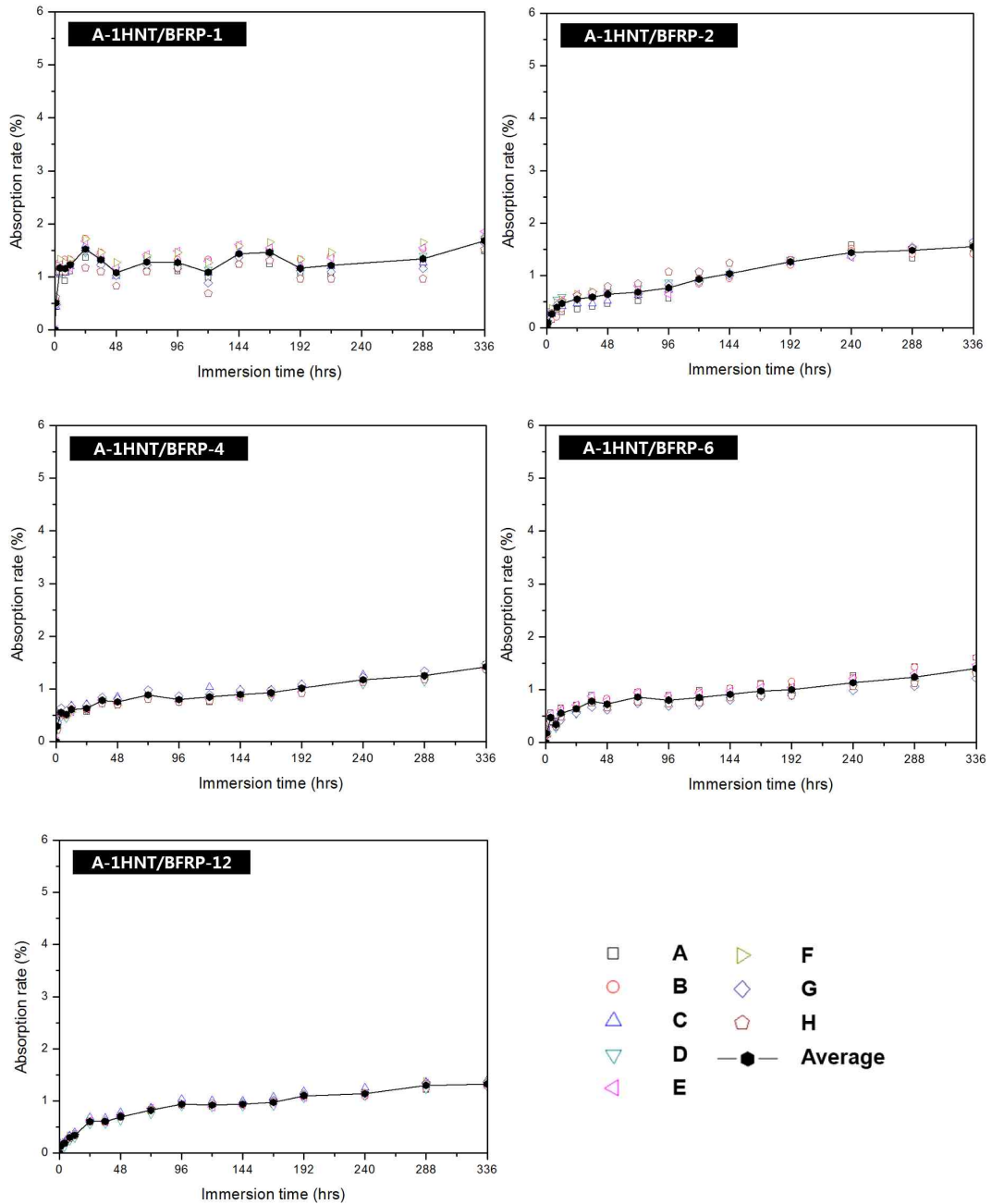


Fig. 36 Absorption rate of A-1HNT/BFRP immersed in distilled water at 70 °C up to 336 h (14 days) according to laminated fiber plies

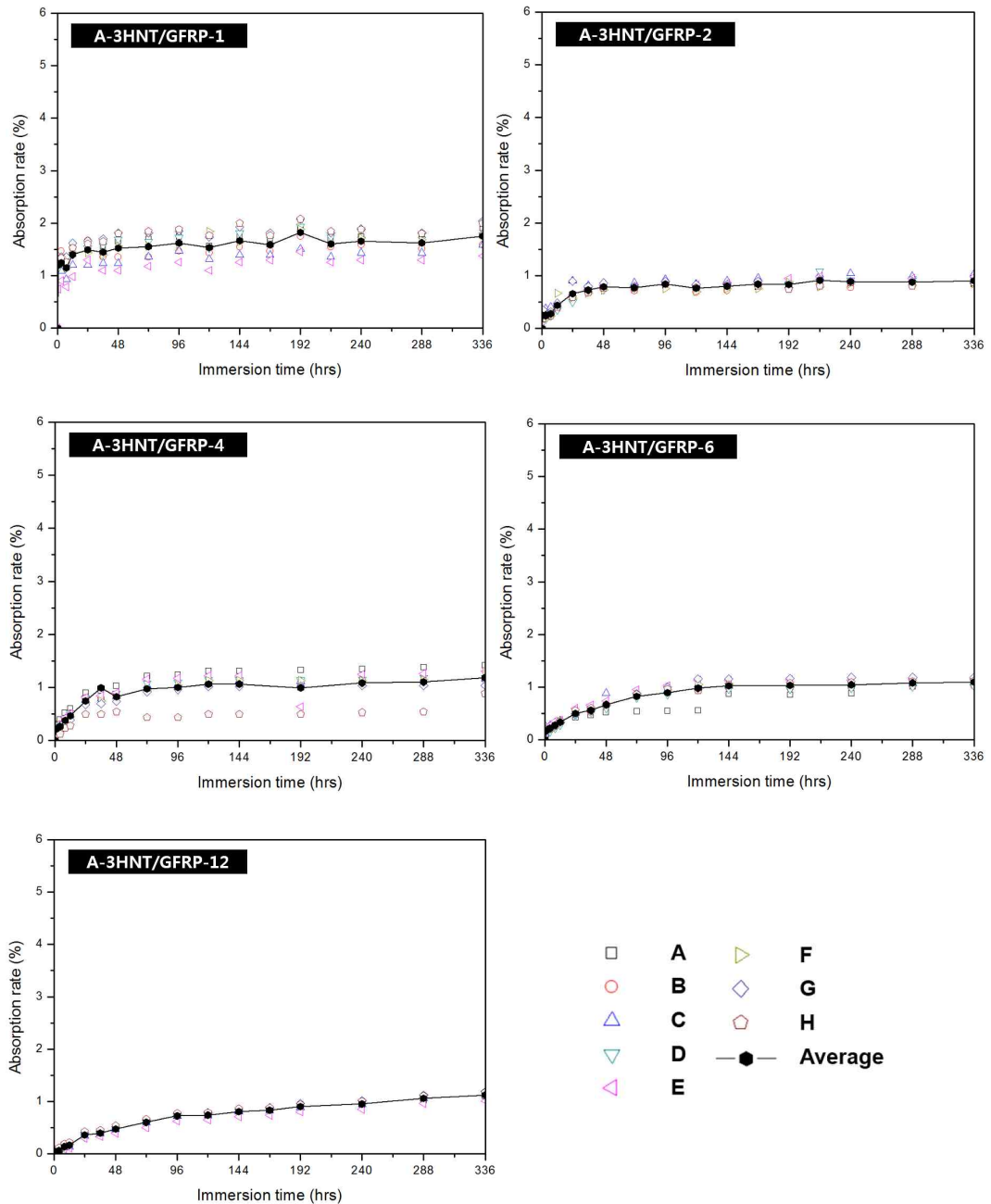


Fig. 37 Absorption rate of A-3HNT/GFRP immersed in distilled water at 70 °C up to 336 h (14 days) according to laminated fiber plies

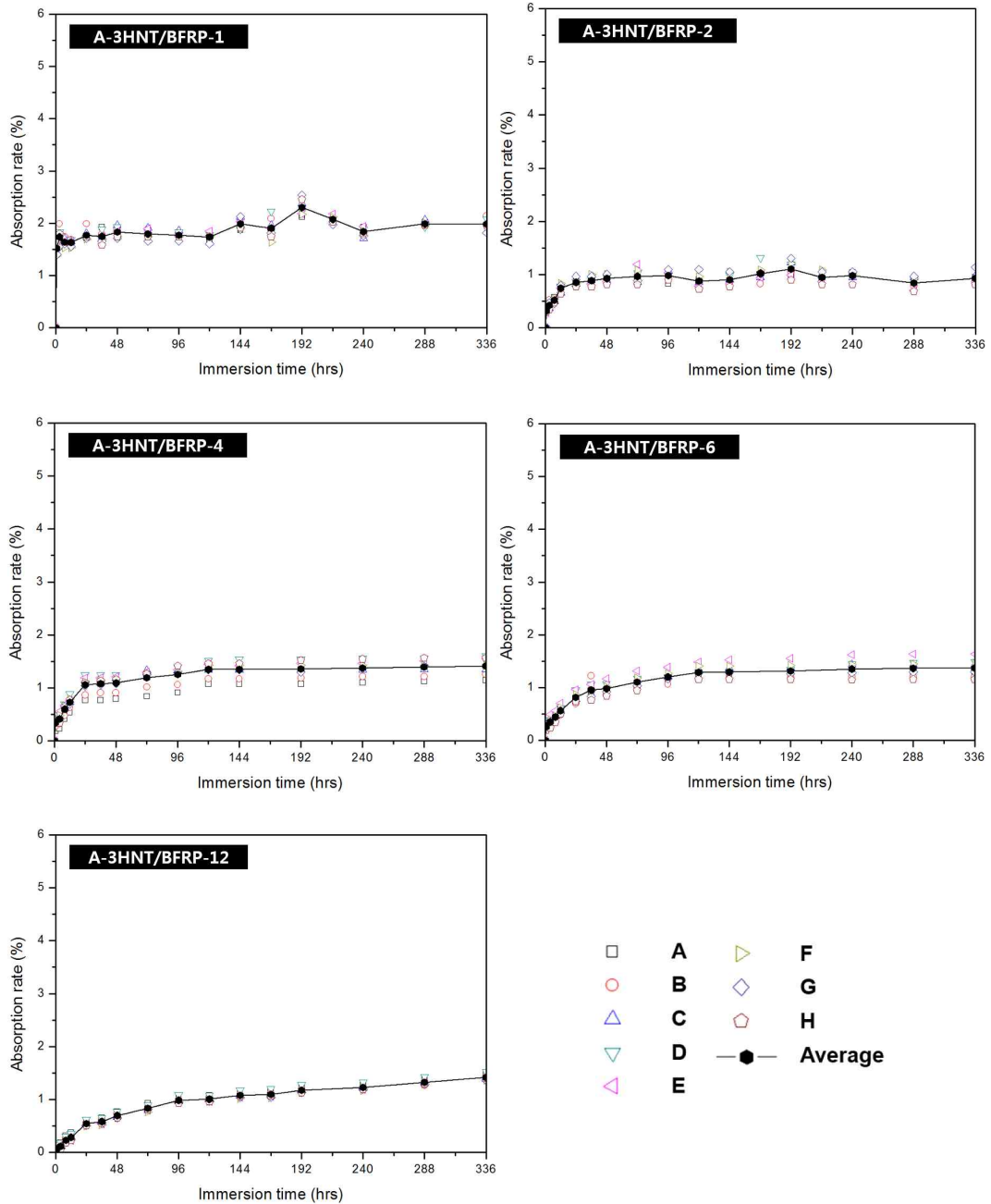


Fig. 38 Absorption rate of A-3HNT/BFRP immersed in distilled water at 70 °C up to 336 h (14 days) according to laminated fiber plies

As shown in Figs. 39 and 40, the moisture absorption rates of A-5HNT/GFRP and A-5HNT/BFRP showed similar variations. However, the moisture absorption rate of A-5HNT/BFRP depended on the amount of particles and showed large variations over the entire time range. A-5HNT/GFRP-4 and A-5HNT/BFRP-6 showed the most stable moisture absorption rates. In the case of 12 plies, the moisture absorption rate was the lowest in the A and B columns. On the other hand, moisture absorption rate was the highest in the D and E columns. This caused resin shrinkage in the direction of air discharge during the vacuum molding, resulting in the re-aggregation of HNT particles. A-5HNT/BFRP showed large variations in moisture absorption with time. This can be attributed to the resin dropout due to the interfacial peeling between the fiber and the resin.

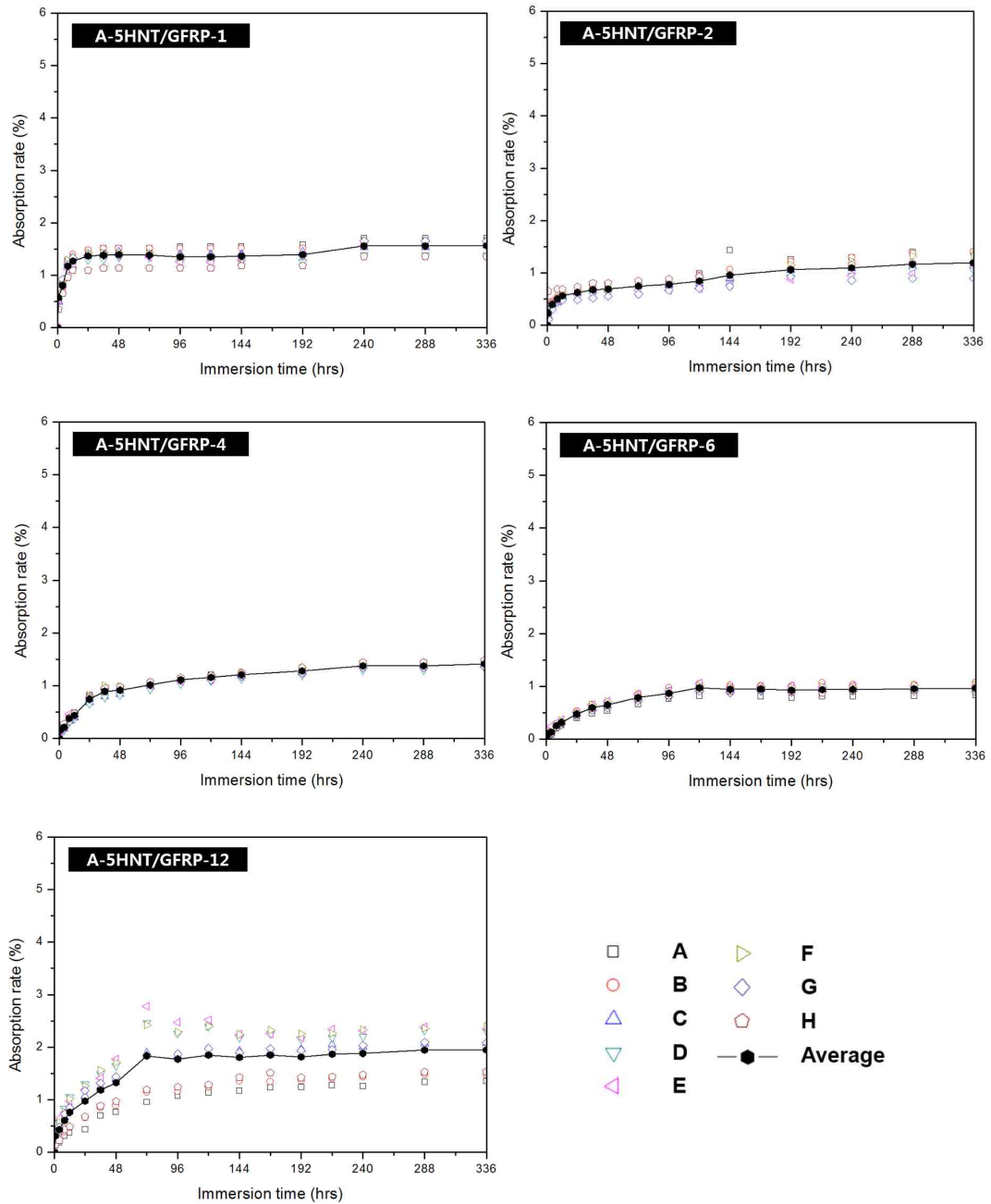


Fig. 39 Absorption rate of A-5HNT/GFRP immersed in distilled water at 70 °C up to 336 h (14 days) according to laminated fiber plies

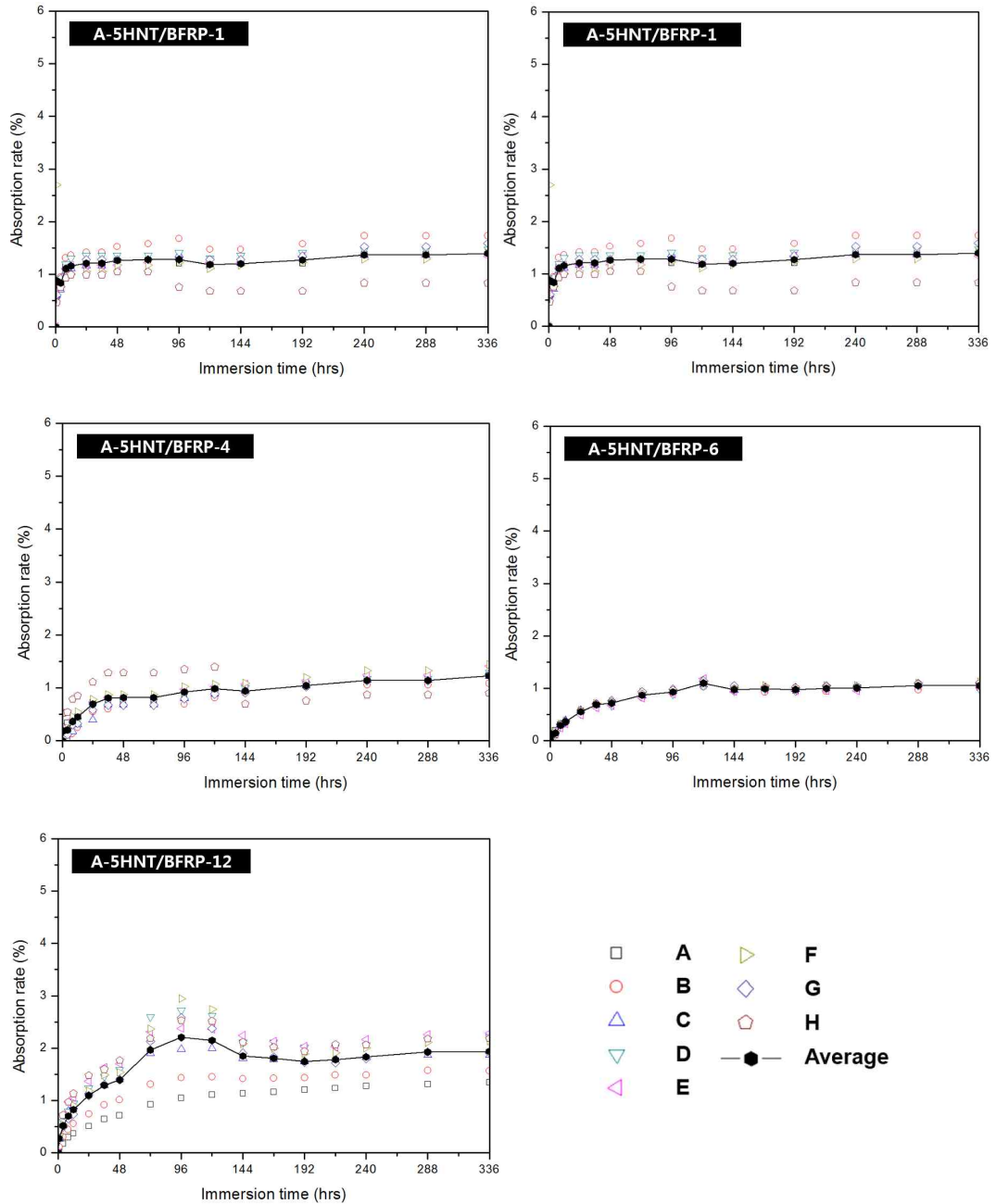
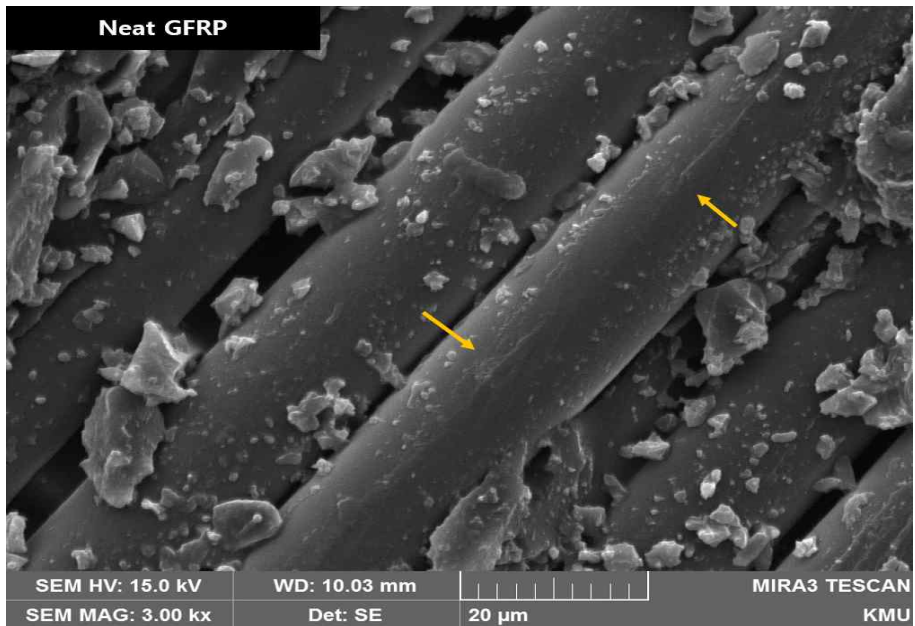


Fig. 40 Absorption rate of A-5HNT/BFRP immersed in distilled water at 70 °C up to 336 h (14 days) according to laminated fiber plies

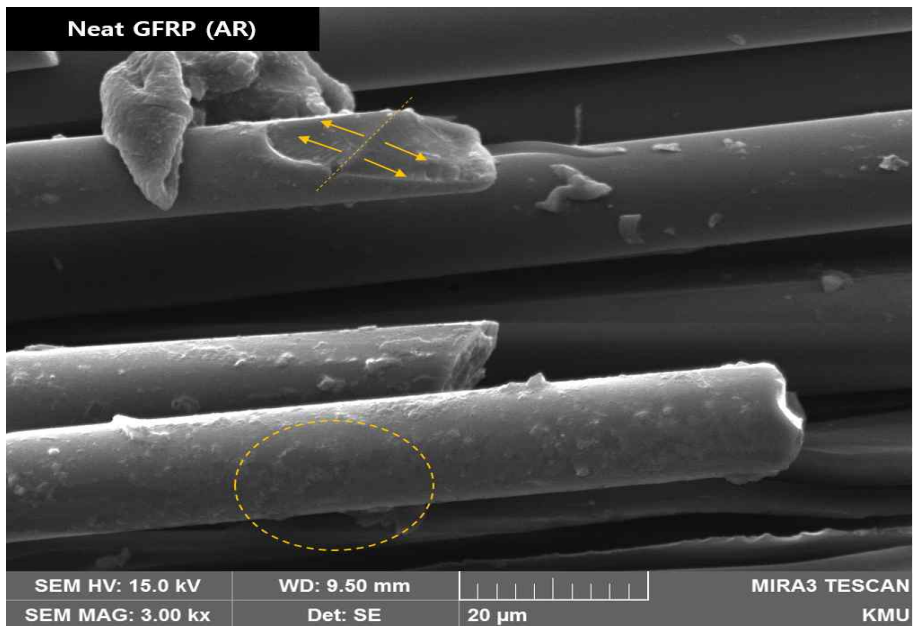
Figs. 41 and 48 show the SEM images of the surfaces of HNT/EP matrix GFRP and BFRP nanocomposites immersed in distilled water at 70 °C for up to 336 h. The interface between fiber and EP, fiber damage behavior due to the delamination of the HNT/EP colloidal solution deteriorated by moisture and cluster effect due to the HNT aggregation phenomenon were analyzed.

Fig. 41 shows the moisture degradation of neat GFRP before and after 336 h of water immersion. Partial bonding with EP was observed prior to the water immersion. Since EP was delaminated by moisture, it was mostly removed and a relatively clean surface was observed. In addition, the EP delamination did not cause any significant damage on the fiber surface. It was confirmed that the fiber cut at the middle of the filament broke in a progressive form over a long period of time instead of undergoing instantaneous fracture. We believe that water caused volume expansion in EP, water transferred from the fiber surface, and the fiber fracture occurred as the water content in the fiber reached the saturation point.

As shown in Fig. 42, in the case of neat BFRP, the interface between EP and BF was bonded very smoothly before the moisture immersion, and there was almost no breakage of EP. This is because BF and EP were uniformly bonded. After the prolonged water immersion EP delamination and fiber fracture occurred simultaneously. In addition, many traces of fibers fell off the fiber surface. This is considered to be a direct effect of EP degradation on the fiber due to moisture and delamination.

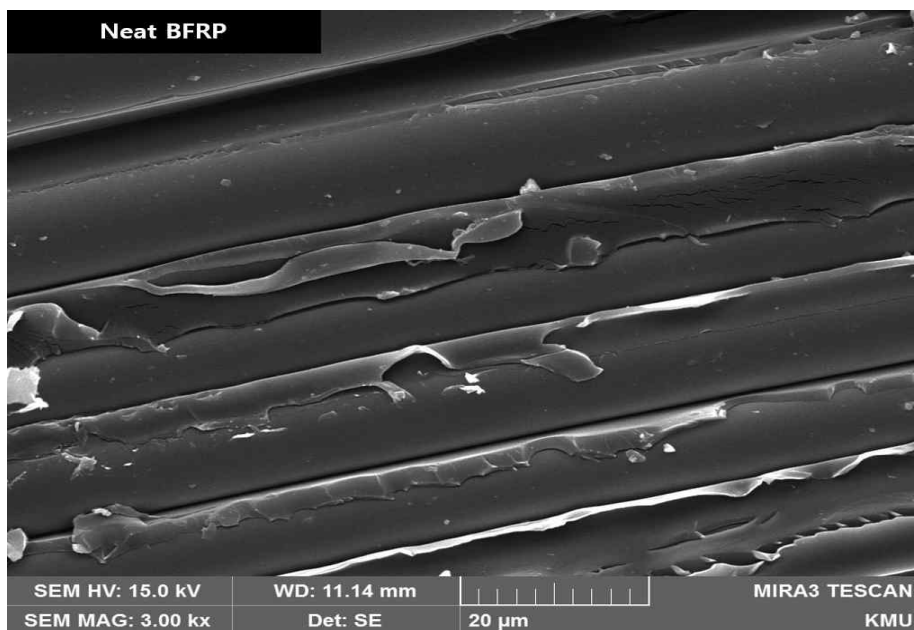


(a)

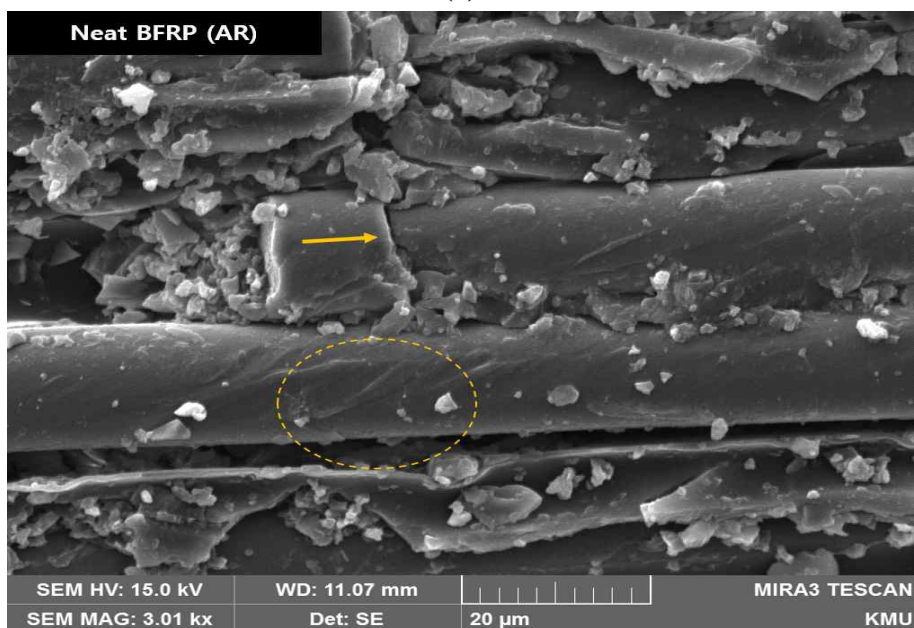


(b)

Fig. 41 Moisture degradation of Neat GFRP by SEM; (a) before and (b) after distilled water immersion



(a)



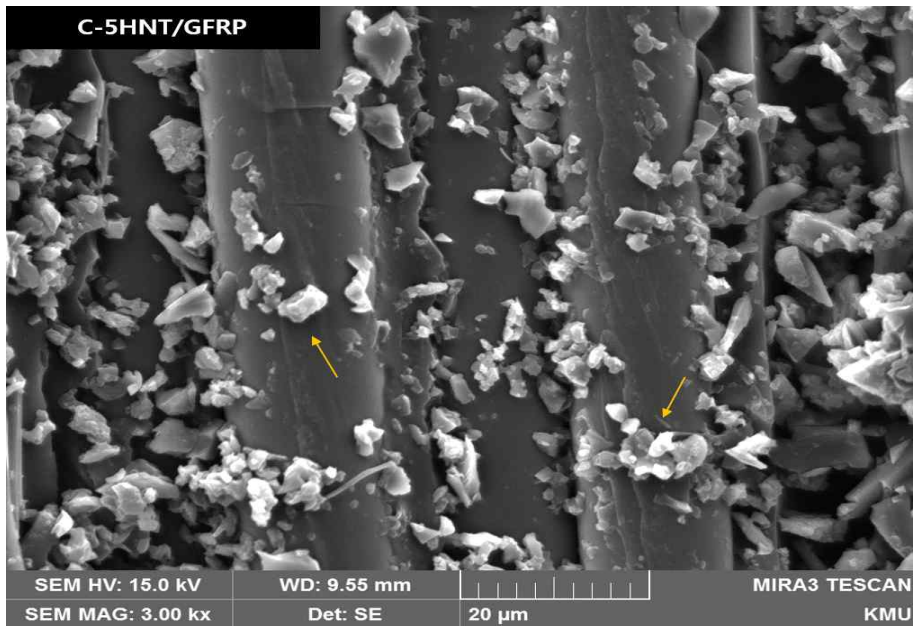
(b)

Fig. 42 Moisture degradation of Neat BFRP by SEM; (a) before and (b) after distilled water immersion

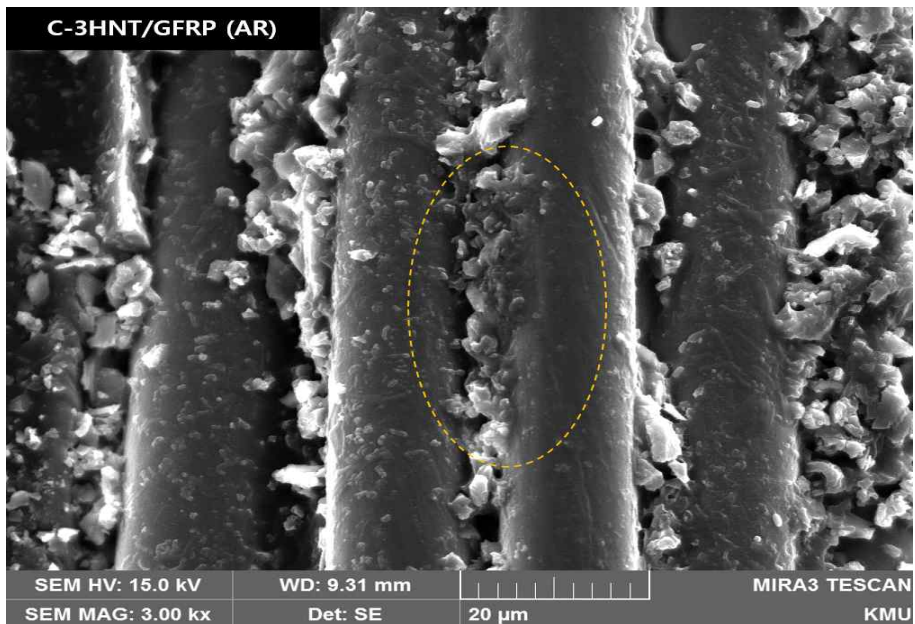
Fig. 43 shows the surface of the C-HNT—dispersed GFRP. As shown in Fig. 43-(a), neat GFRP was densely bonded to the fibers and the size of the delaminated EP was relatively large. After immersion for 336 h, the softened EP bonded to the fiber interface and the bond marks on the fiber surface were swollen and distinct. The swelling of EP, which appeared to be entangled by C-HNT, was caused by moisture absorption. The residual resin, which was not directly involved in the bonding, was removed in the form of the initial EP. HNT combined with water to reduce the effect of moisture on EP.

Fig. 44 shows the water resistance of BFRP by C-HNT. Unlike C-HNT/GFRP, C-HNT/BFRP exhibited relatively smooth fiber surfaces before and after the water immersion with partial damage to the HNT clusters. However, no initial fiber surface damage was observed. However, after the water immersion, fiber damage became predominant, and the size of the delaminated EP was relatively small.

Fig. 45 shows the results of the A-HNT/GFRP surface examinations. Unlike the case of C-HNT/GFRP, in this case, the amount of EP attached to the fiber surface prior to the immersion was low, and a smooth surface was observed. C-HNT/BFRP bonded to a large area of the fiber surface. After the water immersion, the EP of the scratched pieces was stained on the fiber surface, and the delamination of EP and the fibers produced a large amount of interface residue. However, there were almost no traces because of the bonding on the fiber surface, and the damage due to delamination on the surface was higher than that in the interior of the fiber.

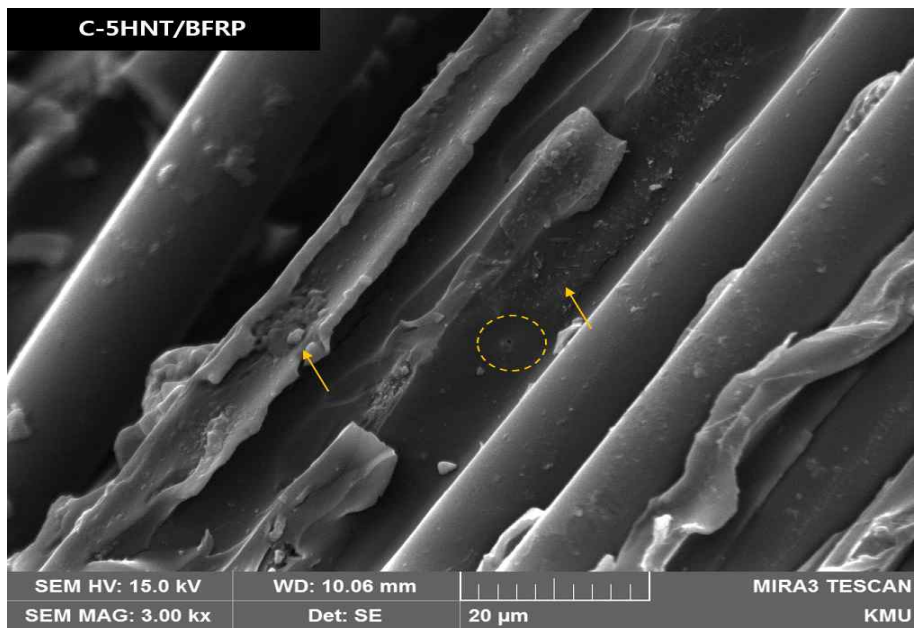


(a)

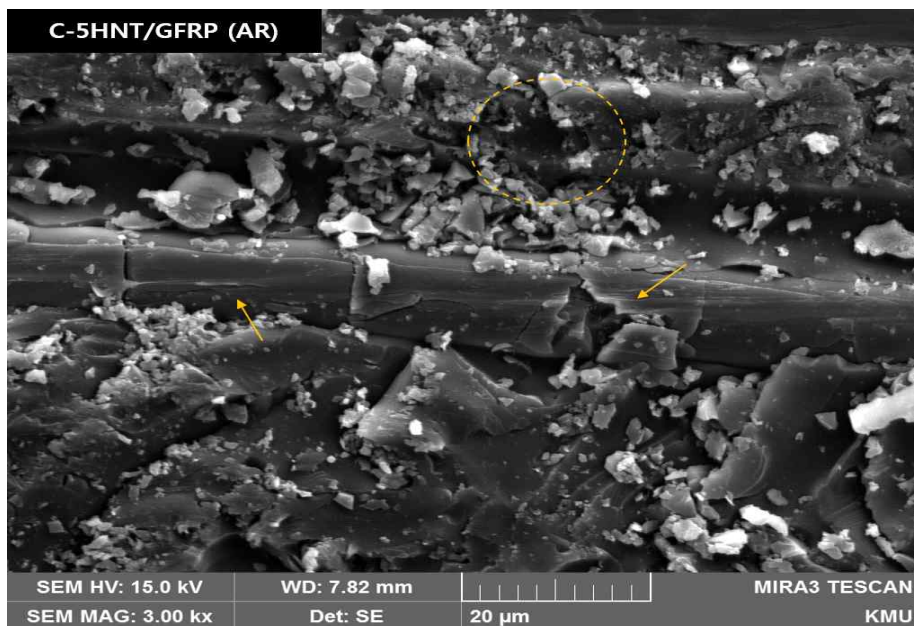


(b)

Fig. 43 Effect of HNT on the moisture degradation of C-HNT/GFRP by SEM;
(a) before and (b) after distilled water immersion

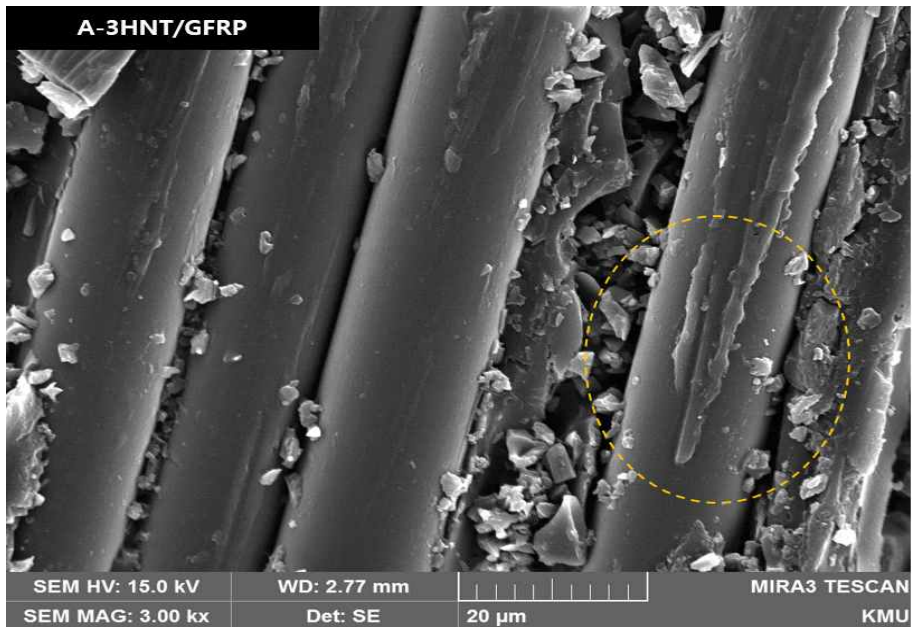


(a)

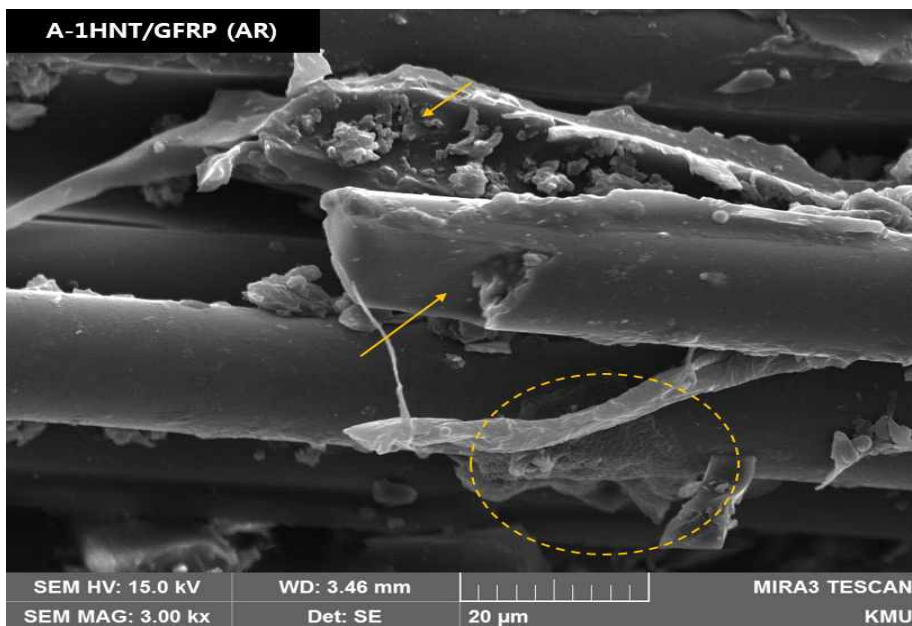


(b)

Fig. 44 Effect of HNT on the moisture degradation of C-HNT/BFRP by SEM;
(a) before and (b) after distilled water immersion



(a)



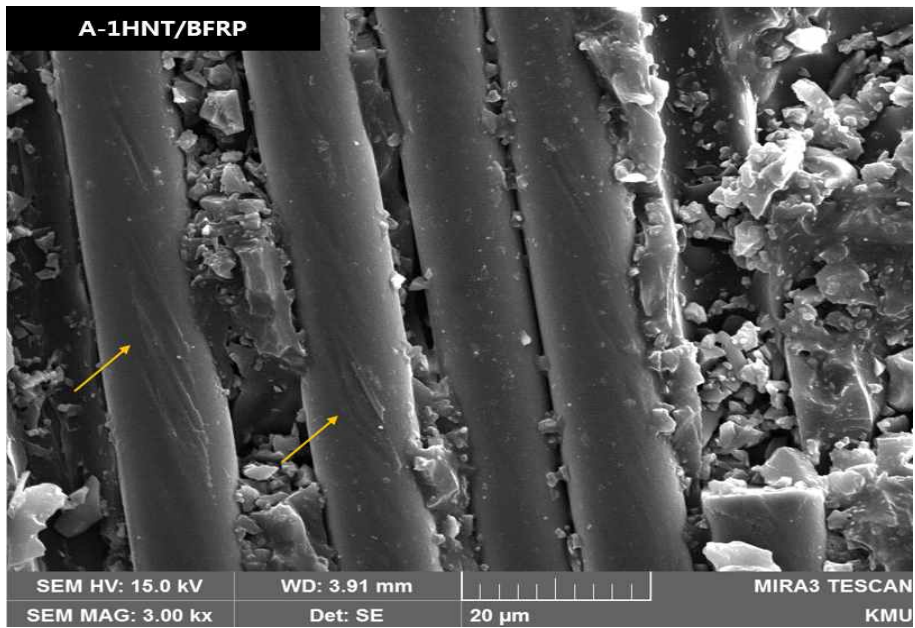
(b)

Fig. 45 Effect of HNT on the moisture degradation of A-HNT/GFRP by SEM;
(a) before and (b) after distilled water immersion

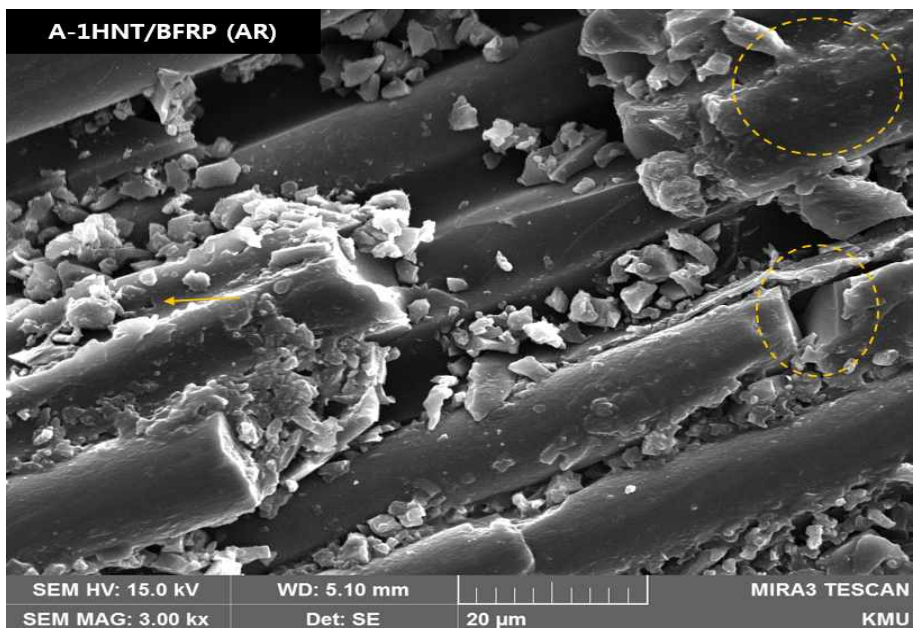
As shown in Fig. 46, before the water immersion, A-HNT/BFRP exhibited an EP-bound form across the surface of the fiber. However, C-HNT/BFRP showed a scattering pattern of HNT clusters on the fiber surface, while A-HNT/BFRP showed long scratched edges at the fiber/EP interface. After the water immersion, grain tearing was observed along the fiber length, and the fiber cut surface showed a sharp shape. A small piece of EP (EP agglomerated with A-HNT) was observed around the fiber.

Fig. 47 shows the samples exposed to distilled water at 70 °C for over 700 h. As shown in Fig. 47-(a), in the case of C-HNT/GFRP (700), the water trapped inside the C-HNT/EP interface gradually expanded its shape. In other words, C-HNT was wrapped around EP and absorbed water directly preventing the moisture-degradation of EP. In this process, supersaturated water diffused into the fibers to repeat the moisture adsorption and desorption process, so that the initial HNT/EP bond remained on the fiber surface. On the other hand, in the case of C-HNT/BFRP (700), moisture adsorption caused the swelling of the C-HNT/EP surrounding the fiber surface over the entire surface and softening of EP. In addition, the adsorption moisture caused delamination in the fiber.

Fig. 48 shows the surfaces of A-HNT/GFRP (700) and A-HNT/BFRP (700). A-HNT showed less C-HNT agglomeration and showed stable bonding with EP on the fiber surface because of uniform particle dispersion. The number of broken EPs was small and did not cause severe damage inside the fibers. However, it showed a greater impact on EP bonding than the fiber and contributed to minimizing the moisture damage of the fibers. In A-HNT/BFRP (Fig. 48-(b)) EP delamination and deterioration was more evident than the delamination between the fibers and EP.

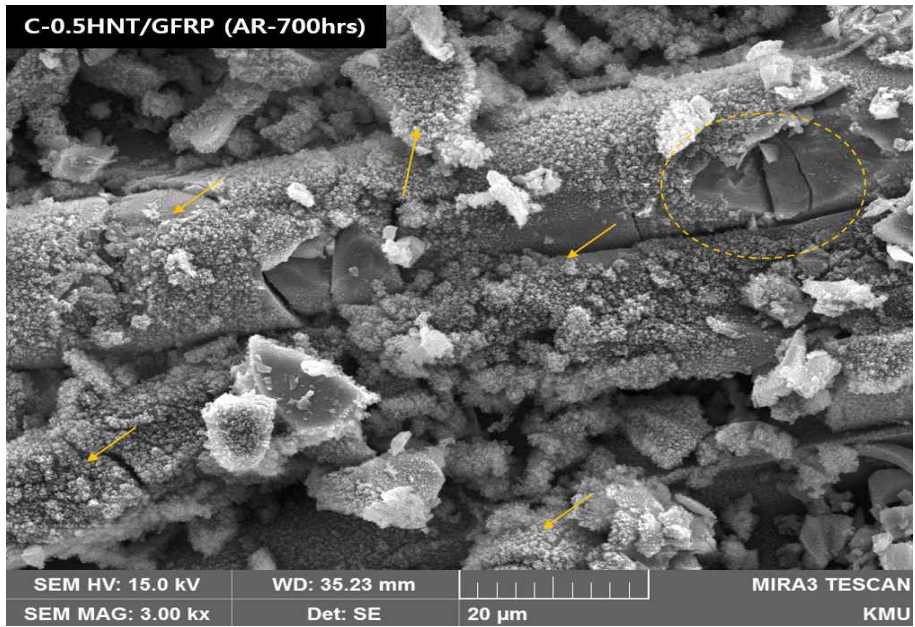


(a)

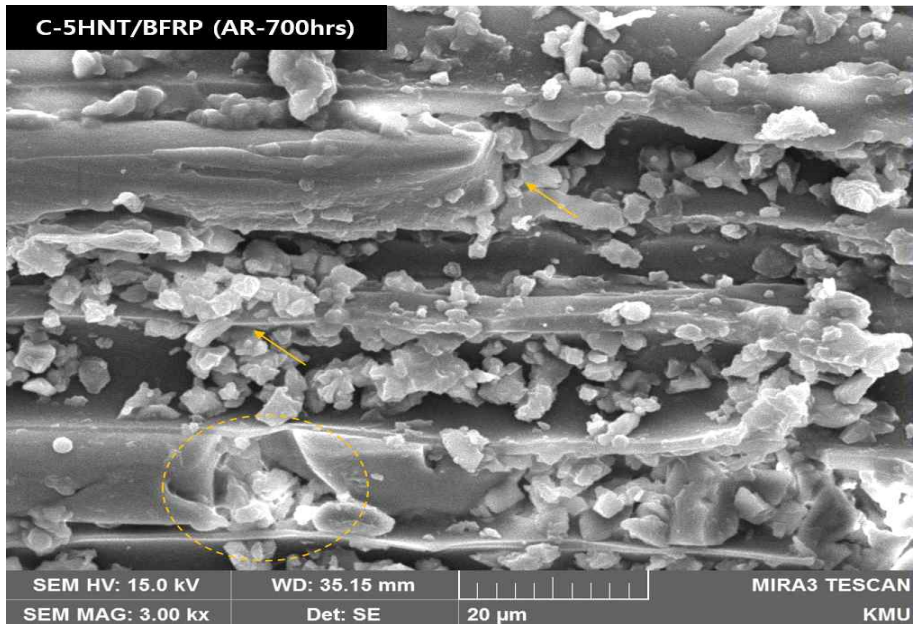


(b)

Fig. 46 Effect of HNT on the moisture degradation of A-HNT/BFRP by SEM;
(a) before and (b) after distilled water immersion

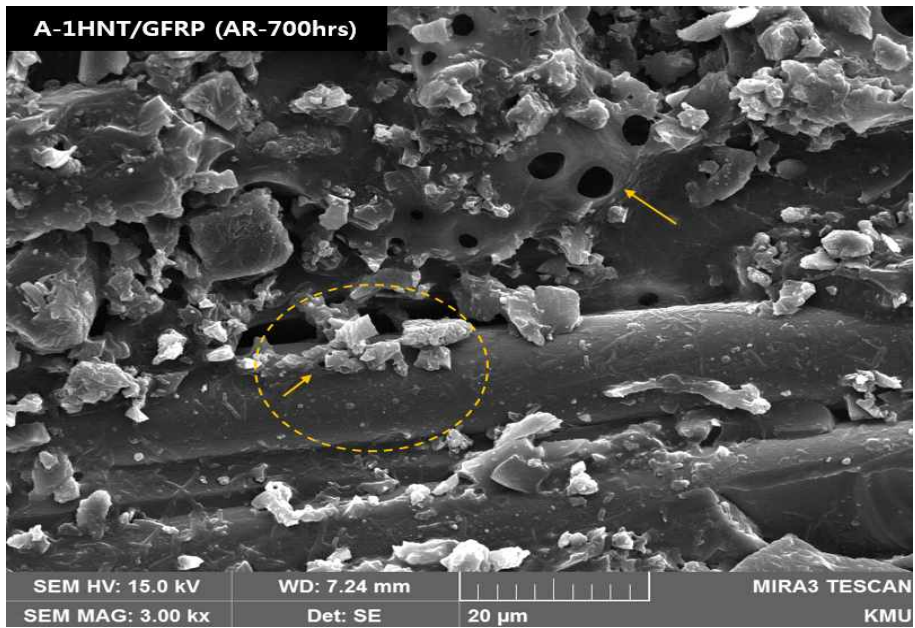


(a)

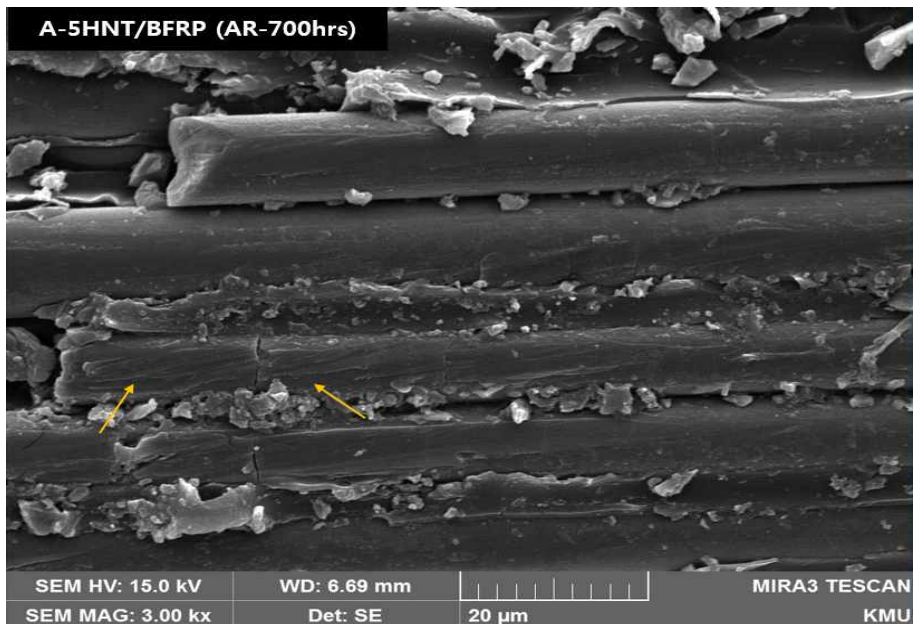


(b)

Fig. 47 Effect of HNT on the moisture degradation by SEM; (a) C-HNT/GFRP and (b) C-HNT/BFRP after distilled water immersion over 700 h



(a)



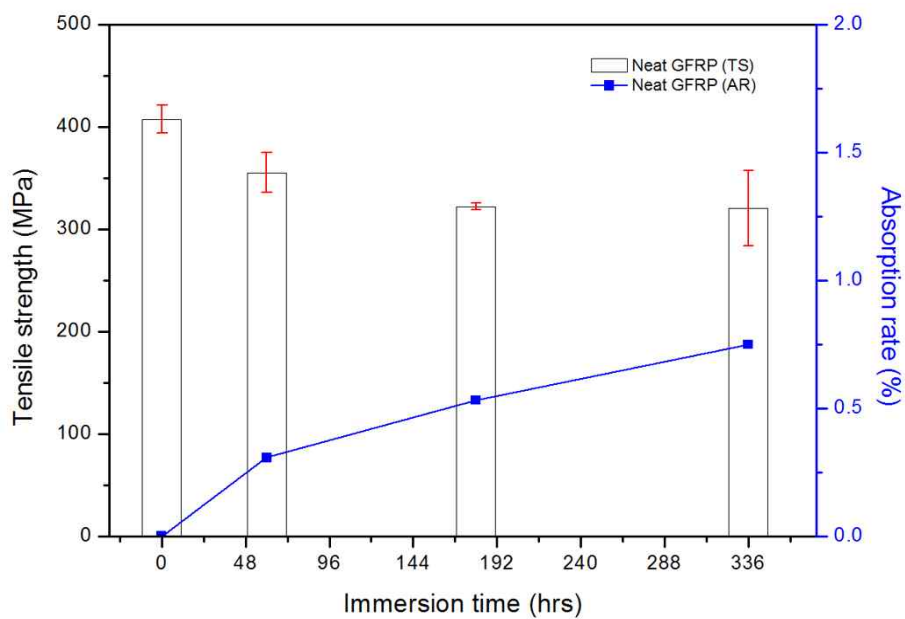
(b)

Fig. 48 Effect of HNT on the moisture degradation by SEM; (a) A-HNT/GFRP and (b) A-HNT/BFRP after distilled water immersion over 700 h

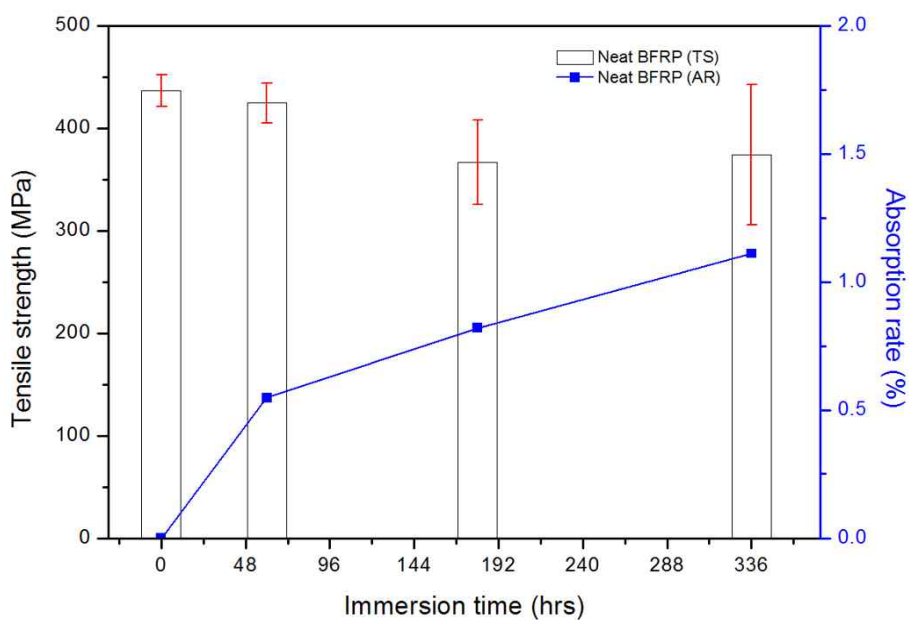
4.4 Mechanical property

4.4.1 Tensile strength

The effect of the absorption rate of HNT/GFRP and HNT/BFRP immersed in distilled water for a long time on mechanical tensile strength was investigated by tensile test. The relationship between the tensile strength and the absorption rate was investigated according to the crystallinity and addition amount of HNT. Fig. 49 compares the tensile (TS) and intermittent moisture absorption (AR) changes between Neat GFRP and Neat BFRP, and the trends of these graphs are similar. The initial tensile strength of Neat BFRP was higher than that of Neat GFRP. The strength of Neat GFRP decreased significantly during 48 h after immersion in distilled water. Neat BFRP showed significant tensile strength decrease after 48 h. Neat GFRP and Neat BFRP used the same EP as the matrix, but Neat BFRP was significantly higher at the absorption rate than Neat GFRP, and there was less damage to tensile strength due to moisture, relative to Neat GFRP. However, the intensity inhibition rate based on the initial tensile strength was measured similarly. The moisture absorptivity tended to increase slowly at 180 h of water immersion, but the tensile strength tended to be maintained. This means that there is little physical/chemical damage due to penetrated moisture, suggesting that mutual moisture diffusion and migration take place via reversible routes. In other words, during this time, the moisture is easily released through the drying process, which means that it has have little effect on the bond between the fiber reinforcement and the matrix.

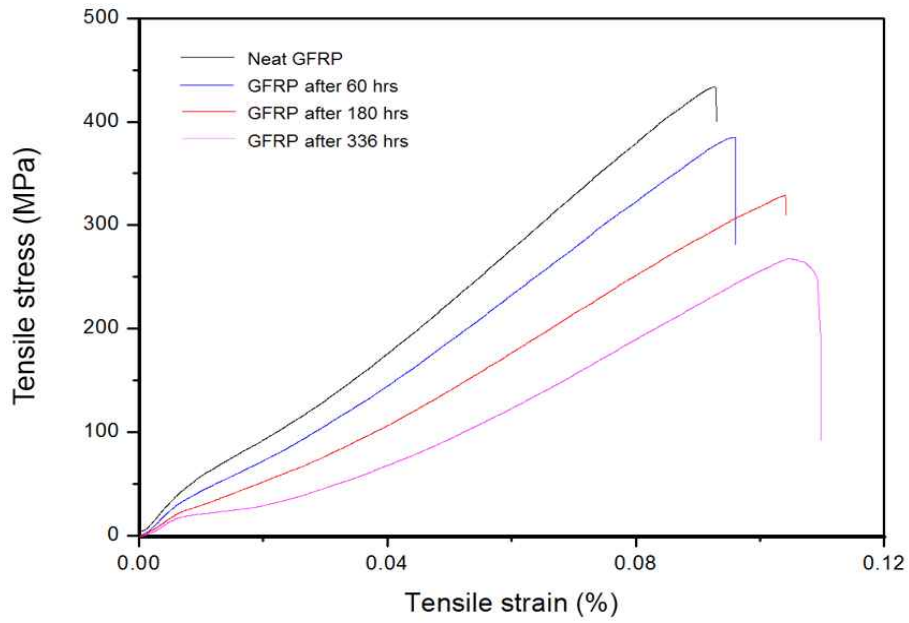


(a)

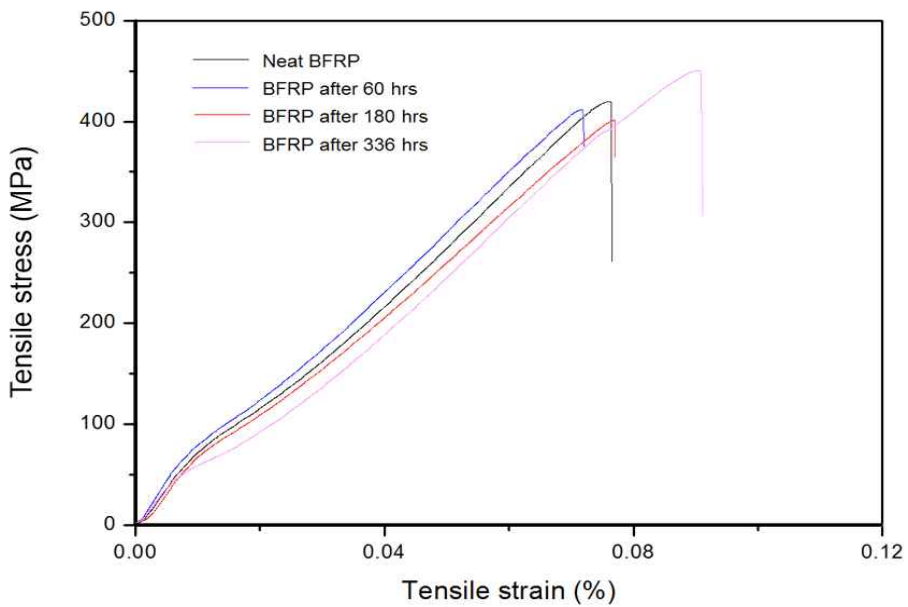


(b)

Fig. 49 Effect of water absorption rate on tensile strength in (a) Neat GFRP and (b) Neat BFRP



(a)



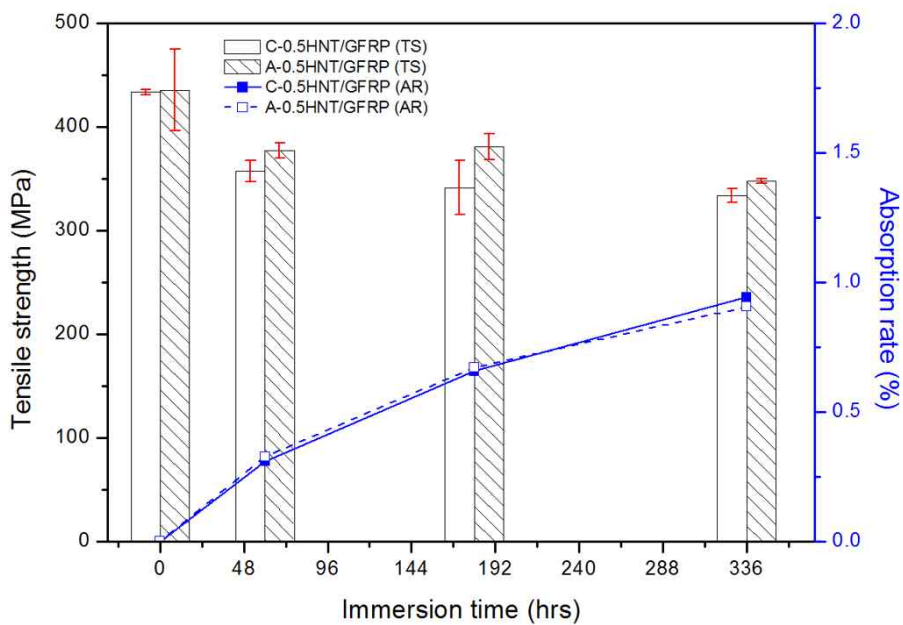
(b)

Fig. 50 Tensile stress-tensile strain curves with water immersion time in (a) Neat GFRP and (b) Neat BFRP

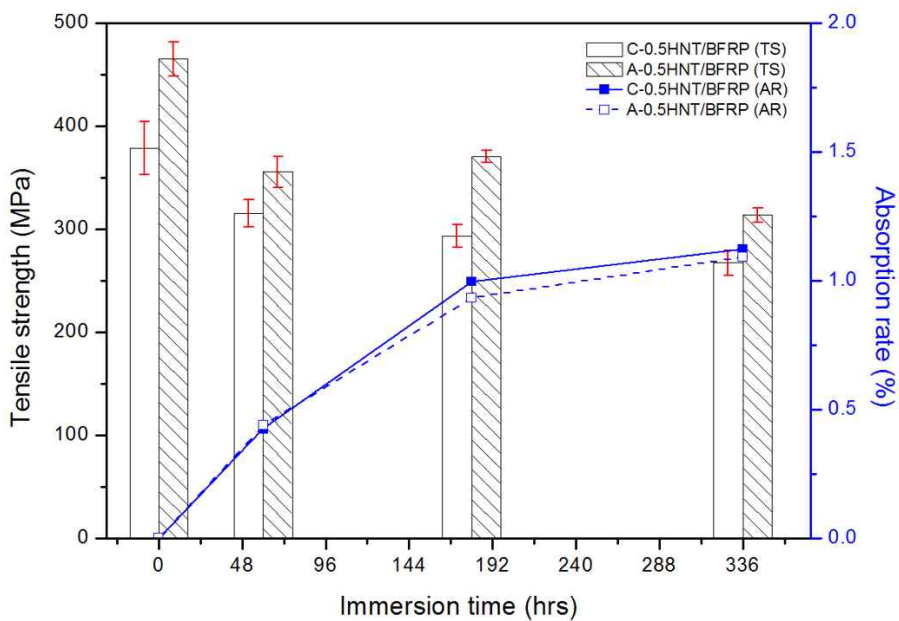
Fig. 50 shows the tensile stress-strain curves. Both Neat GFRP and Neat BFRP showed smaller stiffness and tensile modulus E as the moisture immersion time increased. As a result of the softening of the resin, Neat BFRP was observed to be relatively unaltered, which is related to the interfacial bonding strength at the laminates interface.

Fig. 51 compares the relationship between the tensile strength and the absorption rate with HNT crystallinity when 0.5 wt.% HNT is added, while Fig. 52 shows the tensile strength-tensile strain curves at that time. In general, the hygroscopic rates of 0.5HNT/GFRP and 0.5HNT/BFRP increased sharply in the range of (60–180) h of immersion, regardless of the crystallinity of HNT. It was found that 0.5HNT/BFRP showed a gentle curve, and reached a certain saturation level. However, 0.5HNT/GFRP retained a modest but increasing shape similar to Neat GFRP and Neat BFRP, which was sufficient to predict continuous absorption. In addition, adding C-HNT and A-HNT enhanced the initial tensile strength of 0.5 HNT/GFRP, and the tensile strength reduction rate of A-HNT was lower than that of C-HNT. This is because the interfacial bonding strength and the state of dispersion of A-HNT are relatively good. In addition, tensile strength was lowered by the initial small amount of water, but the effect on moisture mechanical properties was significantly reduced up to 336 h.

In the tensile stress-tensile strain curves of Fig. 52, C-0.5HNT/GFRP and A-0.5HNT/GFRP showed the same shape regardless of the crystallinity of HNT. However, in the case of C-0.5HNT/BFRP and A-0.5HNT/BFRP, the longer the immersion time, the smaller the slope. This suggests that HNT is not sufficiently bound in BFRP laminates, and is softened by the activation of water compared to Neat BFRP.

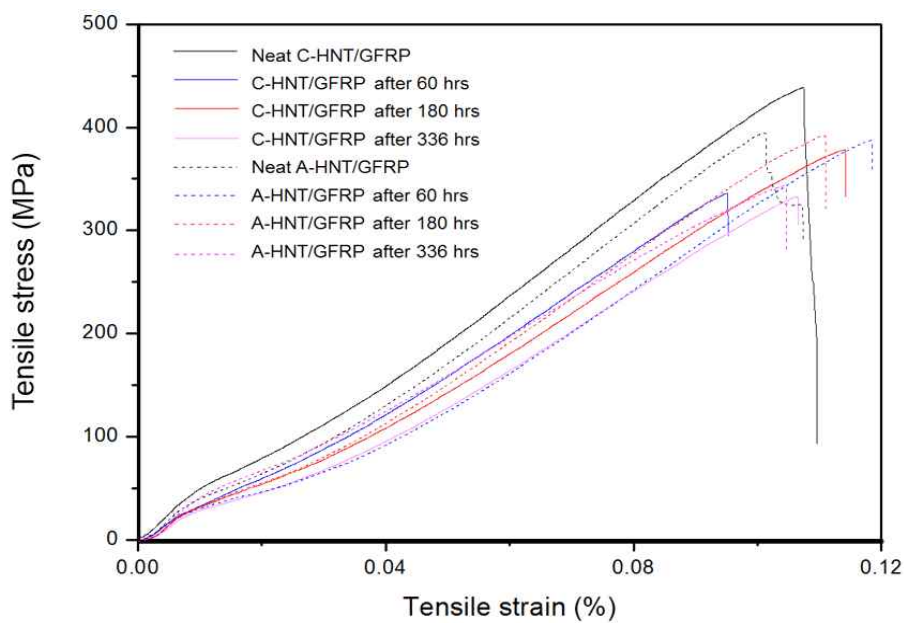


(a)

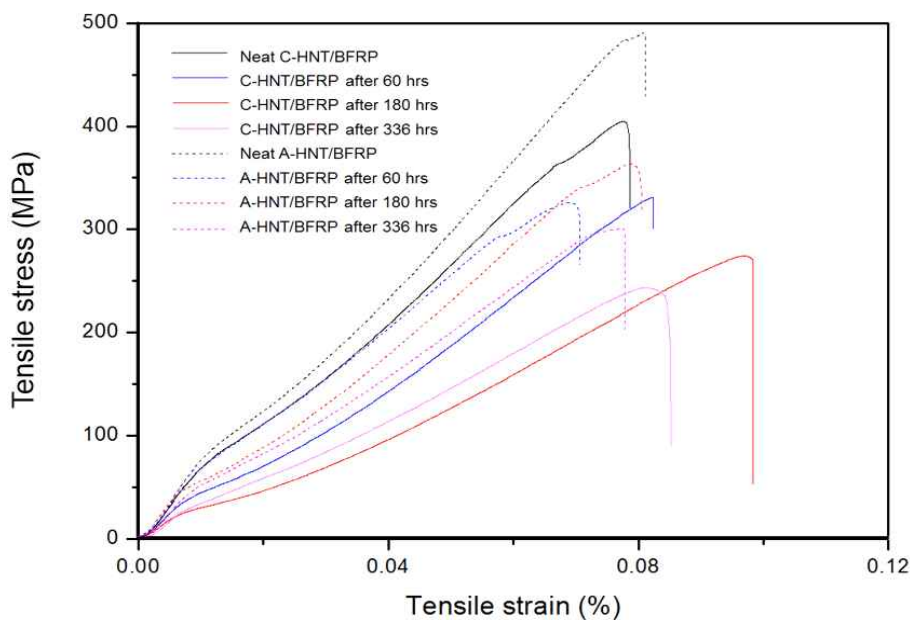


(b)

Fig. 51 Effect of water absorption rate on tensile strength in (a) 0.5HNT/GFRP and (b) 0.5HNT/BFRP according to crystallinity of HNT



(a)



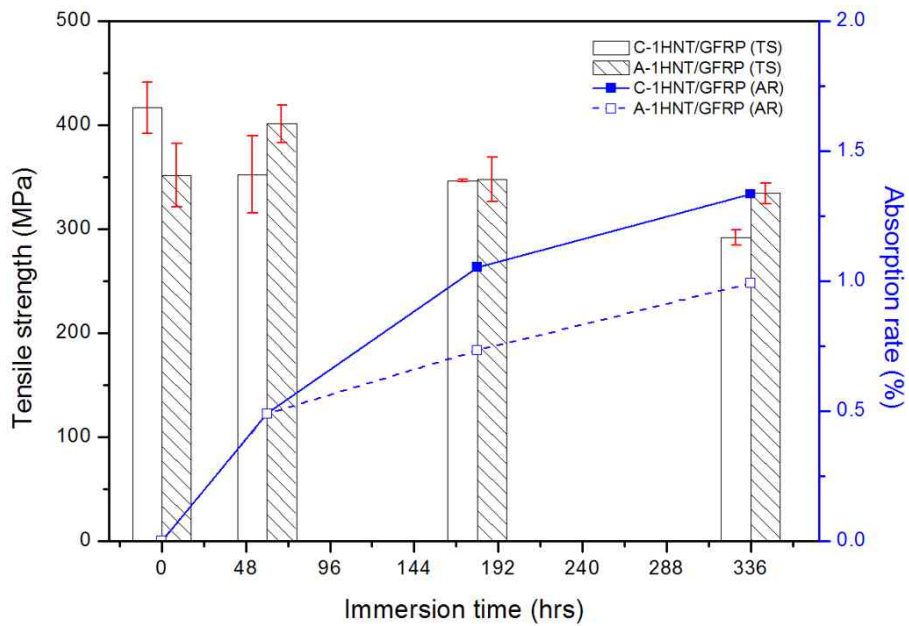
(b)

Fig. 52 Tensile stress-tensile strain curves with water immersion time in (a) 0.5HNT/GFRP and (b) 0.5HNT/BFRP according to crystallinity of HNT

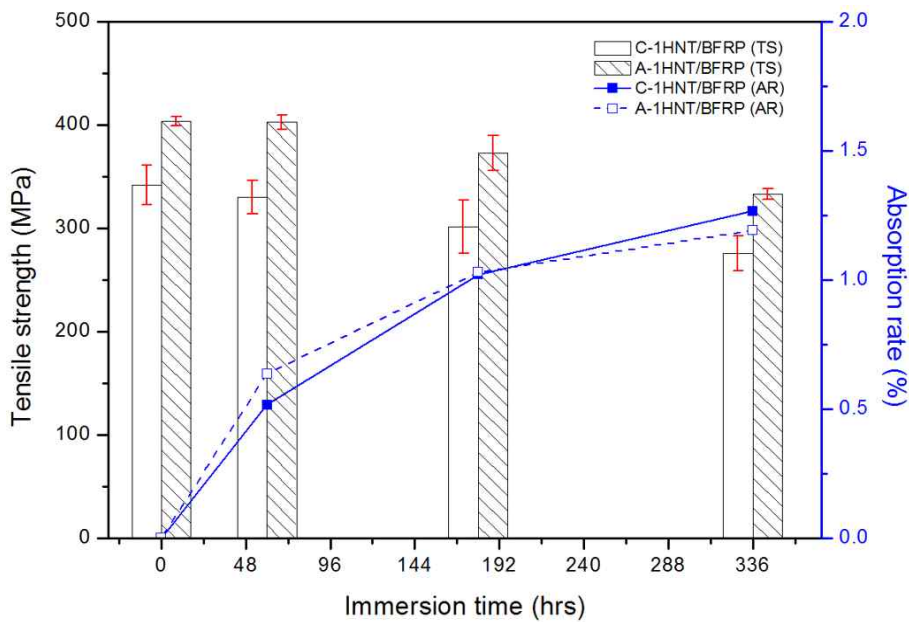
On the other hand, in 0.5HNT/BFRP, the initial tensile strengths were different. The initial tensile strength was improved in A-HNT, but decreased in C-HNT. This suggests that 0.5 wt.% C-HNT did not form a smooth bond in laminates, and it was found that it acted as an inhibitor to decrease the strength. Also, unlike Neat BFRP, the tensile strength decreased sharply from moisture immersion, compared to the moisture absorption rate. In other words, 0.5 wt.% C-HNT and A-HNT showed a relatively high reinforcing effect in GFRP laminates.

Fig. 53 shows the relationship between tensile strength and water absorption rate in 1HNT/GFRP and 1HNT/BFRP, depending on the crystalline state of HNT. Unlike 0.5 wt.% HNT, 1 wt.% HNT showed a large difference in moisture absorption rate depending on the crystal structure. The initial tensile strength was the same or decreased, compared to Neat GFRP and Neat BFRP. In general, the initial tensile strength tends to decrease with exposure to moisture. In A-1HNT/GFRP, the tensile strength increased when exposed to water for 60 h, and then decreased again afterwards. This is because unlike the mutual bonding force with EP, the filling state is changed from the powder state to the liquid state, while the EP is not diffused into the A-HNT cluster, which is considered to increase the resistance against the external load.

Particle clusters are mainly broken by external loads, because they behave like pores in composite laminates. However, filling the empty space with a relatively dense liquid absorbs the external load, and temporarily creates a reinforcing effect. The tensile stress—tensile strain graph of Fig. 54 shows that the C-1HNT/GFRP immersed in water for 60 h has a higher tensile modulus E than the initial value, which means higher stiffness. In addition, the overall water resistance was measured to be low.

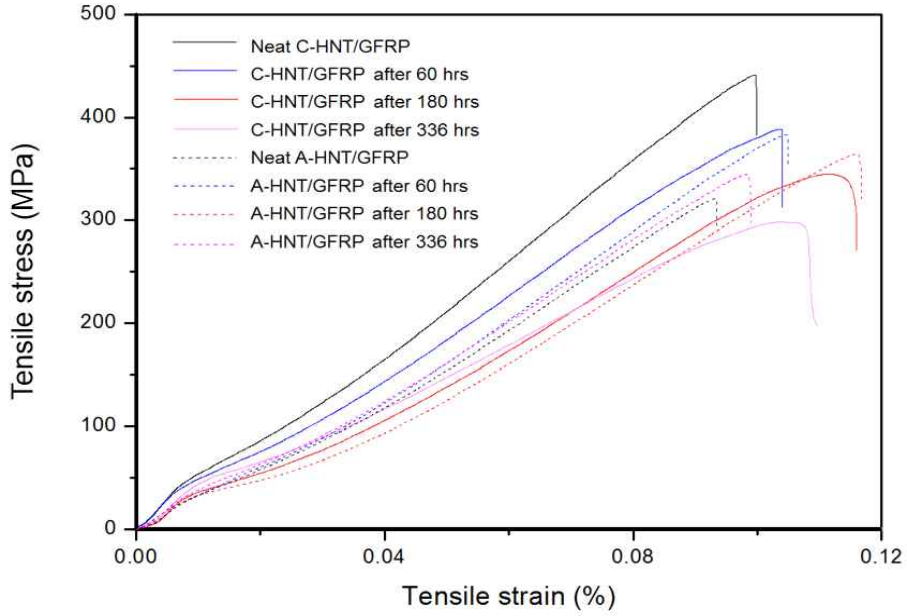


(a)

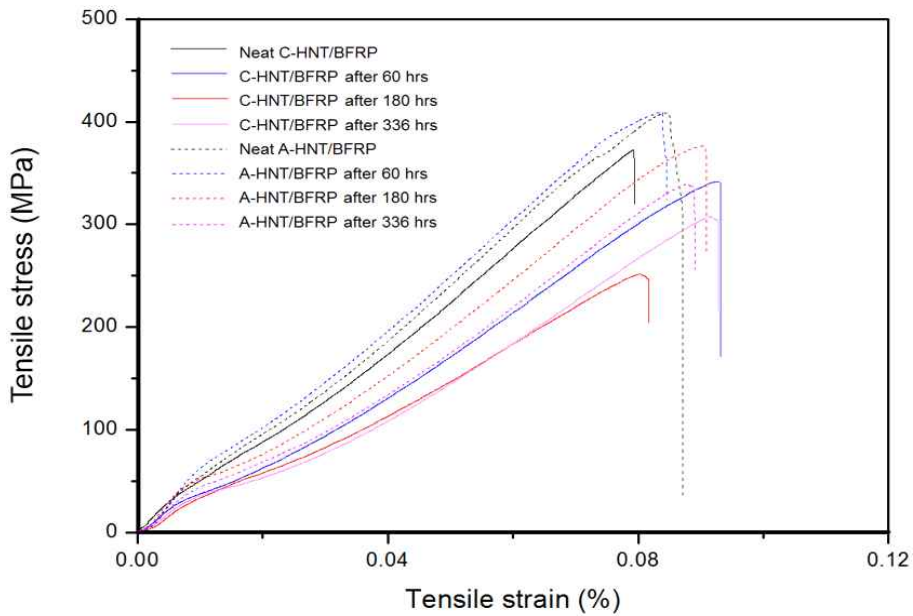


(b)

Fig. 53 Effect of water absorption rate on tensile strength in (a) 1HNT/GFRP and (b) 1HNT/BFRP according to crystallinity of HNT



(a)

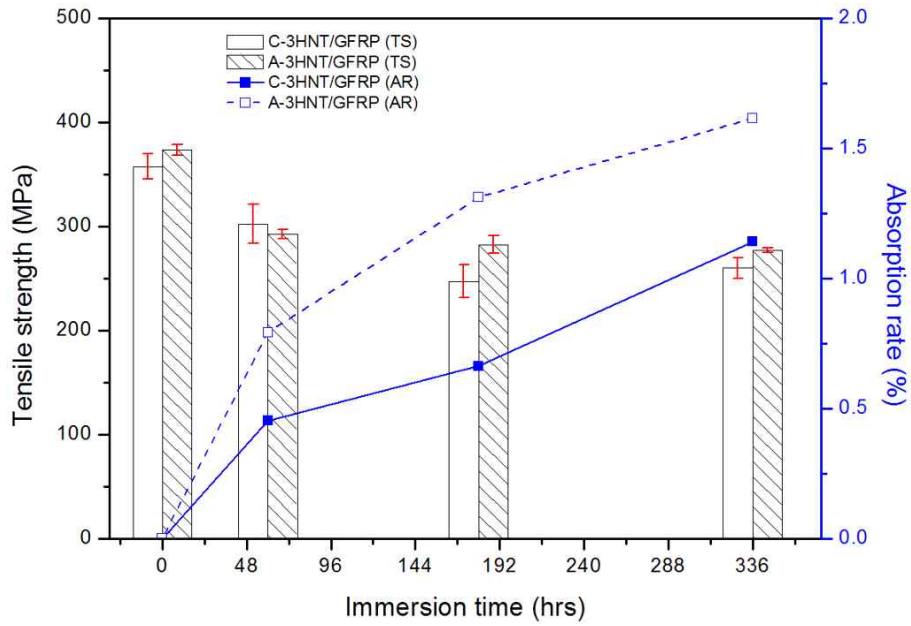


(b)

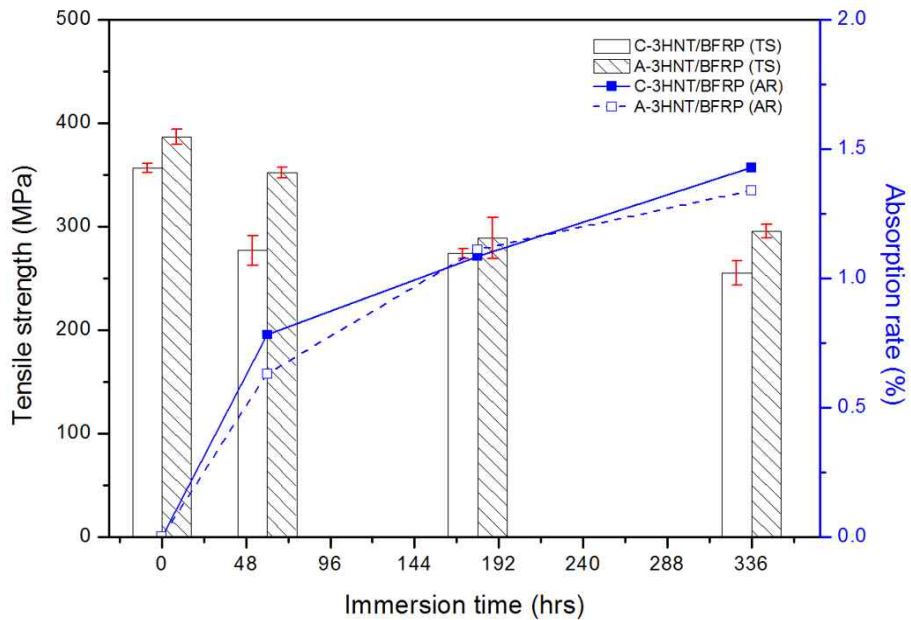
Fig. 54 Tensile stress-tensile strain curves with water immersion time in (a) 1HNT/GFRP and (b) 1HNT/BFRP according to crystallinity of HNT

In particular, the water resistance of C-HNT was relatively lower than that of A-HNT, and these HNTs seem to maintain a stable bonding state in BFRP laminates. In other words, in GFRP laminates, it is necessary to analyze the mechanism of bonding between HNT and GF, as well as the crystallinity of HNT. HNTs in BFRP laminates have a specific tendency to be integrated, but GF, EP, and HNT are independent in GFRP laminates. Therefore, it is necessary to analyze not only the state of dispersion between HNT and EP, but also the combined form at the surface of GF and BF.

Fig. 55 shows the results of HNT/GFRP and HNT/BFRP for 3 wt.% HNT. First, no reinforcing effect was observed due to the addition of HNT. As the amount of HNT was increased, the moisture absorption rate gradually increased. In the case of 3HNT/BFRP, regardless of the crystallinity of HNT, the same values were obtained for the moisture absorption rate, and it is considered that the stability of A-3HNT/BFRP with respect to moisture is relatively high by the modification of the hygroscopicity graph with immersion time. However, 3HNT/GFRP was significantly influenced by the crystallinity of HNT. In particular, the A-3HNT exhibited a significantly higher moisture absorption rate, resulting in softening of the material, but a relatively higher strength than C-HNT. As the amount of A-HNT added increases, the frequency of clusters increases, due to particle agglomeration. However, this does not directly damage the fiber reinforcement or matrix, but rather seals moisture inside the particles, and substantially increases the moisture stability of the material, compared to the moisture absorption rate. As shown in Fig. 56 shows that the addition of HNT increased the ductility by softening the material, but increased the yield, and contributed to improving the material's resistance to fracture.

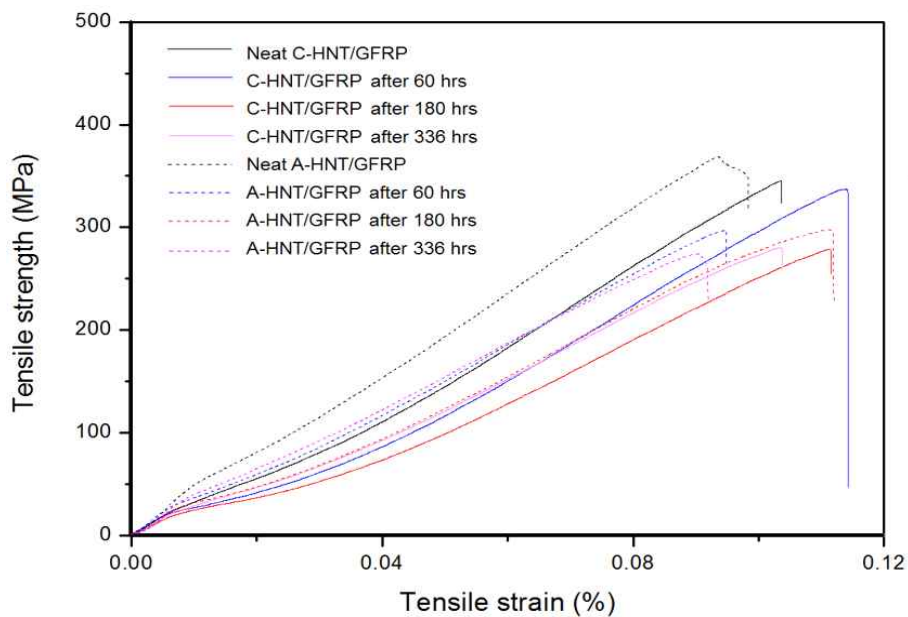


(a)

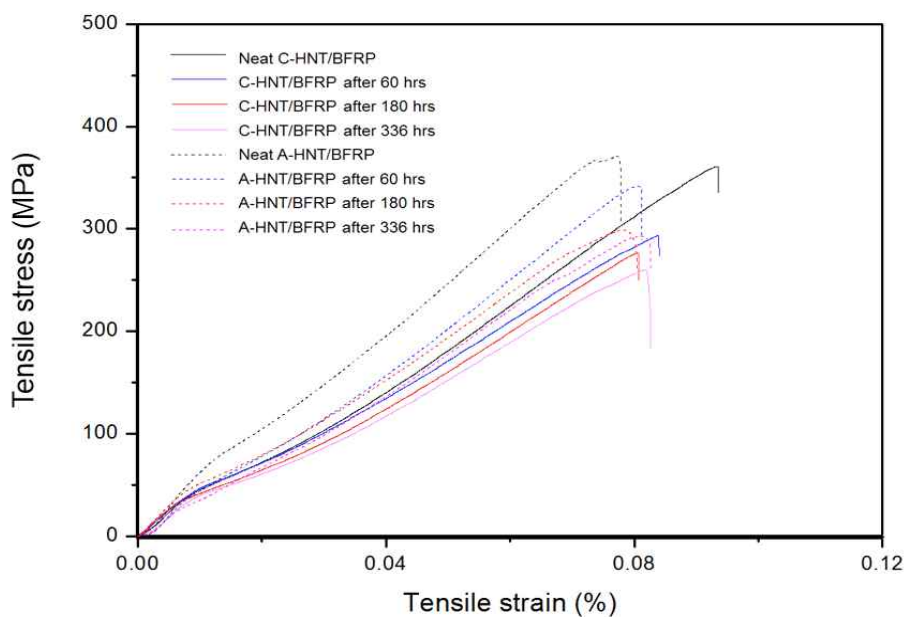


(b)

Fig. 55 Effect of water absorption rate on tensile strength in (a) 3HNT/GFRP and (b) 3HNT/BFRP according to crystallinity of HNT



(a)

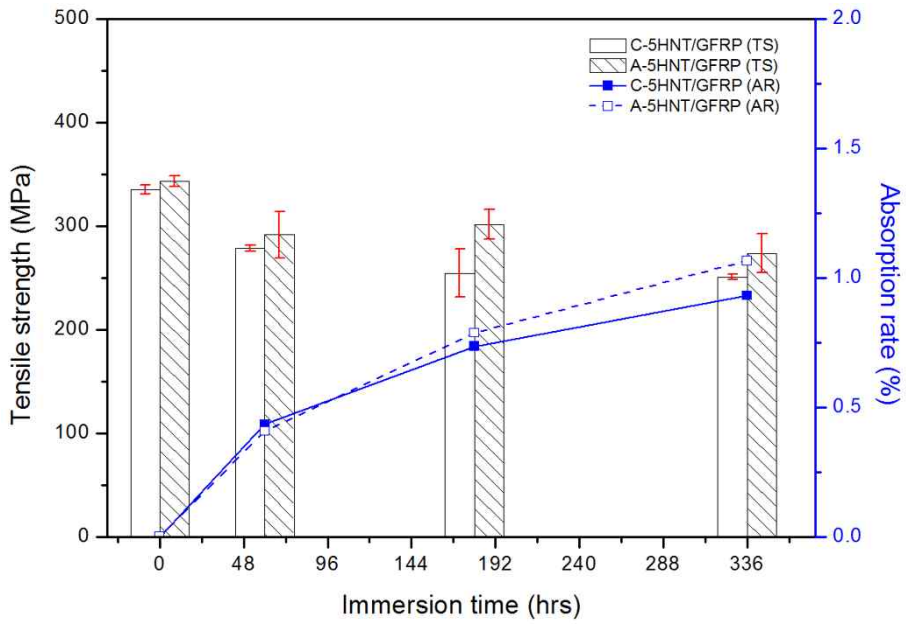


(b)

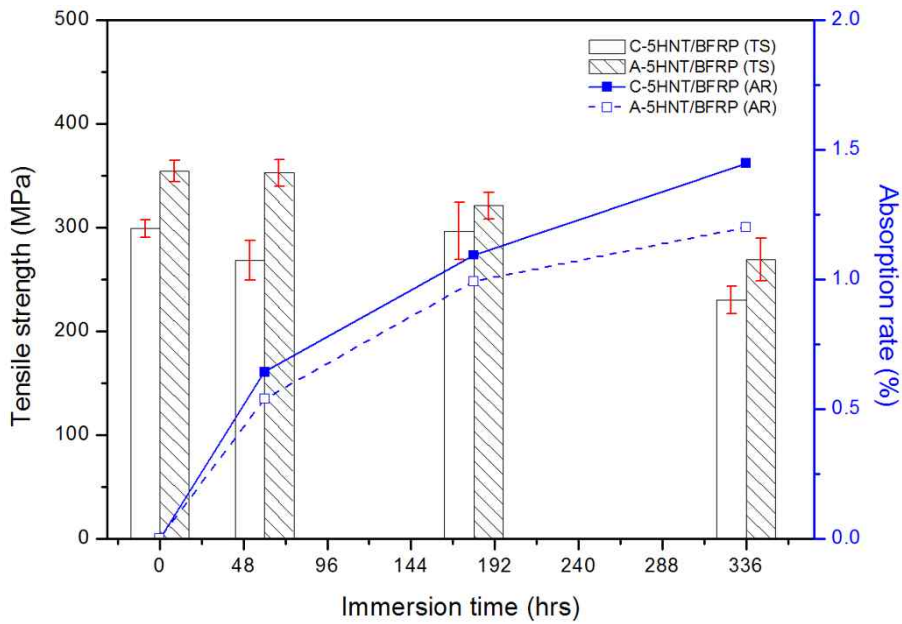
Fig. 56 Tensile stress-tensile strain curves with water immersion time in (a) 3HNT/GFRP and (b) 3HNT/BFRP according to crystallinity of HNT

Fig. 57 shows the results for 5 wt.% HNT. The tensile strength was lowered compared to the initial Neat GFRP and Neat BFRP, and a high moisture absorption rate was also measured with respect to the immersion time. However, C-HNT and A-HNT are similar to each other, suggesting similar absorption behavior in composite laminates. In particular, a large amount of HNT is considered to be a direct factor in lowering the tensile strength. As the HNT clusters are mass produced, the thickness of the surface layer surrounding the non-impregnated portion at the center of the cluster thickens, making it difficult for the water penetrate. In addition, the effect on the specific load varies, depending on the size and shape of the HNT cluster. Fig. 58 shows that there was almost no difference in the tensile modulus E from the initial mechanical properties before moisture absorption.

Therefore, in GFRP laminates, the crystallinity and content of HNT were affected by the mechanical properties and water resistance. In BFRP laminates, there was a difference in the size and shape of the clusters depending on the content of HNT. C-HNT and A-HNT commonly softened the material to increase ductility and delayed the arrival time to yield, reducing deformation by external load, and increasing resistance to damage. In particular, compared to C-HNT, A-HNT was relatively easy to migrate into and out of clusters due to moisture penetration and diffusion, and C-HNT was greatly influenced by the state of dispersion in EP. C-HNT is very likely to act as a factor to inhibit the properties of materials, such as stress concentration, rather than expressing the inherent functions. On the other hand, A-HNT is believed to contribute to the enhancement of stiffness by increasing the tensile modulus E , and preventing the water from directly damaging the material, by blocking moisture in the cluster after forming clusters of clusters.

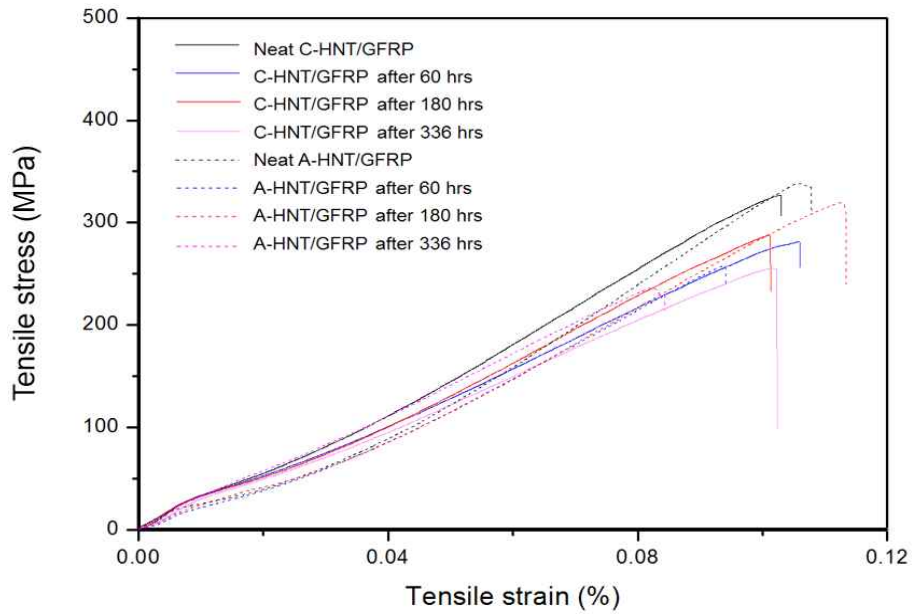


(a)

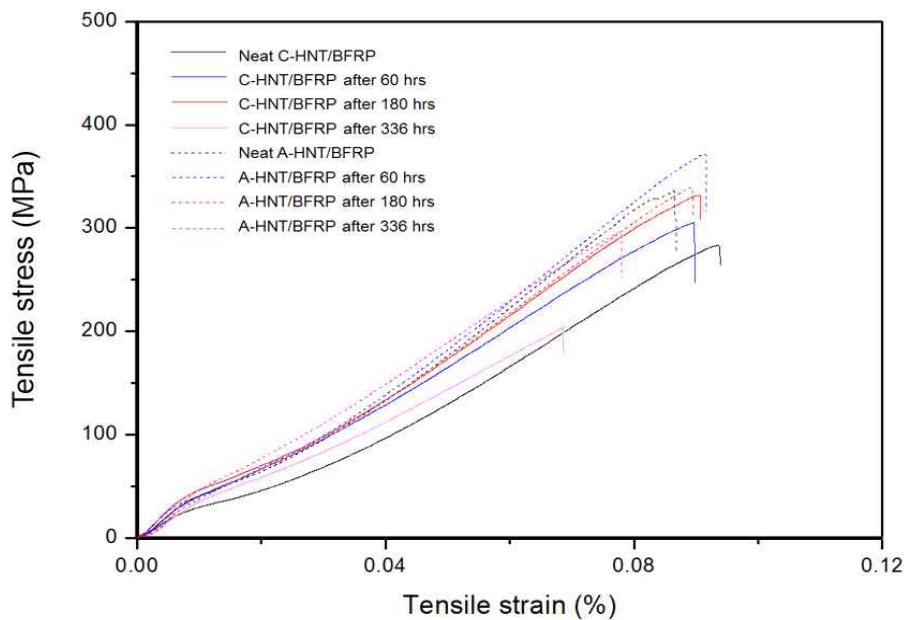


(b)

Fig. 57 Effect of water absorption rate on tensile strength in (a) 5HNT/GFRP and (b) 5HNT/BFRP according to crystallinity of HNT



(a)



(b)

Fig. 58 Tensile stress-tensile strain curves with water immersion time in (a) 5HNT/GFRP and (b) 5HNT/BFRP according to crystallinity of HNT

Previous studies have shown that silica nanoparticles contribute to the improvement of stiffness and toughness of EP; the tensile modulus E can be increased by up to 20 %, and yields greater than that of pure EP can be achieved (Rosso, et al., 2006). In addition, in dense microstructures, nanoparticles can also form voids, which can promote hydration due to the reactivity of the nanoparticles.

4.4.2 Fracture behavior analysis

In this section, the tensile failure shapes of open-hole specimens were observed from a macroscopic point of view, after tensile testing of the HNT/GFRP and HNT/BFRP immersed in distilled water for (0, 60, 180, 336) h. In composite laminates, delamination is generally one of the important failure mechanisms in composites, because of the low interlaminar strength. In isotropic laminates, interlaminar delamination is mainly removed by delamination from free edges. However, delamination is significantly affected by the notch tensile strength, which is the fracture damage due to the stress concentration at the notch (Wisnom & Hallett, 2009; Kedward, et al., 1989; Wisnom, et al., 1996). Therefore, in this study, the HNT dispersed inside of the interlaminar laminates was observed as a stress concentration region around the HNT, due to the HNT acting as a notch for the external stress, and the state of dispersion of the HNT was analyzed. The open-hole tensile specimen was used, and the failure shape of HNT/GFRP and HNT/BFRP according to the crystallinity of HNT was observed based on 6 mm hole.

Table 5 shows the Neat GFRP and Neat BFRP fracture patterns. Generally, cracks occurred along the fibers arranged in the tensile direction, and these cracks were initiated based on the central hole. They were not completely separated, and it was confirmed that the hole was extended in the loading direction. Relatively Neat GFRP was more cracked than Neat BFRP, and fiber loosening at the interface was observed to be reduced. On the other hand, in Neat BFRP, delamination occurred partially along the fiber filament interface.

Table 6 compares C-0.5HNT/GFRP with C-0.5HNT/BFRP, similar to Neat GFRP and Neat BFRP. The longer the immersion time, the more cracks that were generated and propagated.

Table 5 Open-hole tensile failure shape of HNT/FRP nanocomposites with immersion time in hygroscopic environment at 70°C; Neat GFRP and Neat BFRP


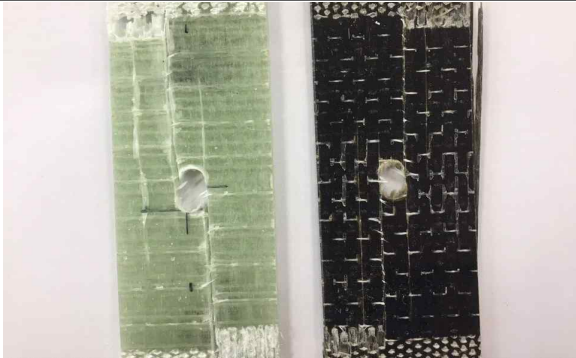
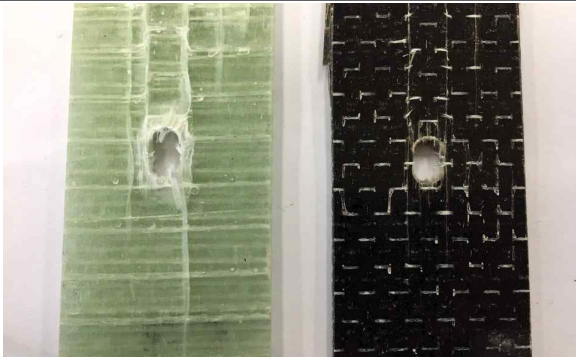

Samples	Water immersion time (h)	
	0	60
Neat FRP (GF-BF)		
	180	336 (14 days)
		

Table 6 Open-hole tensile failure shape of HNT/FRP nanocomposites with immersion time in hygroscopic environment at 70°C; C-0.5HNT/GFRP and C-0.5HNT/BFRP

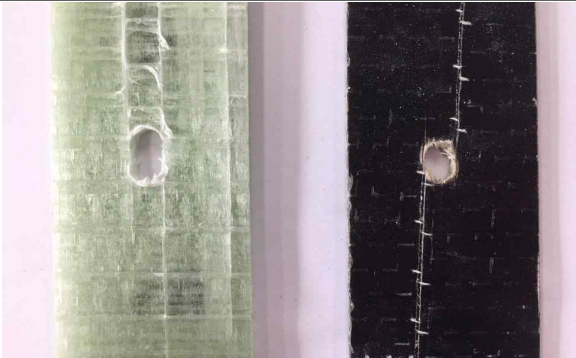

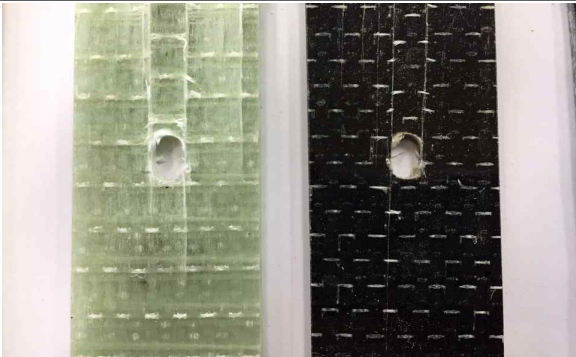
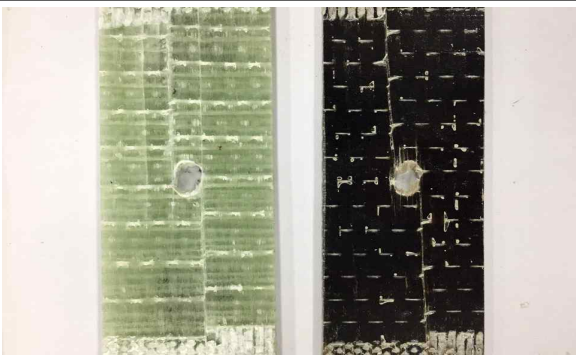
Samples	Water immersion time (h)	
	0	60
C-0.5HNT/FRP (GF-BF)		
	180	336 (14 days)
		

Table 7 shows the tensile failure shape of C-1HNT/GFRP and C-1HNT/BFRP. In the case of C-1HNT/GFRP, partial delamination of GF and EP was observed. As the immersion time increased, the slip phenomenon was small with respect to the hole, and separation into the loading direction occurred. In the case of C-1HNT/BFRP, the delamination of BF and EP was promoted inside the hole based on the hole, and the center of the hole was swollen, and the edge was relatively not delaminated.

Table 8 compares C-3HNT/GFRP with C-3HNT/BFRP. As the amount of HNT was increased, both the delamination between the filament filaments and the layer delamination became severe. Also, on the surface, multiple cracks and pull-out phenomena were observed around the cracks, and the weakest holes and edges were damaged at the same time. This suggests a local vulnerability to moisture at locations where HNTs are involved.

Table 9 compares C-5HNT/GFRP and C-5HNT/BFRP. C-5HNT/GFRP relatively lowered in rigidity before immersion in water, and reached a complete separation failure, due to slip in tensile direction due to external load. It was judged that the material was softened by moisture and increased ductility after the moisture absorption, and cracks at the edge were observed. In the case of C-5HNT/BFRP, fracture was found due to local cracking, and delamination of the fiber was observed at the edge.

Table 10 compares A-0.5HNT/GFRP with A-0.5HNT/BFRP. Overall, interlaminar delamination due to fiber lifting was formed around the hole and edge. The longer the immersion time, the shorter the time to fracture, which could be deduced through the shape of the hole.

Table 7 Open-hole tensile failure shape of HNT/FRP nanocomposites with immersion time in hygroscopic environment at 70°C; C-1HNT/GFRP and C-1HNT/BFRP


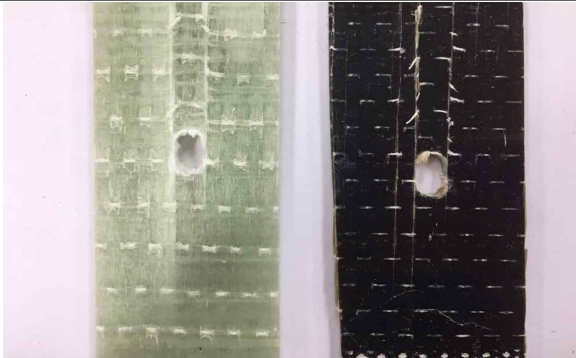

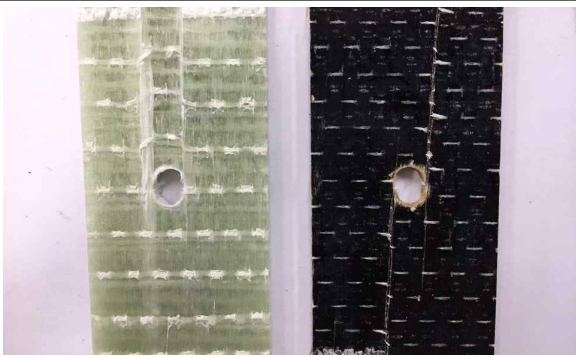
Samples	Water immersion time (h)	
	0	60
C-1HNT/FRP (GF-BF)		
	180	336 (14 days)
		

Table 8 Open-hole tensile failure shape of HNT/FRP nanocomposites with immersion time in hygroscopic environment at 70°C; C-3HNT/GFRP and C-3HNT/BFRP

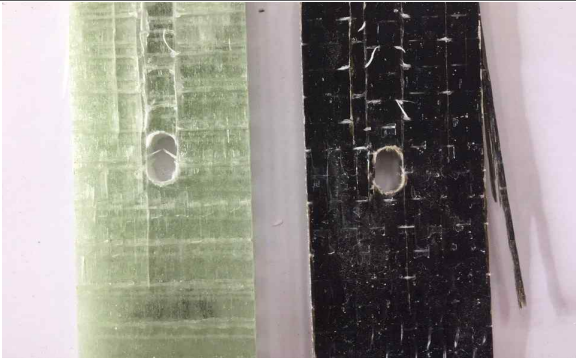

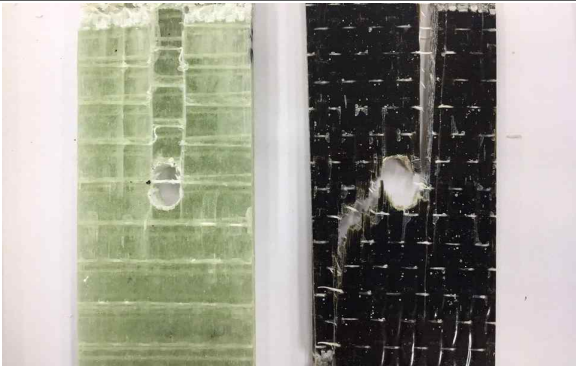
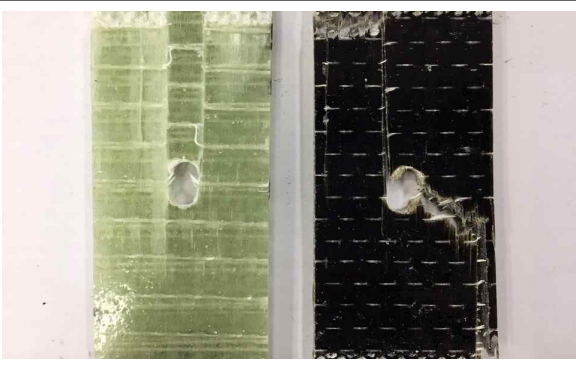
Samples	Water immersion time (h)	
	0	60
C-3HNT/FRP (GF-BF)		
	180	336 (14 days)
		

Table 9 Open-hole tensile failure shape of HNT/FRP nanocomposites with immersion time in hygroscopic environment at 70°C; C-5HNT/GFRP and C-5HNT/BFRP

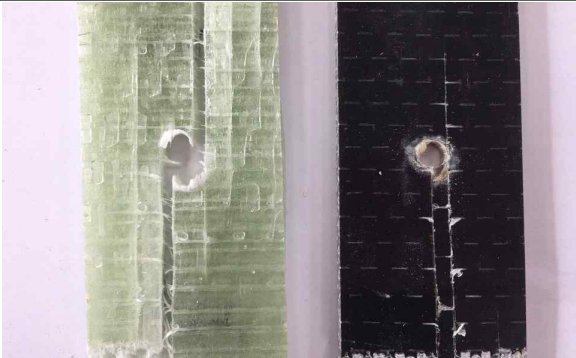


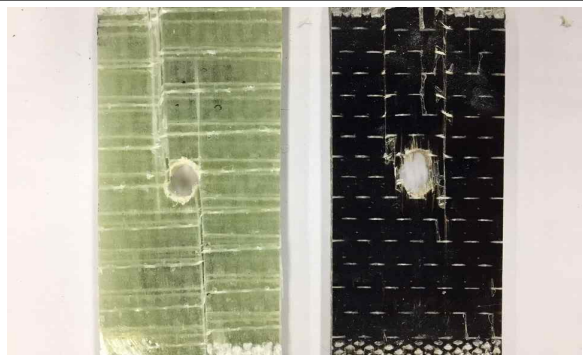
Samples	Water immersion time (h)	
	0	60
C-5HNT/FRP (GF-BF)		
	180	336 (14 days)
		

Table 10 Open-hole tensile failure shape of HNT/FRP nanocomposites with immersion time in hygroscopic environment at 70°C; A-0.5HNT/GFRP and A-0.5HNT/BFRP


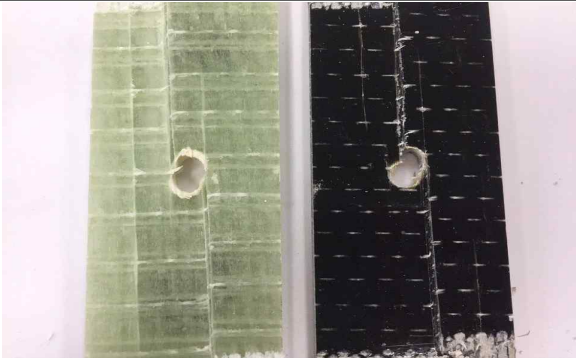


Samples	Water immersion time (h)	
	0	60
A-0.5HNT/FRP (GF-BF)		
	180	336 (14 days)
		

Table 11 Open-hole tensile failure shape of HNT/FRP nanocomposites with immersion time in hygroscopic environment at 70°C; A-1HNT/GFRP and A-1HNT/BFRP



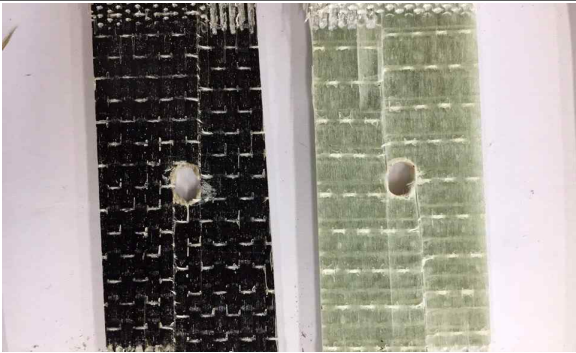
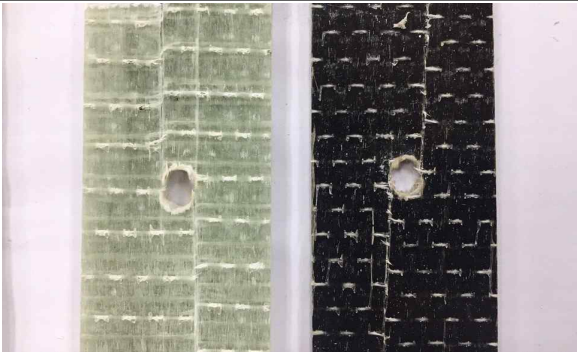
Samples	Water immersion time (h)	
	0	60
A-1HNT/FRP (GF-BF)		
	180	336 (14 days)
		

Table 11 compares the fracture patterns of A-1HNT/GFRP and A-1HNT/BFRP. In the case of A-1HNT/GFRP, the water immersion time and layered delamination phenomena were in inverse proportion. Layered delamination mainly occurred due to fiber floatation. In the case of A-1HNT/BFRP, the cracks generated around the hole part progressed diagonally, rather than in the tensile direction, which is considered to have a large effect due to the slip between the fiber filaments.

Table 12 compares the fracture patterns of A-3HNT/GFRP and A-3HNT/BFRP. Compared with less than 3 wt.% HNT in A-3HNT/GFRP and C-3HNT/GFRP, the interlaminar bond at the laminates interface was stable, and was destroyed by the generation and propagation of surface cracks in the tensile direction. A-3HNT/BFRP also showed no interlaminar delamination and fiber floatation when compared to C-3HNT/BFRP, and no abnormalities were found in the fracture pattern with water immersion time.

Table 13 compares the fracture patterns of A-5HNT/GFRP and A-5HNT/BFRP according to water immersion time. Overall, when compared to A-3HNT/GFRP, delamination of A-3HNT/BFRP occurred at the hole, surface, and edge, fiber pull-out was observed before water immersion, and cracks promoted by hole slip were more prominent than those of A-3HNT/BFRP.

In summary, the bonding strength of A-HNT to the interlayer interface of laminates was stronger than that of C-HNT, and there was less delamination between fiber filaments and fiber filaments. Although the tendency depending on the amount of HNT could not be specified, it is considered that the effect of the crystallinity of HNT on the fracture pattern is significant. In the open-hole tensile test, it is considered that the macroscopic analysis of crack initiation and fracture termination between crack initiation part and interlaminar fracture is effective in determining the strength inhibition factors, except for the central part of the stress hole.

Table 12 Open-hole tensile failure shape of HNT/FRP nanocomposites with immersion time in hygroscopic environment at 70°C; A-3HNT/GFRP and A-3HNT/BFRP

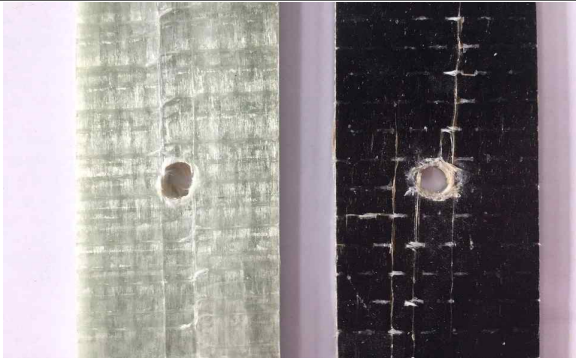
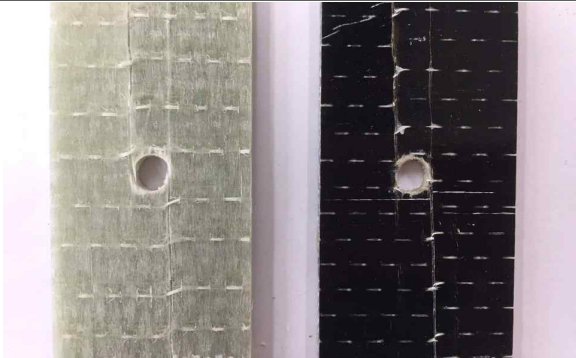
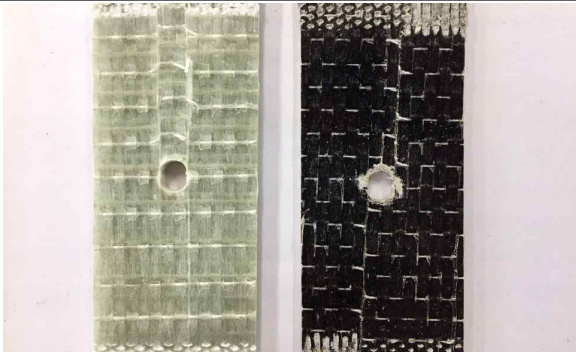



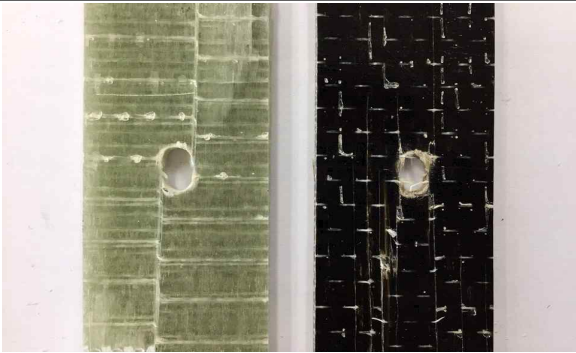
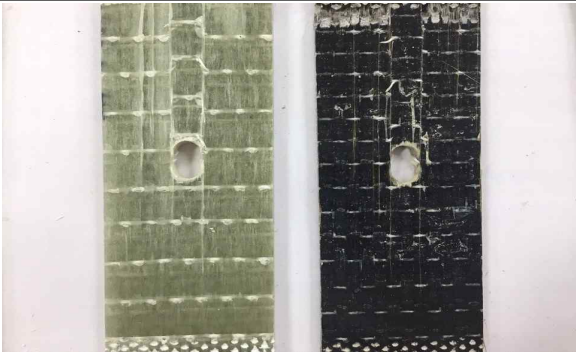
Samples	Water immersion time (h)	
	0	60
A-3HNT/FRP (GF-BF)		
	180	336 (14 days)
		

Table 13 Open-hole tensile failure shape of HNT/FRP nanocomposites with immersion time in hygroscopic environment at 70°C; A-5HNT/GFRP and A-5HNT/BFRP

Samples	Water immersion time (h)	
	0	60
A-5HNT/FRP (GF-BF)		
	180	336 (14 days)
		

4.5 Dispersibility

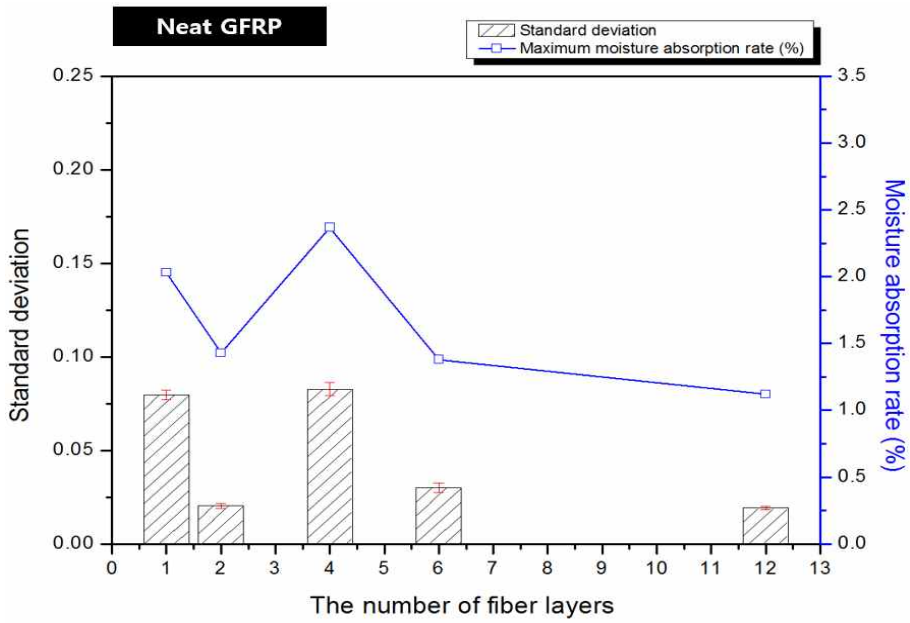
In HNT/EP matrix FRP nanocomposites, the dispersibility of HNT as a nanofiller is an important factor in the physical properties of the material, and was influenced not only by the shape of the product but also by the external molding conditions such as temperature and humidity. Thus, it is necessary to establish the optimum dispersion conditions by analyzing the dispersion behavior of HNT. However, the dispersion inhibition factors of nanoparticles are different from those of microparticles. This can be attributed to their different processing factors. Therefore, in this study, the effects of the polymer curing factors on the HNT dispersibility and shape of the nanocomposite were investigated. In order to investigate the effect of the HNT/EP colloidal solution on the permeability coefficient of the nanocomposite (when impregnated with GF and BF), the particle parameters such as the HNT binding force, cohesion, and free mobility were varied depending on the number of fabric layers forming the laminates and the changes in the absorption rate.

Fig. 59 shows the absorption rates and their standard deviations of neat GFRP and neat BFRP (in the A—H columns of the plate) as a function of the number fiber layers. The uniform states of HNT dispersion in each region of the plate were compared. In the case of neat GFRP, the variations in the moisture absorption rate and standard deviation of each region showed similar trends. In the case of neat BFRP, the absorption rate decreased with an increase in the thickness of the laminates. However, relatively high standard deviations were measured in the 1 and 4 layers as in neat GFRP, depending on the region. In the case of neat BFRP, the absorption rate decreased with an increase in the thickness of the laminates. However, relatively high standard deviations were measured in the 1 and 4 layers as in neat GFRP,

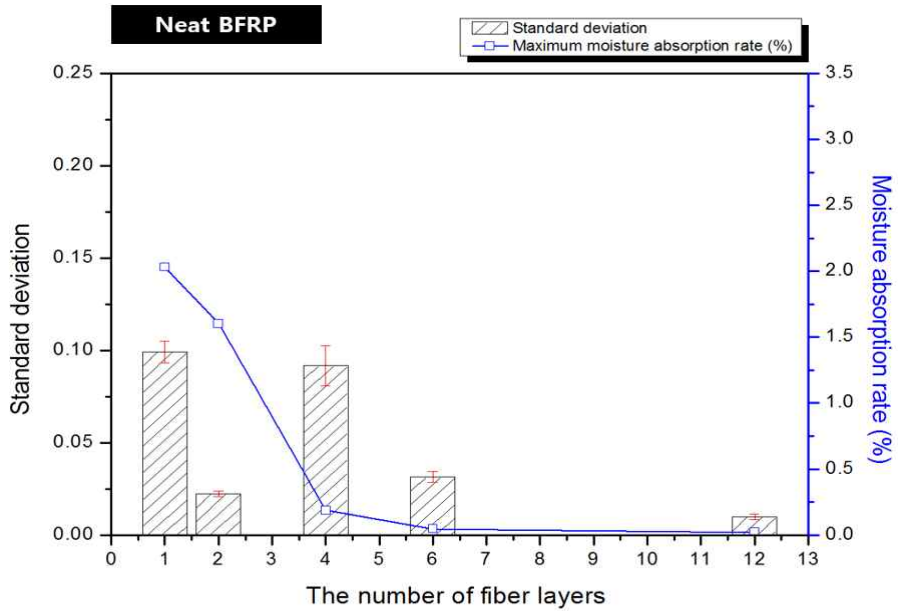
depending on the region. This is because the viscosity of EP decreases with an increase in the temperature of the curing system. Moreover, the degree of freedom of movement of EP in the edge regions of A, B, G, and H increased. This resulted in EP loss, which caused a difference in the volume fraction of the fibers and EP per unit area and the area deteriorated by the water environment. Unlike the case when 1 layer was used, when 4 layers were used, the effect of the trapped pores at the laminate interface was relatively large during the vacuum forming process.

Fig. 60 shows the dispersibility of C-0.5HNT/GFRP and C-0.5HNT/BFRP. The state of dispersion of the plate area in C-0.5HNT/GFRP and C-0.5HNT/BFRP was more stable than that in neat GFRP and neat BFRP. However, the moisture absorption rates of C-0.5HNT/GFRP and C-0.5HNT/BFRP increased with an increase in the number of fiber layers. In general, the absorption rates of C-0.5HNT/GFRP and C-0.5/BFRP in all the regions were proportional to their standard deviations.

As shown in Fig. 61, A-0.5HNT/GFRP and A-0.5HNT/BFRP showed the lowest deviation when 12 plies were used. However, the moisture absorption rate of A-0.5HNT/BFRP was higher than that of A-0.5HNT/GFRP because of the degradation of EP. In addition, the rapid increase in the moisture absorption rate when two plies were used, was not significantly affected by the HNTs acting on the mutual binding force of EP and GF even though the initial one ply area deviation was small, as in A-0.5HNT/GFRP-2. On the other hand, in A-0.5HNT/BFRP, the regional deviation was relatively high and the moisture absorption rate was the lowest when four plies were used. This is partly because of the decrease in the mobility of HNTs due to resin shrinkage.

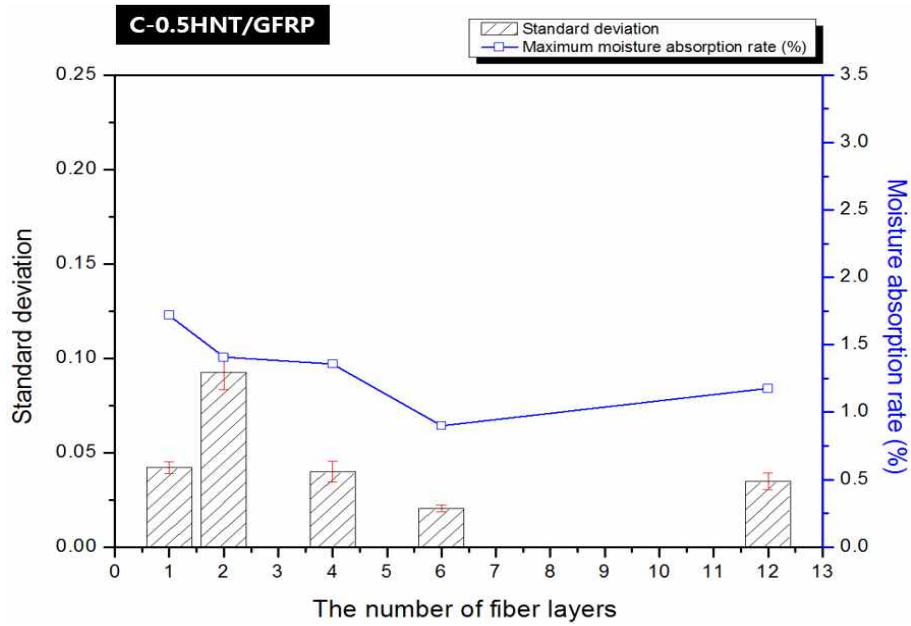


(a)

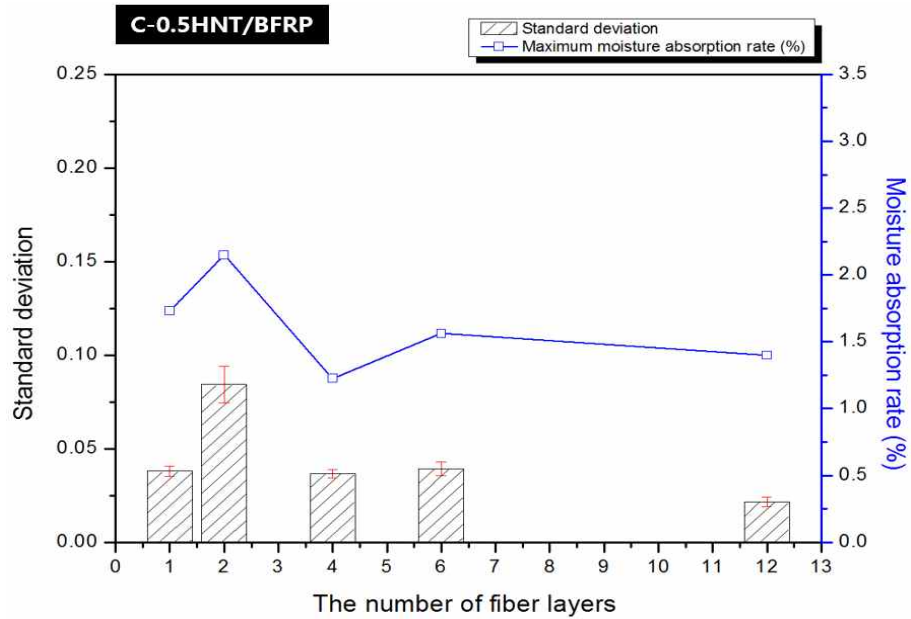


(b)

Fig. 59 Analysis of the state of HNT dispersion in composite laminates through moisture rate and variation with laminated fiber plies; (a) Neat GFRP and (b) Neat BFRP

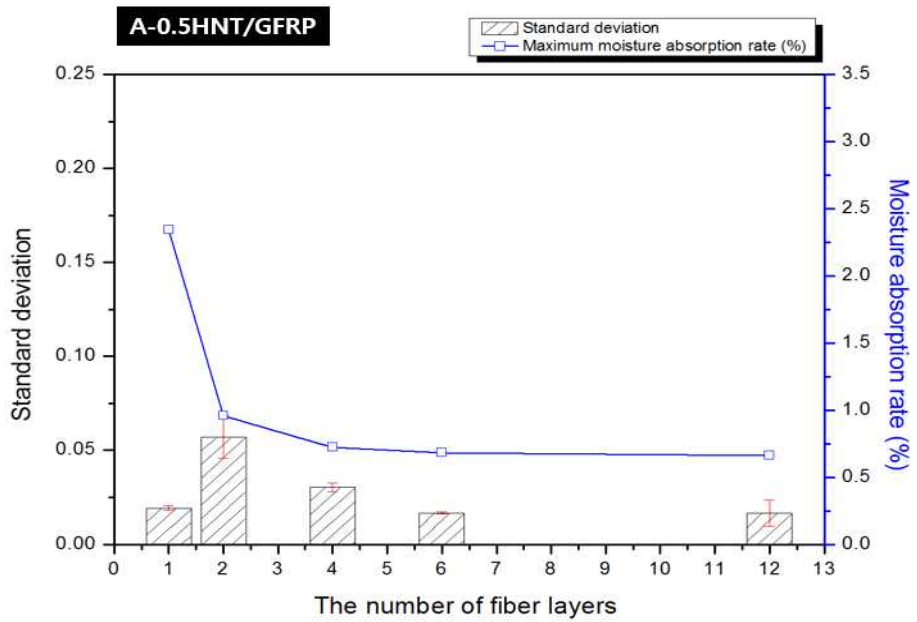


(a)

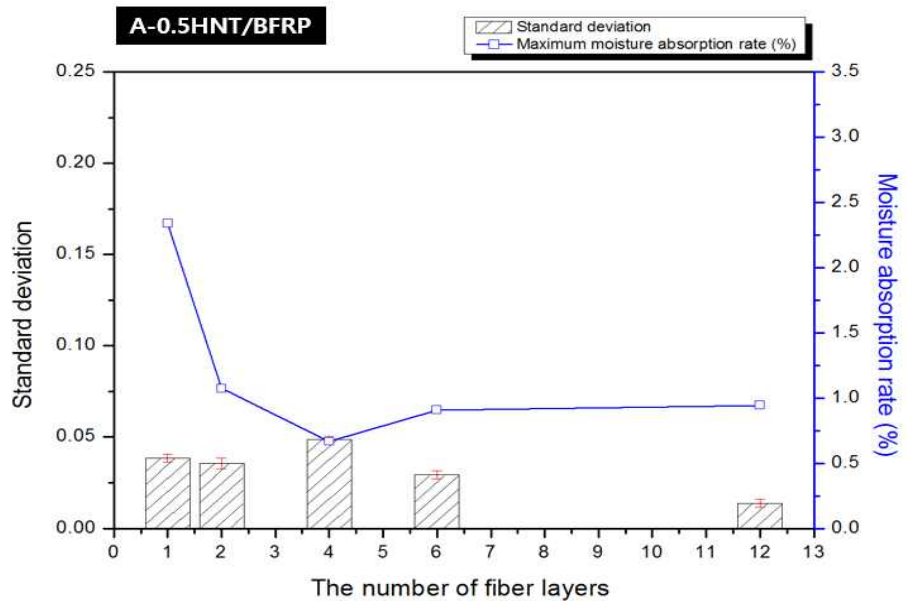


(b)

Fig. 60 Analysis of the state of HNT dispersion in composite laminates through moisture rate and variation with laminated fiber plies; (a) C-0.5HNT/GFRP and (b) C-0.5HNT/BFRP



(a)



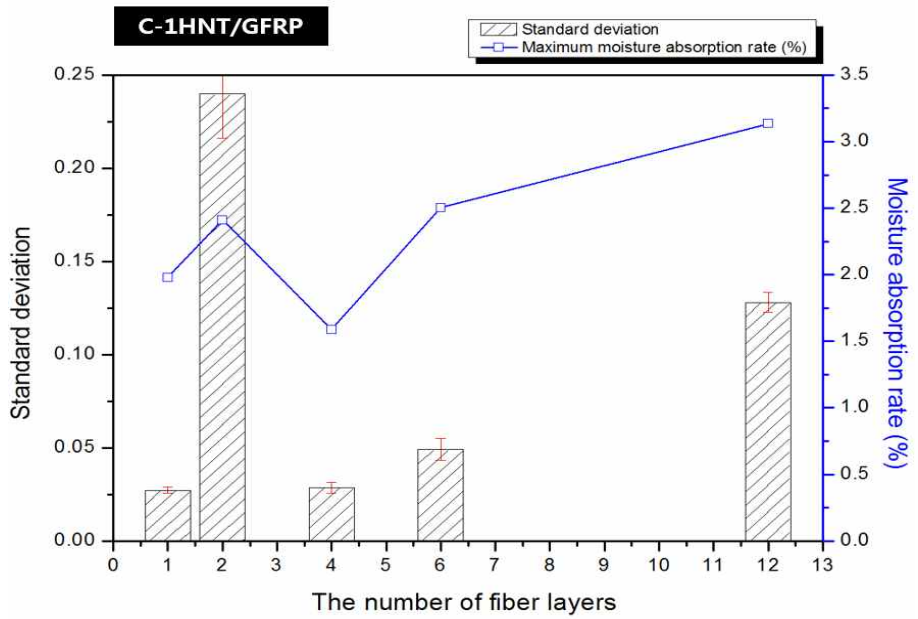
(b)

Fig. 61 Analysis of the state of HNT dispersion in composite laminates through moisture rate and variation with laminated fiber plies; (a) A-0.5HNT/GFRP and (b) A-0.5HNT/BFRP

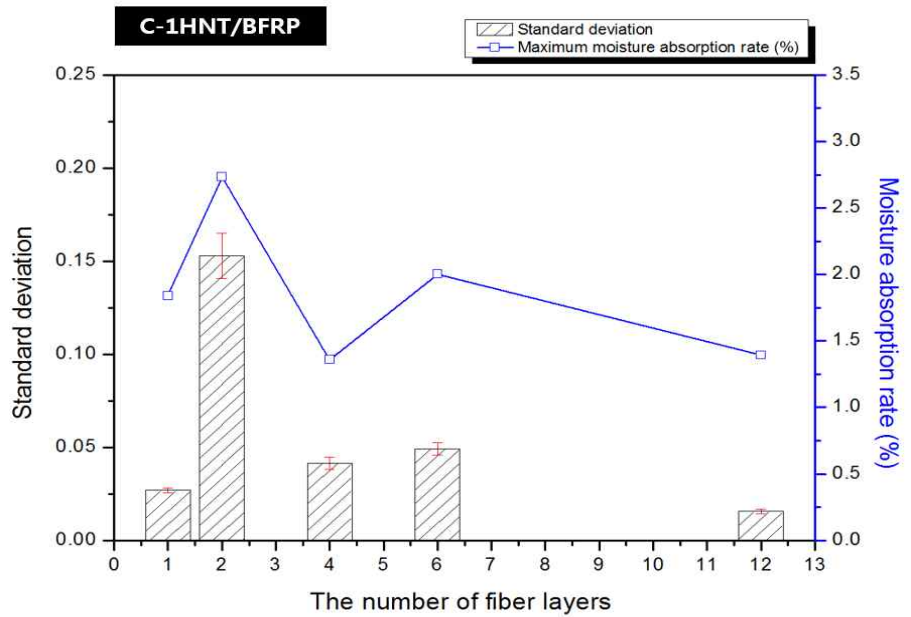
Fig. 62 shows the moisture absorption rates of C-1HNT/GFRP-2 and C-1HNT/BFRP-2. A large difference was observed in moisture absorption rates of the two samples when two plies were used. This indicates that the highly cohesive force between the HNT particles in C-1HNT/GFRP-2 and C-1HNT/BFRP-2 reached a very weak state in water. With an increase in the number of laminate layers, the area-specific deviations decreased. However, the regional deviations increased again in C-1HNT/GFRP-12. This is because of the unstable binding or mixed state between C-HNT and GFRP, and no consistent trend was observed.

Fig. 63 shows the moisture absorption rate of A-1HNT/GFRP and A-1HNT/BFRP. The area-specific deviations decreased with an increase in the number of fiber layers in both the samples and the moisture absorption rate became constant. The constant moisture absorption rate indicates that HNT was stably dispersed in EP and there was little re-aggregation by the curing system. A-1HNT/ FRP showed a stable binding pattern as compared to C-1HNT/BFRP.

As shown in Fig. 64, C-3HNT/GFRP-1 showed a very large variation in area, indicating that the aggregation of HNT occurred on the fiber surface not at the interface. C-3HNT/BFRP-1 showed a large area-dependent variation. This can be attributed to the partial agglomeration in C-3HNT/BFRP-1 when four and five plies were used. However, C-3HNT/GFRP suppressed the formation of HNT clusters and resin degradation at the interface. With an increase in the number of layers, it decreased because of moisture per region; however, the moisture absorption rate did not show any tendency. This can be attributed to the deterioration of EP, which was not affected by HNT.

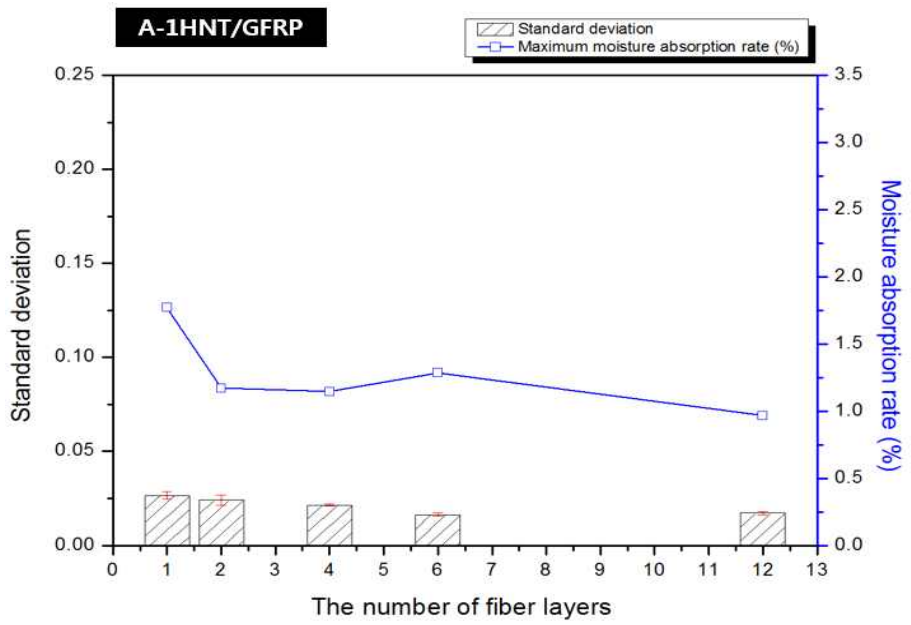


(a)

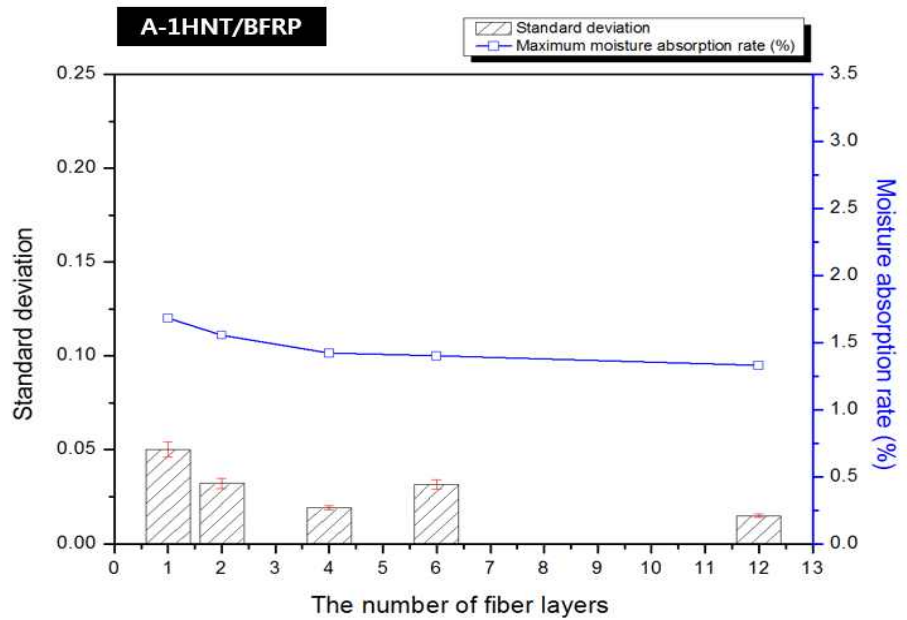


(b)

Fig. 62 Analysis of the state of HNT dispersion in composite laminates through moisture rate and variation with laminated fiber plies; (a) C-1HNT/GFRP and (b) C-1HNT/BFRP



(a)



(b)

Fig. 63 Analysis of the state of HNT dispersion in composite laminates through moisture rate and variation with laminated fiber plies; (a) A-1HNT/GFRP and (b) A-1HNT/BFRP

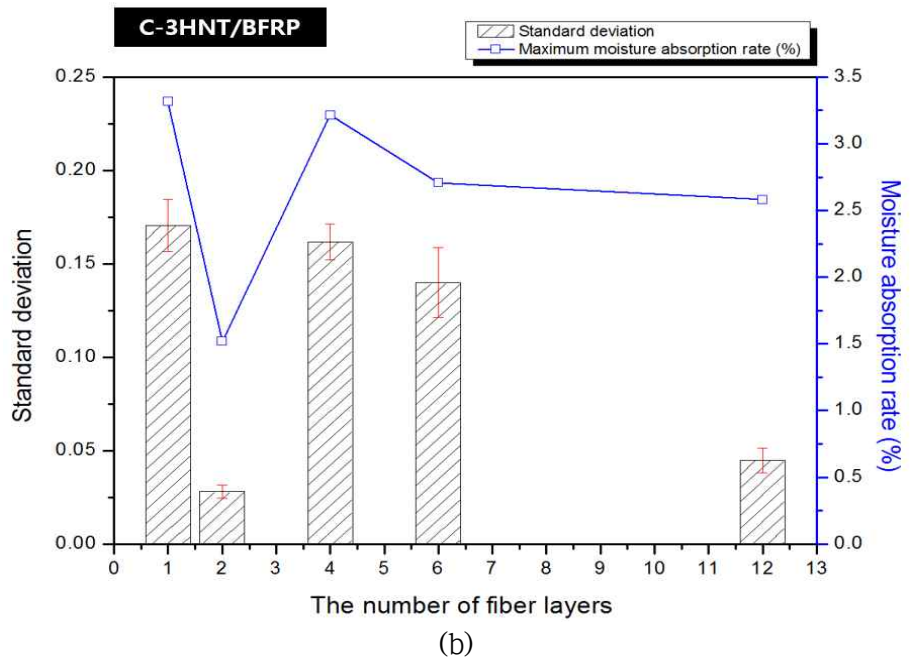
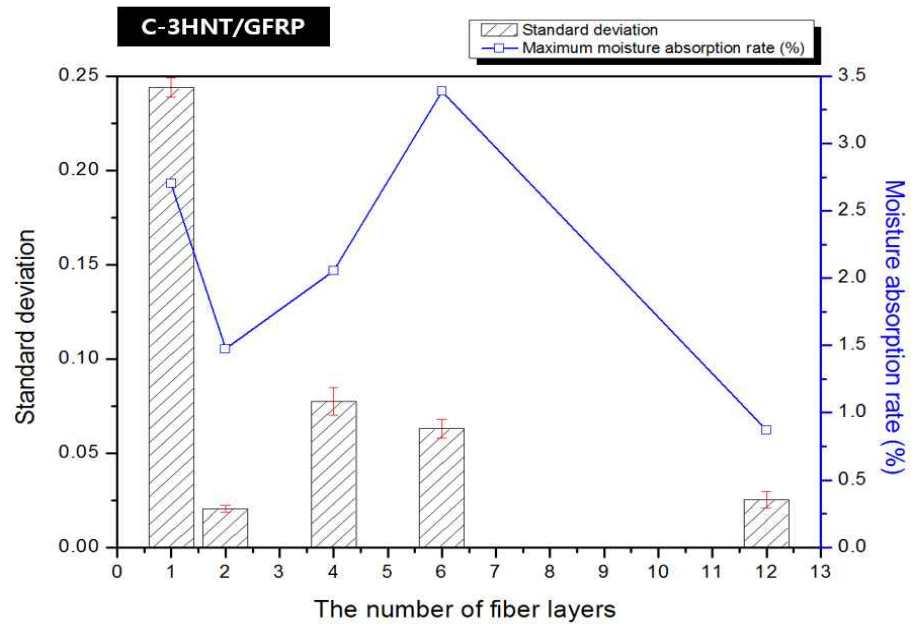
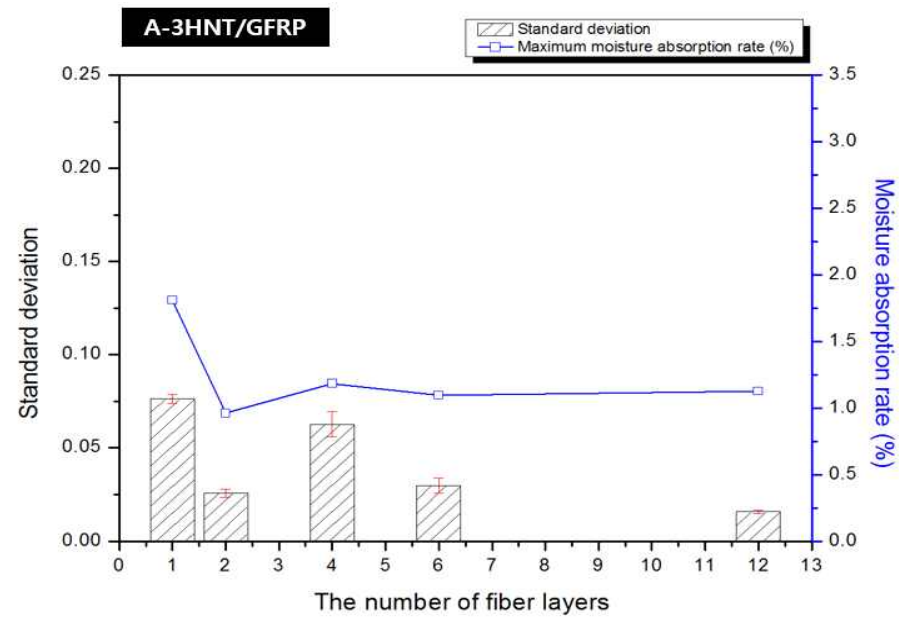


Fig. 64 Analysis of the state of HNT dispersion in composite laminates through moisture rate and variation with laminated fiber plies; (a) C-3HNT/GFRP and (b) C-3HNT/BFRP

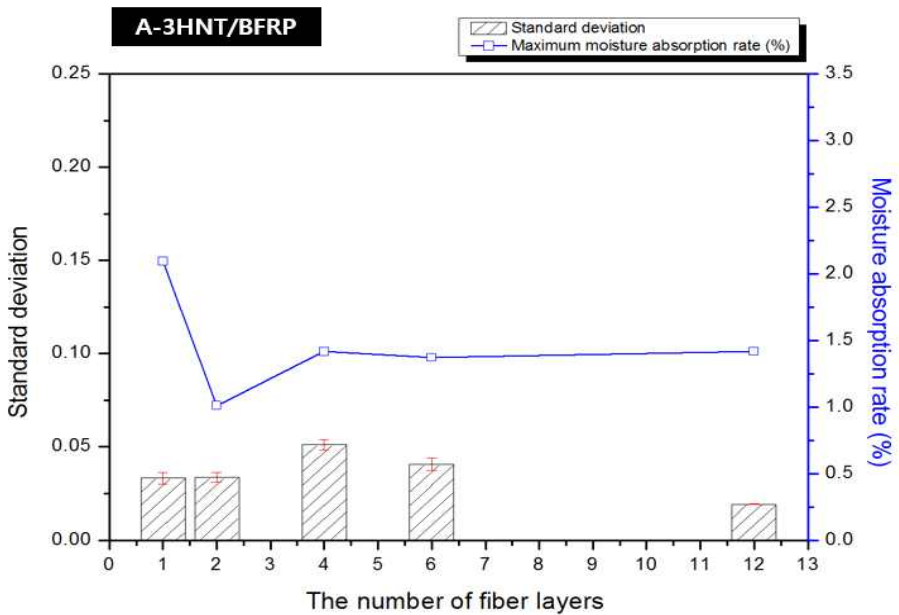
Fig. 65 shows the moisture absorption rates and area deviations of GFRP and BFRP. Both GFRP and BFRP showed absorption rates and area deviations similar to those of A-3HNT. With a decrease in the number of layers, moisture-induced deterioration became prominent and the effect of HNT on the bond strength between the fiber and EP became significant. In the case of A-3HNT/BFRP, the regional deviations remained the same irrespective of the number of fiber layers. However, different moisture absorption rates were observed. The aggregated HNT and EP showed similar dispersibility throughout the region because they exhibited similar moisture degradation.

As shown in Fig. 66, in the case of C-5HNT/GFRP, the deviation in the moisture absorption rate of each region tended to decrease with an increase in the number of fiber layers. A similar tendency was observed, except for a relatively high average moisture absorption rate, when four plies were used. On the other hand, in C-5HNT/BFRP, the moisture absorption rate deviation increased with an increase in the number of fiber layers. In the case of C-5HNT/BFRP-12, this deviation was small because C-5HNT showed the least effect of resin shrinkage because of the curing reaction. Most of the HNT particles showed a thick surface, and their moisture activation was difficult.

Fig. 67 shows that very large variations were observed in the area-specific moisture absorption rate of the samples when 12 plies were used, resulting in an increase in the moisture absorption rate. This is because A-HNTs showed lower mutual cohesion than C-HNTs and could be easily degraded by moisture. In addition, because of the partial delamination, a large amount of HNT was considerably vulnerable to uniform dispersibility.

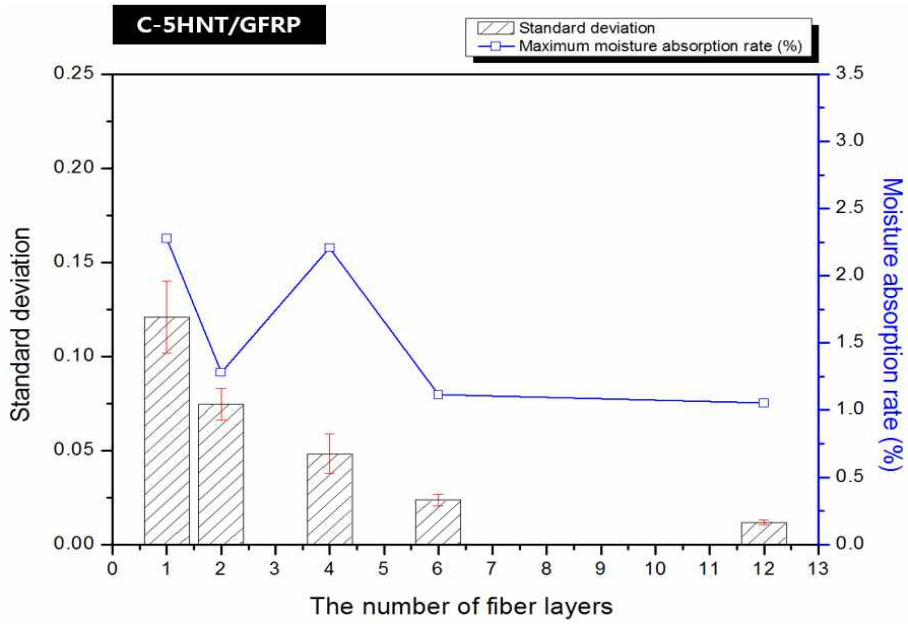


(a)

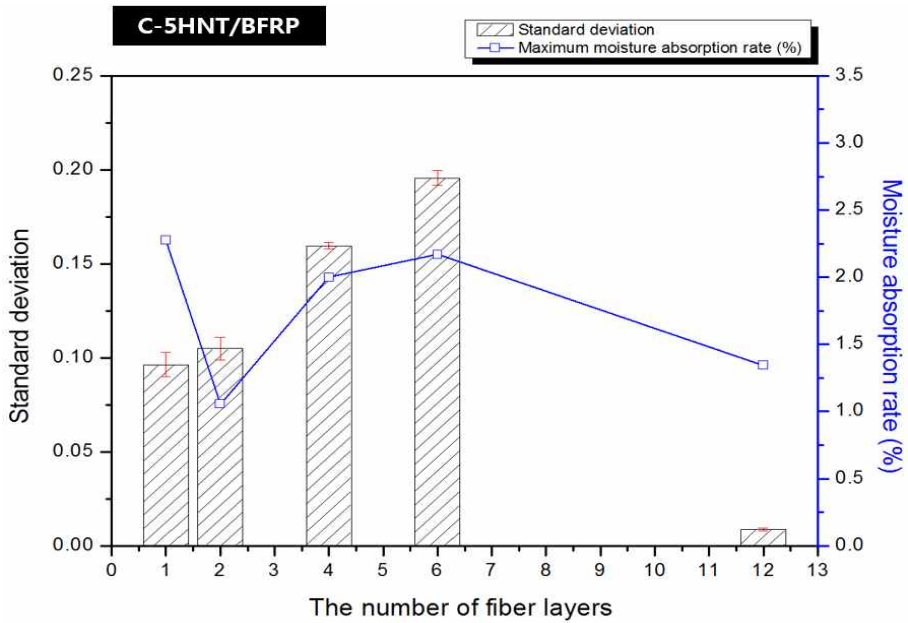


(b)

Fig. 65 Analysis of the state of HNT dispersion in composite laminates through moisture rate and variation with laminated fiber plies; (a) A-3HNT/GFRP and (b) A-3HNT/BFRP

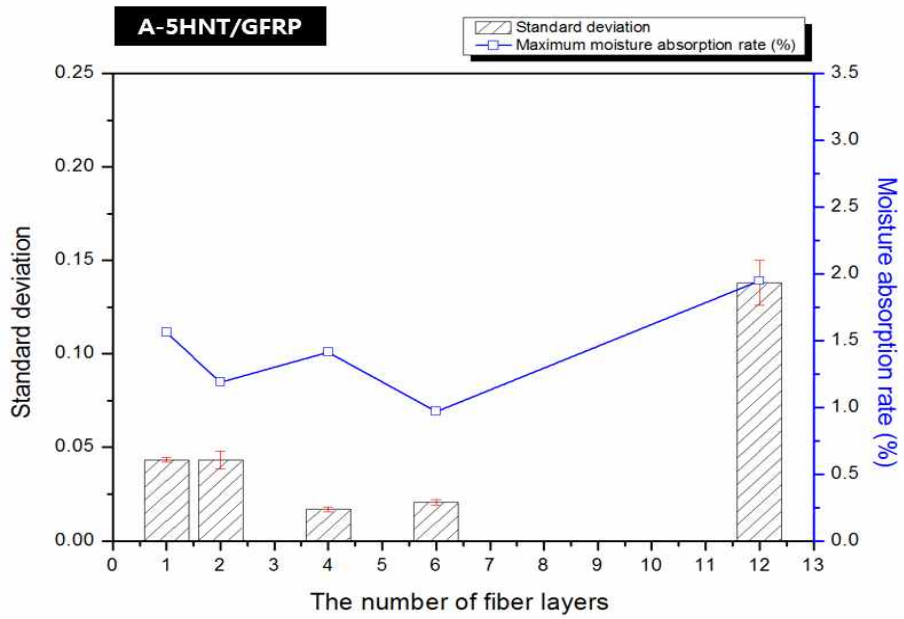


(a)

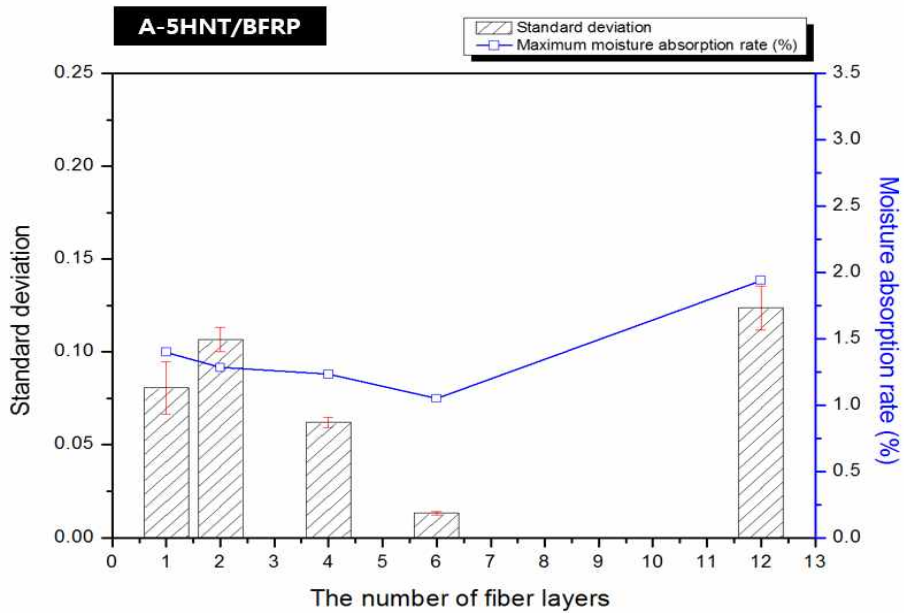


(b)

Fig. 66 Analysis of the state of HNT dispersion in composite laminates through moisture rate and variation with laminated fiber plies; (a) C-5HNT/GFRP and (b) C-5HNT/BFRP



(a)



(b)

Fig. 67 Analysis of the state of HNT dispersion in composite laminates through moisture rate and variation with laminated fiber plies; (a) A-5HNT/GFRP and (b) A-5HNT/BFRP

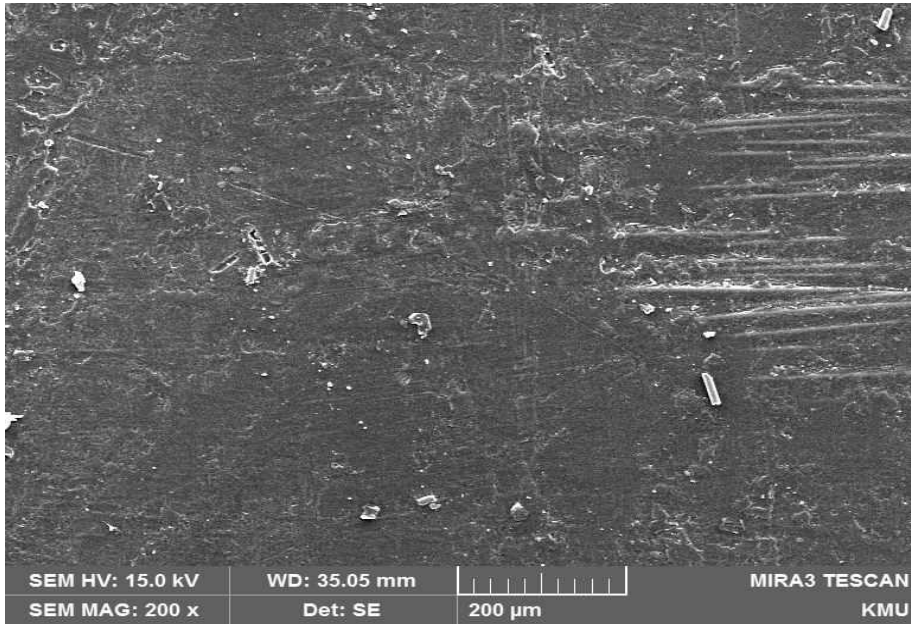
5. Proposal for Various Applications

5.1 High functional structural materials

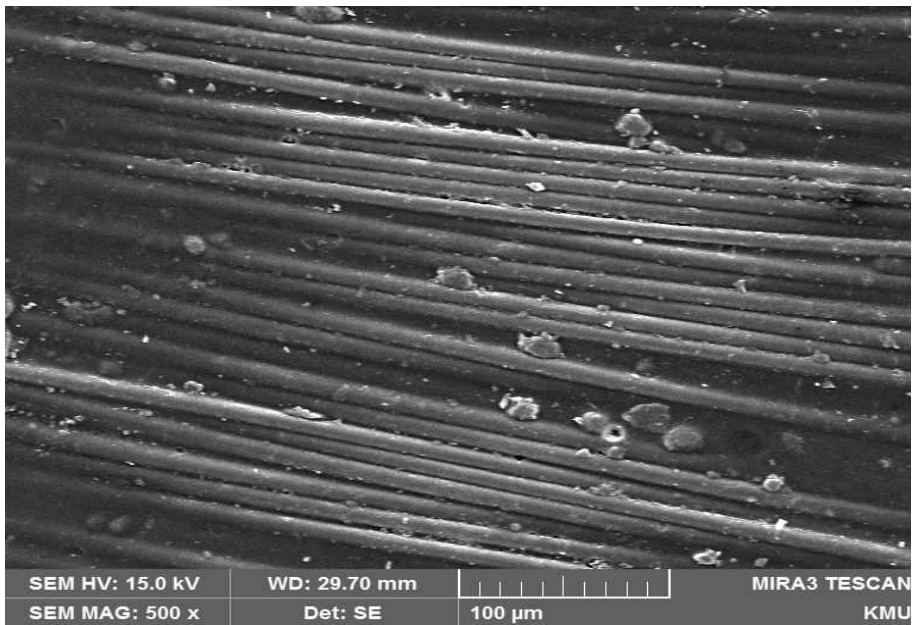
Recent technological innovations have increased the technological demand of preoccupying high technology. In the materials and parts industries, research and development is being carried out in various fields for the development of complex functional materials and new functional fusion-type new materials based on the technical requirements.

Composite materials, such as high-performance structural materials have a great advantage in terms of diversity, functionality and specificity in the advancement of material source technology. Amongst them, nanocomposites are classified as the most promising industries because they can be synthesized between different materials and be applied to specific applications.

However, even though nanocomposites have very good chemical, physical and structural properties, they have many structural and technological limitations. Particularly, in the production of parts and structures as medium and large-sized structural materials, production efficiency and cost competitiveness are low. Therefore, it is difficult to practically utilize them in the manufacture of structural materials. The difference from the conventional bulk scale materials of nanomaterials is that they are able to overcome the limitations of existing technology by manufacturing unique materials or to present convergence technology based on new properties that were not possible in the past. In other words, it is possible to develop a variety of fusion technologies based on the unique characteristics of the nanomaterials. However, it is limited in scale compared to the conventional bulk scale materials. To overcome this, it is necessary to increase productivity and price competitiveness of nanomaterials.

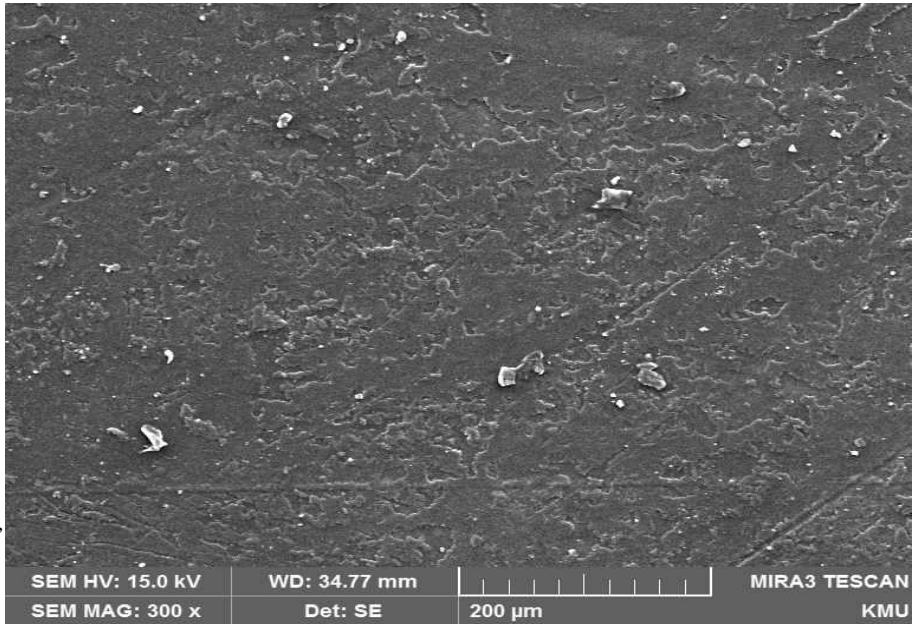


(a)

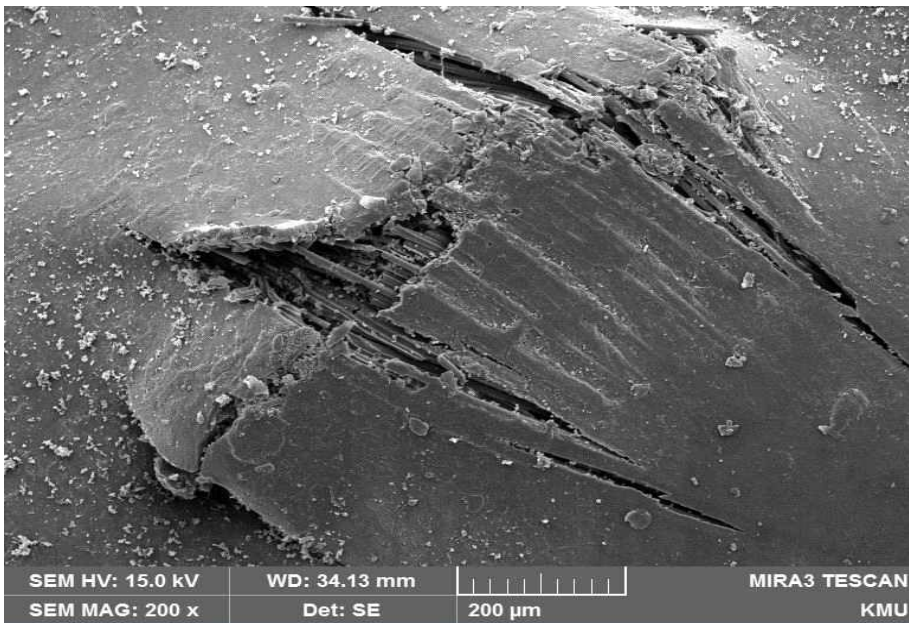


(b)

Fig. 68 SEM observation of carbonized surface by flame; (a) A-HNT/GFRP and (b) A-HNT/GFRP (after UL 94 5V test)



(a)



(b)

Fig. 69 SEM observation of carbonized surface by flame; (a) A-HNT/BFRP and (b) A-HNT/BFRP (after UL 94 5V test)

Therefore, we propose the HNT-polymer nanocomposites as high-performance structural materials. Nanomaterials and nanocomposite materials focus on specific functionality because of the high-risk materials with complicated manufacturing processes, which have very low physical properties and cost ratios as general structural materials. However, HNT is not only a natural reservoir of natural nanomaterials but also has a relatively easy dispersion in the production of polymer nanomaterials. According to the results of this study, it is easy to manufacture laminated composites with uniform states of dispersion by adding only the HNT dispersion process to the existing FRP composites manufacturing process. In addition, HNT has water resistance, heat resistance, environment friendliness, and can be used as a special functional material.

For example, in the case of flammability characteristics, the UL 94 5V test results showed that the C-HNT/GFRP, C-HNT/BFRP, A-HNT/GFRP and A-HNT/BFRP satisfied 5VA levels. As a result of observing the carbonized surfaces of A-HNT/GFRP and AHNT/BFRP by SEM (see Fig. 68–69). After extinguishing the flame that remained on the sample surface, no surface cracks and penetration marks were observed on the surface of the sample. In this regard, they analyzed that the A-HNT formed a physical barrier on the surface of the carbide produced by heat, delaying heat transfer and enhancing the interfacial bonding force between the fibers and EP (Kim, et al. 2019).

Therefore, the results of the state-of-the-dispersion evaluation based on the water resistance of the HNT, aggregation and re-aggregation behavior of the HNT at the interlayer interface of laminates suggest that the possibility of using HNT as a high functional structural material. Additionally, HNT materials have the potential to overcome the utility of bulk-scale structural materials. This research will reiterate its potential.

6. Conclusions

In this study, HNT/EP matrix GFRP and BFRP nanocomposites were manufactured by using C-HNT (Crystalloid) and A-HNT (Amorphous) according to the crystallinity of HNT, additionally the state of dispersion of HNT was evaluated at the interlayer interface of the utilized laminates. The state of dispersion of each laminate nanocomposites was analyzed by dividing the nine (A-H) columns in the direction of the air outlet in vacuum molding, the evaluation of homogeneous dispersion was carried out based on the tendency and the deviation of the absorption rate when immersed in 70 °C distilled water for 336 hours. The reliability of the state of dispersion criterion of nanomaterials was also evaluated at that time. The conclusions are as follows.

(1) C-HNT and A-HNT generally formed agglomerates in the powdered state regardless of crystallinity. In the case of A-HNT thermally treated at 1000 °C, the dehydrogenation reaction occurred with the removal of the physically bonded water layer, and the particle contraction and rearrangement of the structure occurred due to the inner structure fracture of HNT.

(2) It is noted that the EP and HNT have chemically similar components and bond forms, and were influenced by the noted bond strength depending on the bond type of bond atoms present. Since it was shown that the EP and HNT can form bonds not only in chemical bonding but also in independent form, it is possible to improve mutual bonding force through a chemical modification (surface modification) of EP and HNT.

(3) When the heating rate of the curing system is high, the cure proceeds at a high temperature and the temperature at which the cure reaches the fully formed cure is increased. However, when the heating rate is low, the rate of cure tends to decrease rapidly because cure is required. In this case,

C-HNT and A-HNT showed a stable curing reaction at more than 1 and 3 wt.%, respectively, and regardless of crystallinity, HNT was more effective than the noted Neat EP in promoting the curing reaction.

(4) In the case of the reviewed moisture absorption rate of each region, it was influenced by the formation of HNT particle agglomerates due to the occurrence of resin shrinkage in the curing reaction based on the direction of air discharge in vacuum forming. The cohesion of the HNT particles on the surface of the fiber, which resists resin shrinkage, influenced the dispersion stability, which was therefore attributed to A-HNT which was noted as being relatively high.

(5) As the immersion time increased, HNT/GFRP and HNT/BFRP caused a local damage to the fiber as EP and fiber were delaminated from a microscopic point of view. At that time, moisture deterioration and softening of the EP resulted in a noted different roughness of the fiber fracture pattern. The C-HNT was involved in the moisture absorption in EP, fiber-bonded form, and A-HNT affected direct deterioration with EP, although it was not interfaced between the EP and fiber.

(6) GFRP laminates were greatly influenced by the crystallinity and the content of HNT in mechanical properties and water resistance. In the studied BFRP laminates, there were differences in the size and shape of the clusters depending on the content of HNT. Next, it was noted that the C-HNT and A-HNT commonly softened the material to increase ductility and delayed arrival time to yield, which contributed to reducing deformation by the external load and increasing resistance to any damage.

(7) A-HNT has a higher bonding strength to the interlaminar interface of laminates than C-HNT, and has less delamination as noted between the fiber filaments, and is greatly influenced by the crystallinity of HNT in the

mechanical fracture pattern due to external load.

(8) A-HNT showed relatively uniform dispersibility due to its binding to GFRP and BFRP as compared to C-HNT. The variation of the moisture absorption rate of each region was influenced by the binding force of HNT/EP on the fiber surface and fiber interface. The clusters of C-HNT showed a higher cohesive force than of the A-HNT. In this clustering layer (surface layer), the thickness of the bond with EP was too thick to penetrate the water, resulting in less deterioration by moisture.

Acknowledgement

박사학위논문을 마무리하며, 우선 김윤희 지도교수님께 감사인사 드립니다. 교수님의 한결같은 신뢰와 믿음은 제 지나온 시간의 든든한 버팀목이 되어주셨고, 가르침의 매 순간 배움의 깊이를 더해 나아갈 길을 밝혀주셨습니다. 이제는 교수님의 뒤를 이어 넓은 세상을 배우고 돌아오겠습니다. 항상 감사하는 마음으로 지혜롭게 세상을 살아가겠습니다. 그리고 언젠가 교수님의 비비델 언덕이 되어 드리겠습니다. 교수님의 은혜에 진심으로 감사드립니다.

막막했던 20대의 저에게 학문으로서 나아갈 길을 일깨워주시고 지도를 아끼지 않으셨던 문경만 교수님, 이성열 교수님, 이병우 교수님, 김준영 교수님께도 감사의 말씀드립니다.

복합재료실험실에서 연구를 진행하면서 학문적인 성과뿐만 아니라 진정한 삶을 살아가기 위한 관계의 가치를 알게 되었습니다. 제가 가진 부족함을 응원과 격려, 믿음과 조언을 통해 새로운 희망과 용기로 만들어준 소중한 인연— 배창원 교수님, 김국진 박사님, 신도훈 박사님, 하진철 박사님, 윤성원 박사님, 이진우 박사님, 박창욱 박사님, Hanabusa 교수님, Nakagaito 교수님께 깊이 감사드립니다. 더불어 언제나 제 편이 되어 함께 이 길을 걸어 주었고, 앞으로도 서로에게 든든한 희망이 될 정경석, 한석희에게 고생했고 진심으로 고맙다고 전하고 싶습니다.

함께 박사학위를 마무리하는 Chen Zixuan의 새로운 시작을 응원하며, 부족한 저를 믿고 따라준 복합재료실험실 가족— Yu Tianyu, 홍정효 연구원, 최지수, 이교문, 박성재, 조경인에게도 고맙다고 모두가 있었기에 더욱 많은 추억을 간직할 수 있었다고 전하고 싶습니다.

마지막으로, 소중한 가족에게 사랑하고, 감사드립니다. 항상 제 일에 바쁘고, 감정표현에 서툰 딸을 묵묵히 기다려주시고 저와 함께 희망을 그려주셔서 지금까지 올 수 있었습니다. 헌신해주신 마음과 시간, 그 뜻을 잊지 않고 나아가겠습니다.

저에게 따뜻한 관심과 격려를 아끼지 않았던 모든 분께 진심으로 감사드립니다.

References

- 김용석, 2006. *기능성 표면처리 기술*, 고분자과학과 기술, 17(2), pp.171.
- 연구개발특구진흥재단(INNOPOLIS Foundation), 2017. *고분자 나노 복합재료 시장*, 대전:연구개발특구진흥재단.
- 유선희, 2016. *나노기술과 나노소재의 시장 동향*. CERAMIST, 19(1), pp.5-11.
- 이수정, 2007. *천연나노튜브-할로이사이트의 활용현황과 전망*. 광물과 산업, 20(2), pp.76-84.
- 한국과학기술정보연구원(Korea Institute of Science and Technology Information), 2002. *나노복합재료*, 대전:한국과학기술정보연구원.
- Adhikari, M, Majumdar, M.K. & Pati, A.K., 1983. Thermal decomposition of vermiculites: kinetics of dehydration and dehydroxylation processes. *Transactions of the Indian Ceramic Society*, 42(5), pp.124-127.
- Ahn, W.S., 2018. Cure kinetics of a bisphenol-A type vinyl-ester resin using non-isothermal DSC. *Elastomers and Composites*, 53(1), pp.1-5.
- Akil, H.M., Santulli, C., Sarasini, F., Tirillo, J. & Valente, T., 2014. Environmental effects on the mechanical behaviour of pultruded jute/glass fibre-reinforced polyester hybrid composites. *Composites Science and Technology*, 94, pp.62-70.
- Alamri, H. & Low, I.M., 2012. Effect of water absorption on the mechanical properties of nano-filler reinforced epoxy nanocomposites. *Materials & Design*, 42, pp.214-222.
- Alexandre, M. & Dubois, P., 2000. Polymer-layered silicate nanocomposite: preparation, properties and uses of a new class of materials. *Materials Science and Engineering: R: Reports*, 28(1-2), pp.1-63.

- Ashby, M.F., 2005. *Materials selection in mechanical design*. 3rd Ed. Butterworth-Heinemann: Burlington.
- Attia, N.F., Hassan, M.A., Nour, M.A. & Geckeler, K.E., 2014. Flame-retardant materials: synergistic effect of halloysite nanotubes on the flammability properties of acrylonitrile-butadiene-styrene composites. *Polymer International*, 63(7), pp.1168-1173.
- Baek, C.G., Choi, H.W., Yang, Y.S. & Rim, Y.H., 2016. Non-isothermal crystallization kinetics of 0.8Li₂B₄O₇-0.2Fe₂O₃ dielectric glass. *New Physics: Sae Mulli*, 67(2), pp.121-127.
- Barrientos-Ramirez, S. et al., 2011. Surface modification of natural halloysite clay nanotubes with aminosilanes. Application as catalyst supports in the atom transfer radical polymerization of methyl methacrylate. *Applied Catalysis A: General*, 406(1-2), pp.22-33.
- Basara, C., Yilmazer, U. & Bayram, G., 2005. Synthesis and characterization of epoxy based nanocomposites. *Journal of Applied Polymer Science*, 98(3), pp.1081-1086.
- Beata, S. et al., 2015. The effect of chemical modification on the physico-chemical characteristics of halloysite: FTIR, XRF, and XRD studies. *Journal of Molecular Structure*, 1084, pp.16-22.
- Becker, O., Varley, R.J. & Simon, G.P., 2004. Thermal stability and water uptake of high performance epoxy layered silicate nanocomposites. *European polymer journal*, 40(1), pp.187-195.
- Berglund, L., & Kenny, J., 1991. Processing science for high performance thermoset composites. *Sampe Journal*, 27, pp.27-37.

- Blumstein, A., 1965. Polymerization of adsorbed monolayers. I. preparation of the clay-polymer complex. *Journal of polymer science part A: general papers*, 3(7), pp.2653-2664.
- Brantseva, T.V., Antonov, S.V. & Gorbunova, I.Y., 2018. Adhesion properties of the nanocomposites filled with aluminosilicates and factors affecting them: a review. *International Journal of Adhesion and Adhesives*, 82, pp.263-281.
- Brindly, G.W., 1979. Formation and properties of clay-polymer complexes. *Earth Science Reviews*, 15, pp.295-296.
- Cavallaro, G., Donato, D.I., Lazzara, G. & Milioto, S., 2011. Films of halloysite nanotubes sandwiched between two layers of biopolymer: from the morphology to the dielectric, thermal, transparency, and wettability properties. *The Journal of Physical Chemistry C*, 115(42), pp.20491-20498.
- Chen, Z. et al., 2018. Effect of curing cycles using wet prepreg processing on mechanical properties. *International Journal of Modern Physics B*, 32(19), 1840076.
- Choi, H.J. & Lee, S.H., 2017. Evaluation on adequate range of carbonization temperature using swine manure through reaction kinetics. *Journal of Korean Institute of Resources Recycling*, 26(2), pp.25-32.
- Choe, C.R., 2013. Nanocarbon polymer composites. *Composites Research*, 26(3), pp.147-154.
- Cho, M.S. & Lee, Y.K., 2006. Polymer nanocomposites using nano clay. *Prospectives of Industrial Chemistry*, 9(6), pp.22-36.
- Cipriotti, S.V. & Catauro, M., 2016. Synthesis, structural and thermal behavior study of four Ca-containing silicate gel-glasses. *Journal of Thermal Analysis and Calorimetry*, 123(3), pp.2091-2101.

- Deng, S., Ye, L. & Friedrich, K., 2007. Fracture behaviours of epoxy nanocomposites with nano-silica at low and elevated temperatures. *Journal of materials science*, 42(8), pp.2766-2774.
- Deng, S., Zhang, J. & Ye, L., 2009. Halloysite-epoxy nanocomposites with improved particle dispersion through ball mill homogenisation and chemical treatments. *Composites Science and Technology*, 69(14), pp.2497-2505.
- Deng, S., Zhang, J., Ye, L. & Wu, J., 2008. Toughening epoxies with halloysite nanotubes. *Polymer*, 49(23), pp.5119-5127.
- Dionisi, C. et al., 2016. Halloysite clay nanotubes as carriers for curcumin: characterization and application. *IEEE Transactions on Nanotechnology*, 15(5), pp.720-724.
- Divigalpitiya, W.M.R., Frindt, R.F. & Morrison, S.R., 1991. Molecular composite films of MoS₂ and styrene. *Journal of Materials Research*, 6(5), pp.1103-1107.
- Dong, Y., Lisco, B., Wu, H., Koo, J.H. & Krifa, M., 2015. Flame retardancy and mechanical properties of ferrum ammonium phosphate-halloysite/epoxy polymer nanocomposites. *Journal of Applied Polymer Science*, 132(13).
- Duce, C. et al., 2015. Thermal behavior study of pristine and modified halloysite nanotubes. *Journal of Thermal Analysis and Calorimetry*, 121, pp.1011-1019.
- Esbati, A.H. & Irani, S., 2018. Effect of functionalized process and CNTs aggregation on fracture mechanism and mechanical properties of polymer nanocomposite. *Mechanics of Materials*, 118, pp.106-119.
- Fateme, F., Morteza, E. & Ali, J., 2013. Curing kinetics of solid epoxy/DDM/nanoclay: Isoconversional models versus fitting model. *Thermochimica Acta*, 568, pp.67-73.
- Fellahi, S., Chikhi, N. & Bakar, M., 2001. Modification of epoxy resin with kaolin as a toughening agent. *Journal of Applied Polymer Science*, 82(4), pp.861-878.

- Fr  chette, M.F. et al., 2013. Preparation and dielectric responses of solid epoxy composites containing a mixture of epoxy powder ball-milled with GO. *2013 Annual Report Conference on Electrical Insulation and Dielectric Phenomena. IEEE*, pp.746-750.
- Gao, F., 2004. Clay/Polymer Composites: the story. *Materials today*, 7(11), pp.50-55.
- Gasparini, E. et al., 2013. Thermal dehydroxylation of kaolinite under isothermal conditions. *Applied Clay Science*, 80, pp.417-425.
- Georga, J., Bhagawan, S.S. & Thomas, S. 1998. Effects of environment on the properties of low-density polyethylene composites reinforced with pineapple-leaf fibre. *Composites Science and Technology*, 58(9), pp.1471-1485.
- Glaskova, T. & Aniskevich, A., 2009. Moisture absorption by epoxy/montmorillonite nanocomposite. *Composites Science and Technology*, 69(15-16), pp.2711-2715.
- Hiller, S. et al., 2016. Correlations among the mineralogical and physical properties of halloysite nanotubes (HNTs). *Clay Minerals*, 51(3), pp.325-350.
- Horvath, E. et al., 2003. Hydrazine-hydrate intercalated halloysite under controlled-rate thermal analysis conditions. *Journal of Thermal Analysis and Calorimetry*, 71(3), 707-714.
- Hu, P. & Yang, H., 2012. Sb-SnO₂ nanoparticles onto kaolinite rods: assembling process and interfacial investigation. *Physics and Chemistry of Minerals*, 39(4), pp.339-349.
- Huang, Y. & Kinloch, A.J., 1992. The toughness of epoxy polymers containing microvoids. *Polymer*, 33(6), pp.1330-1332.
- Hwang, S.H., Kang, D.W. & Kang, H.J., 2016. Modification of nano silica for multi-functional organic/inorganic hybrid hard coating. *Polymer*, 40(6), pp.967-971.

- Idumah, C.I., Hassan, A. & Affam, A.C., 2015. A review of recent developments in flammability of polymer nanocomposites. *Reviews in Chemical Engineering*, 31(2), pp.149-177.
- Iijima, S., 1991. Helical microtubules of graphitic carbon. *Nature*, 354(6348), pp.56.
- Irshidat, M.R. & Al-Saleh, M.H., 2018. Thermal performance and fire resistance of nanoclay modified cementitious materials. *Construction and Building Materials*, 159, pp.213-219.
- Jeong, J.W. et al., 2018. Curing Behavior and Thermal Properties of DGEBA/phenol novolac epoxy resin. *Textile Science and Engineering*, 55, pp.44-47.
- Jiuli, Z. et al., 2011. High-viscosity polylactide prepared by in situ reaction of carboxyl-ended polyester and solid epoxy. *Journal of Applied Polymer Science*, 123, pp.2996-3006.
- Kadi, S. et al., 2012. Preparation, characterisation and application of thermally treated Algerian halloysite. *Microporous and Mesoporous Materials*, 158, pp.47-54.
- Kanatidis, M.G., Wu, C.G., Marcy, H.O. & Kannewurf, C.R., 1989. Conductive-polymer bronzes. Intercalated polyaniline in vanadium oxide xerogels. *Journal of the American Chemical Society*, 111(11), pp.4139-4141.
- Kaynak, C., Nakas, G.I. & Isitman, N.A., 2009. Mechanical properties, flammability and char morphology of epoxy resin/montmorillonite nanocomposites. *Applied Clay Science*, 46(3), pp.319-324.
- Kedward, K.T., Wilson, R.S. & McLean, S.K., 1989. Flexure of simply curved composite shapes. *Composites*, 20(6), pp.527-536.
- Kibria, M.A., Anisur, M.R., Mahfuz, M.H., Saidur, R. & Metselaar, I.H.S.C., 2015. A review on thermophysical properties of nanoparticle dispersed phase change materials. *Energy Conversion and Management*, 95, pp.69-89.

- Kim, J.H., Choi, K.Y., Joo, H.J., Jin, F.L. & Park, S.J., 2005. A study on the water resistance and thermo-mechanical behaviors of epoxy adhesives. *Elastomer*, 40(3), pp.166-173.
- Kim, J.K., Hu, C., Woo, R.S. & Sham, M.L., 2005. Moisture barrier characteristics of organoclay-epoxy nanocomposites. *Composites Science and Technology*, 65(5), pp.805-813.
- Kim, J.S., Kim, B.H. & Joe, C.R., 2014. Development and analysis of the autoclave alternative composite material molding process using a pressure device. *Composites Research*, 27(6), pp.254-259.
- Kim, Y.H. et al., 2008. A study on degradation and recovery mechanisms of composites under the moisture environment. *Composites research*, 21(2), pp.8-14.
- Kim, Y.H. et al., 2015. A study on the effect of halloysite nanoparticle addition on the strength of glass fiber reinforced plastic. *Modern Physics Letters B*, 29(06n07), 1540003.
- Kim, Y.H., Choi, J.S. & Park, S.J., 2019. Effect of carbonization on mechanical properties of halloysite nanotube-FRP nanocomposites with different morphological structures. *Modern Physics Letters B*, 1940021.
- Kim, Y.H. et al., 2018. Effects of heat-treated HNTs on the mechanical properties of GFRP under moisture absorption. *International Journal of Modern Physics B*, 32(19), pp.1840070.
- Kim, Y.H., Park, S.J. & Nakagaito, A.N., 2017. Optimization of processing condition of nanocomposites according to the structural changes of halloysite nanotubes under impact behavior. *Metallurgical and Materials Transactions B*, 48(4), pp.1933-1937.
- Klevtsov, D.P. et al., 1988. Kinetics of kaolinite dehydration and its dependence on mechanochemical activation. *Journal of Thermal Analysis*, 33(2), pp.531-535.

- Kojima, Y. et al., 1993. Mechanical properties of nylon 6-clay hybrid. *Journal of Materials Research*, 8(5), pp.1185-1189.
- Kornmann, X., Lindberg, H. & Berglund, L.A., 2001. Synthesis of epoxy-clay nanocomposites: influence of the nature of the clay on structure. *Polymer*, 42(4), pp.1303-1310.
- Kwon, H., 2014. *Out-of autoclave process using a novel semi-preg system for aircraft structures*. Ph.D. Korea Aerospace University.
- Kwon, H. et al., 2014. Cure shrinkage behavior of polymer matrix composite according to degree of cure. *Composites Research*, 27(3), pp.90-95.
- Kwon, H.J. et al., 2018. Study of the curing reaction rate of a glass fiber reinforced bisphenol-A (BPA) epoxy prepreg by differential scanning calorimetry (DSC). *Composites Research*, 31(1), pp.30-36.
- Lan, T., Kaviratna, P.D. & Pinnavaia, T.J., 1996. Epoxy self-polymerization in smectite clays. *Journal of Physics and Chemistry of Solids*, 57(6-8), pp.1005-1010.
- Lasfargues, M., 2014. *Nitrate based high temperature nano-heat-transfer-fluids: formulation & characterisation*. Ph.D., Leeds: University of Leeds.
- Lee, J.H., Rhee, K.Y. & Lee, J.H., 2010. Effects of moisture absorption and surface modification using 3-aminopropyltriethoxysilane on the tensile and fracture characteristics of MWCNT/epoxy nanocomposites. *Applied Surface Science*, 256(24), pp.7658-7667.
- Lee, J.W., Park, S.J. & Kim, Y.H., 2017. Improvement of interfacial adhesion of incorporated halloysite-nanotubes in fiber-reinforced epoxy-based composites. *Applied Sciences*, 7(5), pp.441.
- Lee, S.C. et al., 2015. Improvement in mechanical and wear properties of WC-Co by ultrasonic nanocrystal surface modification technique. *Journal of the Korean Society of Tribologists & Lubrication Engineers*, 31(2), pp.56-61.

- Lee, W.I., Loos, A.C. & Springer, G.S., 1982. Heat of reaction degree of cure, and viscosity of Hercules 350-6 resin, *Journal of Composite Materials*, 16(6), pp.510-520.
- Levis, S.R. & Deasy, P.B., 2002. Characterisation of halloysite for use as a microtubular drug delivery system. *International Journal of Pharmaceutics*, 243(1-2), pp.124-134.
- Li, C. et al., 2008. Polymer-modified halloysite composite nanotubes. *Journal of Applied Polymer Science*, 110, pp.3638-3646.
- Li, C., Liu, J., Qu, X. & Yang, Z., 2009. A general synthesis approach toward halloysite-based composite nanotube. *Journal of Applied Polymer Science*, 112, pp.2647-2655.
- Lin, Y.G., Sautereau, H. & Pascault, J.P., 1987. Processing property relationship for dicyandiamide-cured epoxy networks. *Journal of applied polymer science*, 33(2), pp.685-691.
- Liu, H. et al., 2012. Kinetic study of goethite dehydration and the effect of aluminium substitution on the dehydration. *Thermochimica acta*, 545, pp.20-25.
- Liu, M., Guo, B., Du, M., Cai, X. & Jia, D., 2007. Properties of halloysite nanotube-epoxy resin hybrids and the interfacial reactions in the systems. *Nanotechnology*, 18(45), pp.455703.
- Liu, M., Jia, Z., Jia, D. & Zhou, C., 2014. Recent advance in research on halloysite nanotubes-polymer nanocomposite. *Progress in polymer science*, 39(8), pp.1498-1525.
- Liu, P. & Zhao, M., 2009. Silver nanoparticle supported on halloysite nanotubes catalyzed reduction of 4-nitrophenol (4-NP). *Applied Surface Science*, 255(7), pp.3989-3993.

- Liu, W., Hoa, S.V. & Pugh, M., 2005. Organoclay-modified high performance epoxy nanocomposite. *Composites Science and Technology*, 65(2), pp.307-316.
- Liu, X.Y. et al., 2003. Novel bismuth nanotube arrays synthesized by solvothermal method. *Chemical Physics Letters*, 374(3-4), pp.348-352.
- Lun, H., Ouyang, J. & Yang, H., 2014. Enhancing dispersion of halloysite nanotubes via chemical modification. *Physics and Chemistry of Minerals*, 41(4), pp.281-288.
- Nakamura, R., Netravali, A.N., Morgan, A.B., Nyden, M.R. & Gilman, J.W., 2013. Effect of halloysite nanotubes on mechanical properties and flammability of soy protein based green composites. *Fire and Materials*, 37(1), pp.75-90.
- Nakamura, Y., Yamaguchi, M., Okubo, M. & Matsumoto, T., 1992. Effect of particle size on the fracture toughness of epoxy resin filled with spherical silica. *Polymer*, 33(16), pp.3415-3426.
- Nam, K.S. et al., 2013. Influence of the duty cycle on the characteristics of Al₂O₃ coatings formed on the Al-1050 by plasma electrolytic oxidation. *Journal of the Korean Ceramic Society*, 50(2), pp.108-115.
- Ng, K.M., Lau, Y.T.R., Chan, C.M., Weng, L.T. & Wu, J., 2011. Surface studies of halloysite nanotubes by XPS and ToF-SIMS. *Surface and Interface Analysis*, 43(4), pp.795-802.
- Manfredi, L.B., De Santis, H. & Vazquez, A., 2008. Influence of the addition of montmorillonite to the matrix of unidirectional glass fibre/epoxy composites on their mechanical and water absorption properties. *Composites Part A: Applied Science and Manufacturing*, 2008, 39(11), pp.1726-1731.
- Mazuki, A.A.M., Akil, H.M., Safiee, S., Ishak, Z.A.M. & Bakar, A.A., 2011. Degradation of dynamic mechanical properties of pultruded kenaf fiber reinforced

- composites after immersion in various solutions. *Composites Part B: Engineering*, 42(1), pp.71-76.
- Mohan, T.P. & Kanny, K., 2011. Water barrier properties of nanoclay filled sisal fibre reinforced epoxy composites. *Composites Part A: Applied Science and Manufacturing*, 42(4), pp.385-393.
- Park, S.J., 2016a. *Changes of the structural and mechanical properties on nanocomposites based on halloysite nanotubes with the optimization of dispersion by ultrasonic waves*. Master Thesis. Busan: Korea Maritime and Ocean University.
- Park, S.J., 2016b. *Changes of the structural and mechanical properties on nanocomposites based on halloysite nanotubes with dispersion optimization by ultrasonication*. Master Thesis, Tokushima: Tokushima University.
- Park, S.J., 2019. Influence of fiber laminated thickness on the hygrothermal property of HNT-GFRP nanocomposites for the RFI process-based structures. *Modern Physics Letters B*, pp.1940051
- Park, S.J. et al., 2019. Influence of nanoparticle dispersibility on hydrothermal properties of HNT-GFRP/BFRP nanocomposites. *Modern Physics Letters B*, pp.1940020
- Pavlidou, S. & Papaspyrides, C.D., 2008. A review on polymer-layered silicate nanocomposites. *Progress in polymer science*, 33(12), pp.1119-1198.
- Picard, E., Gerard, J.F. & Espuche, E., 2008. Water transport properties of polyamide 6 based nanocomposites prepared by melt blending: on the importance of the clay dispersion state on the water transport properties at high water activity. *Journal of Membrane Science*, 313(1-2), pp.284-295.
- Qiao, J., Adams, J. & Johannsmann, D., 2012. Addition of halloysite nanotubes prevents cracking in drying latex films. *Langmuir*, 28(23), pp.8674-8680.

- Rawtani, D. & Agrawal, Y.K., 2012. Halloysite as support matrices: a review. *Emerging materials Research*, 1(4), pp.212-220.
- Ray, S.S. & Okamoto, M., 2003. Polymer/layered silicate nanocomposites: a review from preparation to processing. *Progress in polymer science*, 28(11), pp.1539-1641.
- Rosso, P., Ye, L., Friedrich, K. & Sprenger, S., 2006. A toughened epoxy resin by silica nanoparticle reinforcement. *Journal of Applied Polymer Science*, 100(3), pp.1849-1855.
- Ryu, J.G., Park, G.R., Lyu, S.G., Rhew, J.H. & Sur, G.S., 1998. Synthesis and characterization of montmorillonite-epoxy nanocomposites. *Polymer*, 22(2), pp.328-334.
- Saharudin, M., Atif, R. & Inam, F., 2017. Effect of short-term water exposure on the mechanical properties of halloysite nanotube-multi layer graphene reinforced polyester nanocomposites. *Polymers*, 9(1), pp.27.
- Saharudin, M.S., Atif, R., Shyha, I. & Inam, F., 2016. The degradation of mechanical properties in polymer nano-composites exposed to liquid media-a review. *RSC Advances*, 6(2), pp.1076-1089.
- Saharudin, M.S., Wei, J., Shyha, I. & Inam, F., 2016. The degradation of mechanical properties in halloysite nanoclay-polyester nanocomposites exposed in seawater environment. *Journal of Nanomaterials*.
- Samir, K. et al., 2012. Preparation, characterisation and application of thermally treated algerian halloysite. *Microporous and Mesoporous Materials*, 158, pp.47-54.
- Schmidt, D., Shah, D. & Giannelis, E.P., 2002. New advances in polymer/layered silicate nanocomposites. *Current Opinion in Solid State and Materials Science*, 6(3), pp.205-212.

- Schubel, P.J., Warrior, N.A. & Rudd, C.D., 2007. Surface quality prediction of thermoset composite structures using geometric simulation tools. *Plastics, Rubber and Composites*, 36(10), pp.428-437.
- Seo, D.K. et al., 2015. Property evaluation of epoxy resin based aramid and carbon fiber composite materials. *Textile Coloration and Finishing*, 27(1), pp.11-17.
- Shah, D.U. & Schuble, P.J., 2010. Evaluation of cure shrinkage measurement techniques for thermosetting resins. *Polymer Testing*, 29, pp.629-639.
- Shin, D.W. et al., 2015. The change of degree of cure and specific heat capacity according to temperature of thermoset resin. *Composites Research*, 28(3), pp.99-103.
- Shchukin, D.G., Sukhoroukov, G.B., Price, R.R. & Lvov, Y.M., 2005. Halloysite nanotubes as biomimetic nanoreactors. *Small*, 1(5), pp.510-513.
- Shu, Z. et al., 2015. Nanoporous-walled silica and alumina nanotubes derived from halloysite: controllable preparation and their dye adsorption applications. *Applied Clay Science*, 112-113, pp.17-24.
- Sohlerg, K., Pennycook, S.J. & Pantelides, S.T., 1999. Hydrogen and the structure of the transition aluminas. *Journal of the American Chemical Society*, 121(33), pp.7493-7499.
- SunMoon University, 2012. *A Development of Nano Crystalline Surface Modification Technology*, Asan:SunMoon University.
- Szczepanik, B. et al., 2015. The effect of chemical modification on the physico-chemical characteristics of halloysite: FTIR, XRF, and XRD studies. *Journal of Molecular Structure*, 1084, pp.16-22.

- Tang, Y. et al., 2011. Effects of unfolded and intercalated halloysites on mechanical properties of halloysite-epoxy nanocomposites. *Composites Part A: Applied Science and Manufacturing*, 42(4), pp.345-354.
- Teil, H., Page, S.A., Michaud, V. & Manson, J.-A.E., 2004. TTT-Cure diagram of an anhydride-cured epoxy system including gelation, vitrification, curing kinetics model, and monitoring of the glass transition temperature. *Journal of Applied Polymer Science*, 93(4), pp.1774-1787.
- Vergaro, V. et al., 2010. Cytocompatibility and uptake of halloysite clay nanotubes. *Biomacromolecules*, 11(3), pp.820-826.
- Vyazovkin, S. & Sbirrazzuoli, N., 2000. Effect of viscosity on the kinetics of initial cure stages. *Macromolecular Chemistry and Physics*, 201(2), pp.199-203.
- Wang, H., Bai, Y., Liu, S., Wu, J. & Wong, C.P., 2002. Combined effects of silica filler and its interface in epoxy resin. *Acta Materialia*, 50(17), pp.4369-4377.
- Wang, K. et al., 2005. Epoxy nanocomposites with highly exfoliated clay: mechanical properties and fracture mechanisms. *Macromolecules*, 38(3), pp.788-800.
- Wang, L., Wang, K., Chen, L., He, C. & Zhang, Y., 2006. Hydrothermal effects on the thermomechanical properties of high performance epoxy/clay nanocomposites. *Polymer Engineering & Science*, 46(2), pp.215-221.
- Wisnom, M.R., Dixon, R. & Hill, G., 1996. Delamination in asymmetrically tapered composites loaded in tension. *Composite Structures*, 35(3), pp.309-322.
- Wisnom, M.R. & Hallett, S.R., 2009. The role of delamination in strength, failure mechanism and hole size effect in open hole tensile tests on quasi-isotropic laminates. *Composites Part A: Applied Science and Manufacturing*, 40(4), pp.335-342.

- Xiao, K. & Ye, L., 2006. Effects of rubber-rich domains and the rubber-plasticized matrix on the fracture behavior of liquid rubber-modified araldite-F epoxies. *Polymer Engineering & Science*, 40(11), pp.2288-2298.
- Xu, B., Zheng, Q., Song, Y. & Shangguan, Y., 2006. Calculating barrier properties of polymer/clay nanocomposites: Effects of clay layers. *Polymer*, 47(8), pp.2904-2910.
- Ye, Y., Chen, H., Wu, J. & Chan, C.M., 2011. Evaluation on the thermal and mechanical properties of HNT-toughened epoxy/carbon fibre composites. *Composites Part B: Engineering*, 42(8), pp.2145-2150.
- Ye, Y., Chen, H., Wu, J. & Ye, L., 2007. High impact strength epoxy nanocomposites with natural nanotubes. *Polymer*, 48(21), pp.6426-6433.
- Yu, T. et al., 2019. Electrophoresis deposited halloysite nanotubes as modifying additive for carbon fiber and CFRP. *Modern Physics Letters B*, 1940023.
- Yuan, P., Tan, D. & Annabi-Bergaya, F., 2015. Properties and applications of halloysite nanotubes: recent research advances and future prospects. *Applied Clay Science*, 112, pp.75-93.
- Yuan, P., Tan, D., Annabi-Bergaya, F., Yan, W., Fan, M., Liu, D. & He, H., 2012. Changes in structure, morphology, porosity, and surface activity of mesoporous halloysite nanotubes under heating. *Clays and Clay Minerals*, 60(6), pp.561-573.
- Zhang, J.Xu., Xu, Y.C. & Huang, P., 2009. Effect of cure cycle on curing process and hardness for epoxy resin. *Express Polymer Letters*, 3(9), pp.534-541.
- Zhang, M.Q., Rong, M.Z., Yu, S.L., Wetzels, B. & Friedrich, K., 2002. Effect of particle surface treatment on the tribological performance of epoxy based nanocomposites. *Wear*, 253(9-10), pp.1086-1093.

- Zhang, W.L. & Choi, H.J., 2012. Fabrication of semiconducting polyaniline-wrapped halloysite nanotube composite and its electrorheology. *Colloid and Polymer Science*, 290(17), pp.1743-1748.
- Zhang, Yi. & Yang, H., 2012. Co₃O₄ nanoparticles on the surface of halloysite nanotubes. *Physics and chemistry of minerals*, 39(10), pp.789-795.
- Zhao, H. & Li, R.K., 2008. Effect of water absorption on the mechanical and dielectric properties of nano-alumina filled epoxy nanocomposites. *Composites Part A: Applied Science and manufacturing*, 39(4), pp.602-611.